MIXED SILICILCASTIC-SILICEOUS SUCCESSION, MIOCENE MONTEREY FORMATION, POINT DUME TO PARADISE COVE, MALIBU, CALIFORNIA

A THESIS

Presented to the Department of Geological Sciences

California State University, Long Beach

In Partial Fulfillment

of the Requirements for the Degree

Master of Science in Geology

Committee Members:

Richard J. Behl, Ph.D. (Chair)
Tom Kelty, Ph.D.
Marc Kamerling, Ph.D

College Designee:

Richard J. Behl, Ph.D.

By Wanjiru Margaret Njuguna

B.S., 2001, Tufts University, Boston, Massachusetts

December 2016

ABSTRACT

MIXED SILICICLASTIC-SILICEOUS SUCCESSION,

MIOCENE MONTEREY FORMATION,

POINT DUME TO PARADISE COVE,

MALIBU, CALIFORNIA

By

Wanjiru Margaret Njuguna

December 2016

The 752 meter section of the Miocene Monterey exposures between Point Dume and Paradise Cove is described in detail using meter-by-meter Spectral Gamma Ray data, lithologic descriptions, sandstone analysis (percent sandstone and thin section petrography) and X-ray diffraction data. Samples were analyzed to determine total organic carbon (% TOC) and diatom assemblages. The stratigraphic section is subdivided into four distinct members and is portrayed in a new stratigraphic column. In stratigraphic order, the members are the Dolomitic Phosphatic Shale Member, the Porcelanite and Shale Member, the Mixed Clastics Member and the Cherty Diatomite Member. High TOC values in the Dolomitic Phosphatic Shale range between 4.2 and 7.5%. Opal-CT phase silica occurs in cherts and porcelanite and biogenic Opal-A phase silica occurred in the diatomites. Rocks showing a complete digenesis to Quartz phase silica are not in the section. Bedding confined fractures and joint sets between different siliceous rocks are abundant in the Porcelanite and Shale Member. The base of the Mixed Clastics member has high energy deposits indicating downslope movement with major sandstones and conglomerates. The top of the section contains the Cherty Diatomite member and consists of rhythmically bedded pure diatomite, “speckled” beds, muddy diatomites, siliceous/calcareous mudrocks and

Opal-CT chert. Dolostone forms a significant component of the rock type throughout the section. The Monterey Formation is found throughout Coastal California and in most of the Neogene sedimentary basins in the State. It is highly petroliferous, forming both the source and reservoir rock. Understanding the exposures in Malibu, California contributes to the understanding of this economically important formation.

ACKNOWLEDGEMENTS

I would like to thank all the people who supported me throughout my undergraduate and graduate education. Your constant encouragement and gentle nudging helped me plod along and see this project to the finish. This thesis would not have been possible were it not for the incredible mentorship, example and encouragement of my advisor, Dr. Rick Behl. You are awesome and I am SO grateful. To my committee members Dr. Tom Kelty and Dr. Marc Kamerling, I thank you all for the support, guidance, wisdom, good humor and patience.

To my dear parents Dr. Celia Nyamweru and Mr. Njuguna Mwangi, thank you for always being close by and rolling with the good times and the not so good times that were part of this journey. I am so lucky to have you both. To my siblings I love you all and thank you for your support. Thanks also to my classmates at CSULB who were amazing sources of encouragement and support as the wonderful MARS family. Thanks to Pilar and Tim for the delicious family dinners and steady encouragement that kept me nourished physically and mentally through this time. My "Running Ladies" who ALWAYS show up at Signal Hill before the crack of dawn for a run – you inspired and encouraged me to get up and keep moving forward…on the pavement and with the studies.

I also want to thank my various supervisors from California Resources Corporation and Occidental Petroleum for granting me the financial support and approval to continue with my studies and attend this program. I am so grateful. And, a big thanks to my wonderful colleagues and mentors Dr. Michael Clark and Mr. Michael Moniz. You have both played such a huge part in offering steady and consistent words of wisdom and advice along the academic and professional journey. Thank you for everything.

TABLE OF CONTENTS

ABSTRACT ii

ACKNOWLEDGEMENTS iv

LIST OF TABLES vi

LIST OF FIGURES vii

1. INTRODUCTION 1
2. BACKGROUND 3
3. METHODOLOGY 12
4. RESULTS 16
5. DISCUSSION 54
6. CONCLUSION 75
7. FUTURE WORK 78

APPENDICES 80

A. SPECTRAL GAMMA RAY AND ROCK TYPE DESCRIPTIONS 81

B. PALEOCURRENT DATA 110

C. DIATOM ANALYSIS 112

REFERENCES 119

LIST OF TABLES

1. Sandstone Petrography..... 40

2. Total Organic Carbon (%) Results..... 44

LIST OF FIGURES

2.1 Paradise Cove area 4

2.2 Map of Los Angeles basin blocks 5

2.3 Stratigraphy of the Los Angeles basin 7

2.4 Stratigraphic distribution of rocks south of the Malibu Coast Fault 9

2.5 Upper Mohnian submarine-fan facies map 10

2.6 Reconstruction of the Los Angeles region during the Middle Miocene 11

4.1 Stratigraphic column for Point Dume and Paradise Cove section 17

4. 2 Extent of the four members of the stratigraphic column 18

4.3 Sedimentologic and stratigraphic features of the Dolomitic Phosphatic Shale member 21

4.4 Sedimentologic and stratigraphic features of the Porcelanite and Shale member 25

4.5 Sedimentologic and stratigraphic features of the Porcelanite and Shale (cont.) 27

4.6 Sedimentologic and stratigraphic features of the Mixed Clastics member 30

4.7 Sedimentologic and stratigraphic features of the Mixed Clastics (cont.) 33

4.8 Sedimentologic and stratigraphic features of the Mixed Clastics (cont.) 36

4.9 Sedimentologic and stratigraphic features of the Cherty Diatomite member 38

4.10 Stratigraphic sandstone abundance graph 41

4.11 Total Organic Carbon (weight %) 43

4.12 Uranium concentrations (ppm) 46

4.13 Potassium (%) 47

4.14 Thorium concentration (ppm) 48

4.15 Locations for radiometrically dated Zuma Volcanics 53

5.1 Stratigraphic column with locations of radiometric and biostratigraphic samples 66

5.2 Possible pathway for Tarzana fan 68

5.3 West to east correlation from Malibu and the Point Dume-Paradise Cove section 71

5.4 Paleocurrent data from ripple cross-laminations 74

CHAPTER 1

INTRODUCTION

The Los Angeles Basin is a highly petroliferous region with a complex tectonic and depositional history. It is located on the Pacific plate, but within the broad transition zone with the North American plate termed the California Continental Borderland. Widespread extension and strike-slip movement along the California Margin during the mid-Miocene led to the creation of many sedimentary basins including the Los Angeles Basin (Biddle, 1991). Increasingly intense upwelling of nutrient-rich seawater along the north Pacific Rim and California margin occurred about the same time, driven by global changes in oceanic and atmospheric conditions (Ingle, 1981). These changes led to deposition and enhanced preservation of organic-rich, diatomaceous sediments in the various sedimentary basins formed during this time.

Within the Los Angeles Basin, oil is thought to be sourced in the Monterey Formation and its stratigraphic equivalents – parts of the Topanga, Modelo and Puente formations (Blake, 1991). Although part of the same regional unit, there are significant differences in the stratigraphy and sedimentology of the Monterey when compared to some of the better-studied outer basins of California like the Santa Barbara, Santa Maria and San Joaquin. The Los Angeles Basin is much more clastic-rich than more outboard basins (Pisciotto and Garrison, 1981) and contains a distinct suite of detrital minerals (Lanners, 2013). In spite of the different composition, portions of the Monterey (and equivalents) in the Los Angeles Basin are still quite organic-rich. The relationship between the highly petroliferous nature and the detrital content of the basin still remains to be understood completely. One of the challenges in understanding the relationship between trends in lithology between basins is the paucity of complete sections that

are well-exposed in outcrop. Most of the largely complete sections available in the region have been chiefly studied for biostratigraphic and paleoenvironmental purposes with little lithostratigraphic detail (e.g., Blake, 1991).

The Point Dume-Paradise Cove section is a relatively unstudied exposure that appears to be a nearly complete succession of a portion of the Monterey Formation. It is located in the part of the Los Angeles Basin that is interpreted to be the boundary between the rifting and rotating Western Transverse Ranges, also called the northwestern block / Santa Monica Mountain block, and the translating southwestern block / Inner Continental Borderland (Wright, 1991). Hoots (1930) describes a composite stratigraphic succession of the Modelo Formation in the eastern Santa Monica Mountains, some 10's of km from Point Dume. Yerkes and Campbell (1979) briefly describe the stratigraphic sequence in the area south of the Malibu Coast fault near Paradise Cove as being similar to that of the western Santa Monica Mountains but with important-enough differences to separate it stratigraphically. Understanding the geologic history of the Santa Monica-Los Angeles-Point Dume-Paradise Cove area will aid in understanding and further the interpretation of the subsurface data obtained from well logs.

CHAPTER 2

BACKGROUND

Tectonic History and Structural Setting

The southern Californian margin of North America has a tectonically complex history with dramatic transitions recorded by Miocene deposits in the Los Angeles basin. After approximately 30 Ma, the western plate boundary of North America began a transition from a long-lived convergent margin to a transform geometry by undergoing a complex sequence of faulting, rifting and block rotation (Atwater, 1989). The margin fragmented into a number of geologic provinces that experienced different structural and depositional histories. These provinces include the Peninsular Ranges, Transverse Ranges and the Continental Borderland (Nicholson et al., 1994). In the middle to late Miocene, initial rifting was followed by strike-slip movement along newly created faults and the more localized clock-wise rotation of the Transverse Ranges, ultimately placing them in their current east-west trending orientation (Kamerling and Luyendyk, 1979). At the juncture of these three provinces is the Los Angeles Basin (Wright, 1991) and the location of the Point Dume-Paradise Cove study area.

Of the many Neogene wrench-fault related basins created along the California margin (Blake, 1991), the Los Angeles basin is one of the most proximal to sources of coarse clastic sediments. It extends from the Ventura basin to the north to the Santa Ana Mountains and San Joaquin Hills to the south. The Los Angeles basin is subdivided into four fault-bounded blocks (Yerkes et al., 1965) that experienced different depositional histories and that developed distinct stratigraphic successions (Blake, 1991). The Point-Dume-Paradise Cove study location is located at the southern boundary of the Northwestern block which is bounded by the Santa

Monica-Raymond Hill-Cucamonga fault system to the east and the Anacapa-Dume fault system to the west (Blake, 1991).

The boundary between the rotating Transverse Ranges and the translating Inner Borderland blocks of the basin is not defined by a single fault trace but is rather a transition zone defined by several subparallel, named and unnamed faults or splays. The study location (Figure 2.1) is within such a transition zone; located between the east-west-trending Malibu Coast fault, and the offshore Anacapa-Dume fault. The Malibu Coast fault is related to the Santa Monica-Raymond Hill fault system that is the boundary between the Northwestern Block and the Southwestern/Central Block (Dolan et. al., 2000). The stark differences between the older Paleogene-Neogene sedimentary basement of the northwestern Los Angeles basin block and the schist basement of the southwestern Los Angeles basin block (Figure 2.2, Blake, 1991) also indicate that the Point Dume-Paradise Cove region is located at an important tectonic boundary.

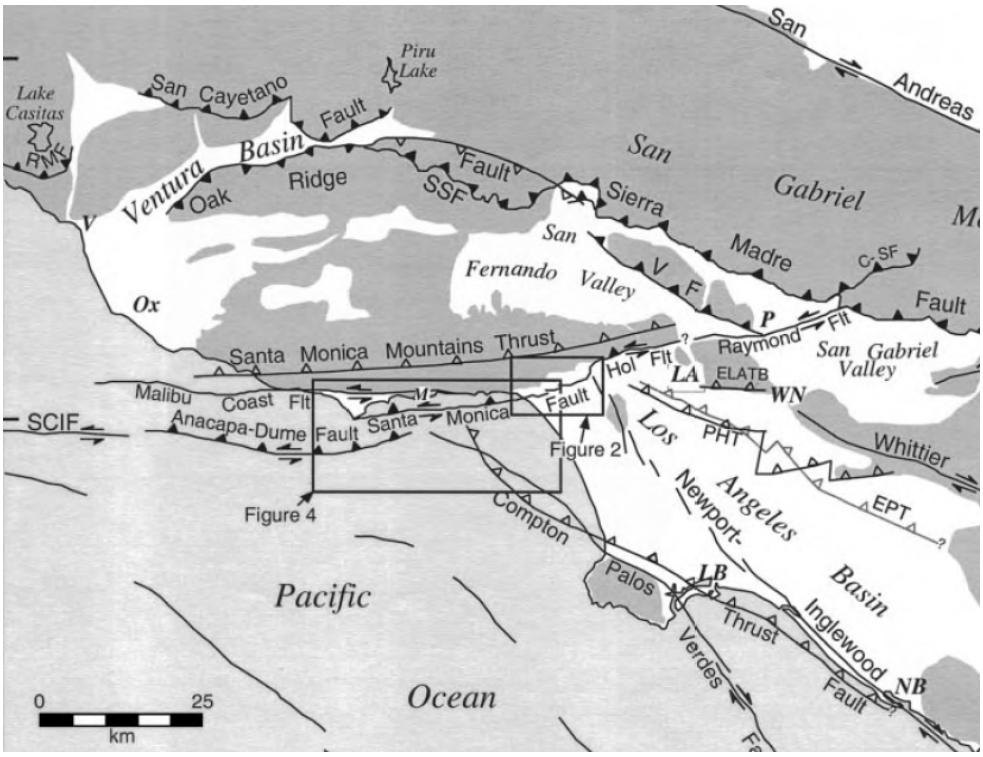

FIGURE 2.1. Paradise Cove area. Bounded by Anacapa-Dume fault to the south and Malibu Coast fault to the north (Dolan et. al., 2000).

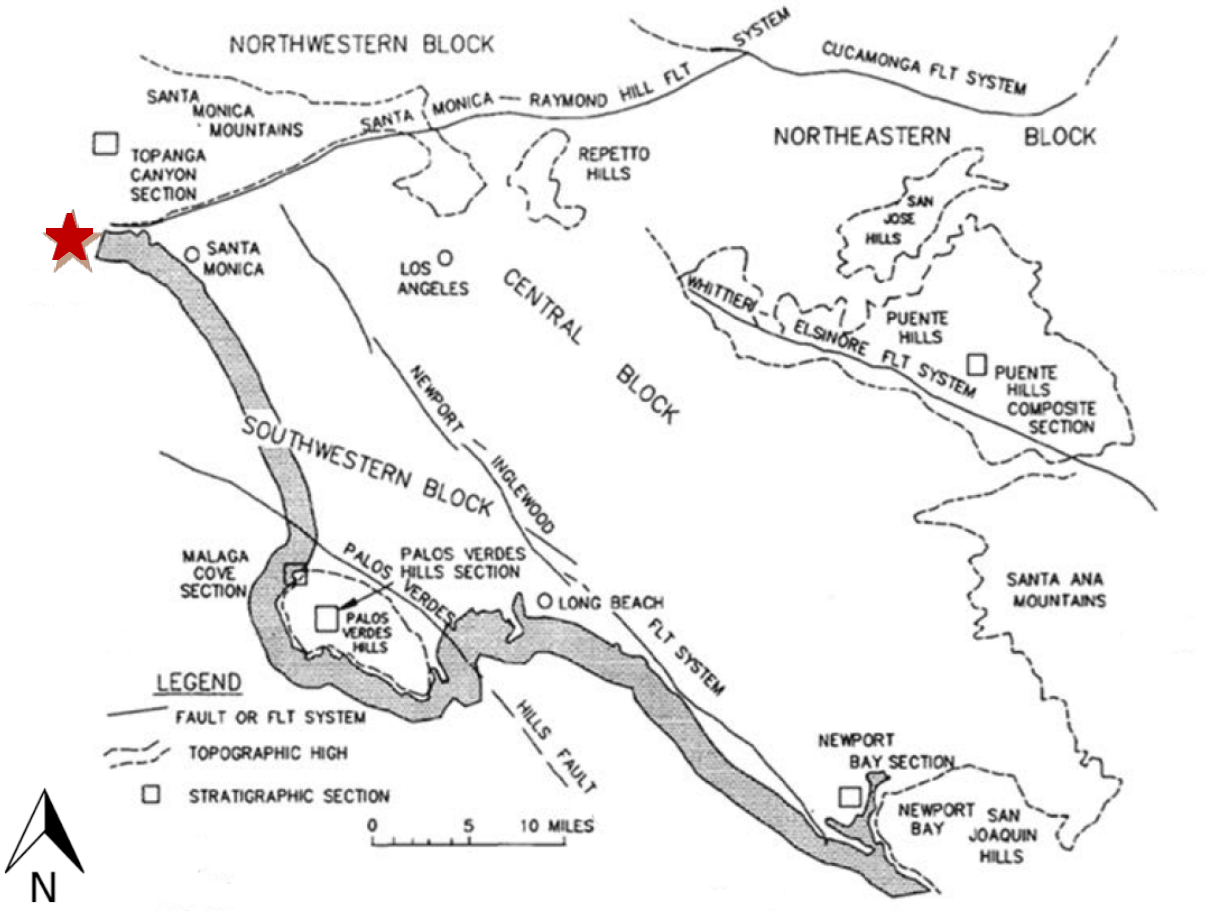

FIGURE 2.2. Map of Los Angeles basin blocks. Paradise Cove located west of Santa Monica modified from Blake (1991).

Stratigraphy

Los Angeles Basin

Within the southern California and Los Angeles basin region, the middle to upper Miocene deep-water deposits of the Monterey Formation have stratigraphic equivalents termed the Puente, Modelo and the upper Topanga formations (Figure 2.3, Blake, 1991). The Puente crops out in the Puente Hills and northern Santa Ana Mountains and is found throughout the subsurface of the Los Angeles basin. It is composed of lower, middle and upper members that overlie the Topanga Group. The subsurface Los Angeles basin can be divided into two terranes:

the La Habra section which overlies the Southern California Batholith and the San Pedro section which overlies Catalina Schist. At the southwestern part of the Los Angeles basin, the strata that crop out in the Palos Verdes Hills include a section of the Monterey Formation that overlies the Catalina Schist. Similarly, the Point Dume-Paradise Cove section also overlies the Catalina Schist (Yerkes and Campbell, 1979) with that being one factor that distinguishes the succession from that in the adjacent Santa Monica Mountains.

Northwestern Los Angeles Basin and the Point Dume-Paradise Cove Study Area

The stratigraphy of the northwestern block (i.e., Santa Monica Mountain block) of the Los Angeles basin in Blake (1991) progresses from the Jurassic Santa Monica Slate to the Pleistocene Fernando Formation. Within this section are the Miocene Topanga Group and Modelo Formation. The Santa Monica fault (and its westward extension, the Malibu Coast fault) marks the boundary between the northwestern block and the central and southwestern blocks of the Los Angeles basin and is the intersection between markedly different geologic terrains (Yerkes and Campbell, 1979). To the north are the sediments described in Blake's compilation of stratigraphic information for the Santa Monica Mountains; to the south are the Miocene exposures in the Point Dume-Paradise Cove area that are the focus of this study. South of the Malibu Coast fault, the basement rock is the Catalina Schist that is overlain by the Miocene Trancas Formation, Zuma Volcanics and the Monterey Shale (Figure 2.4, Yerkes and Campbell, 1979).

The Zuma Volcanics intrude and are interfingered with the Trancas Formation that is composed of schist-bearing, marine sedimentary rocks, and that, in turn, interfingers with the Monterey. In this area, the Monterey Formation is a deep-water deposit of Luisian and Mohnian age (Wright, 1991).

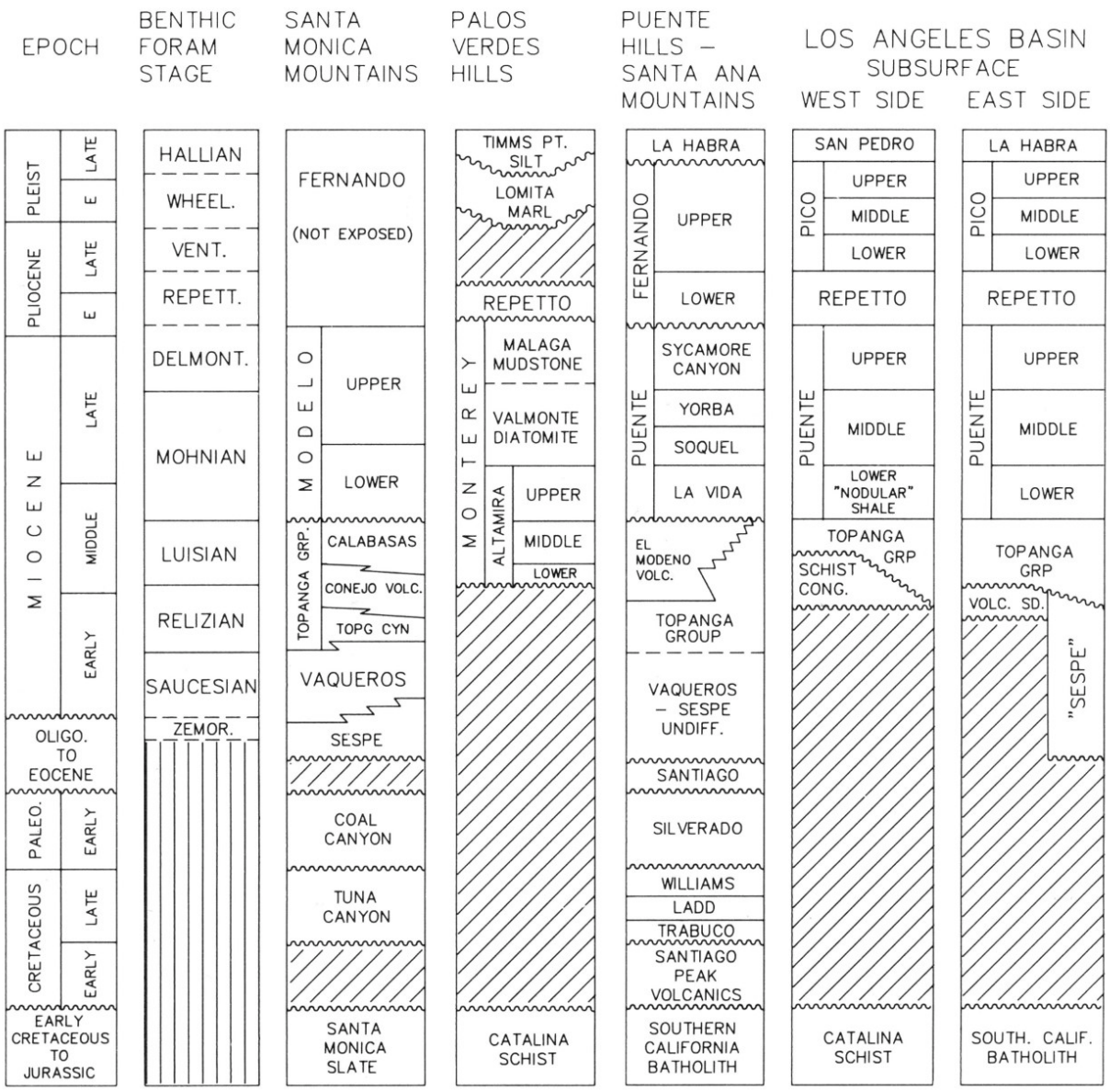

FIGURE 2.3. Stratigraphy of the Los Angeles basin. Modified from Blake (1991).

The Zuma Volcanics are radiometrically dated at 15.0 +/- 1.0 Ma (Berry et al., 1976, updated by Stanley et al., 2000) and are considered related to the Conejo Volcanics that crop out to the north of the Malibu Coast fault. While the Trancas Formation is age-equivalent to the Topanga group described to the north of the Malibu Coast fault, presence of glaucophane schist fragments only south of the fault suggest that the Point Dume-

Paradise Cove area is either a transitional zone, or part of the southern block entirely (Yerkes and Campbell, 1979).

Well log data, collected from the exploratory well Sovereign Oil Co. Malibu 1, confirmed the sequence of rocks as being the Monterey Shale (spud location), the Trancas Formation and the Zuma Volcanics. The base of the well encountered either the Catalina Schist or the San Onofre Breccia (Yerkes and Campbell, 1979).

Palos Verdes Hills

Located in the southwestern tip of the Los Angeles basin, the Palos Verdes Hills are one of the best-studied exposures of the Monterey Formation in the basin (Figure 2.2; Blake, 1991). Palos Verdes is located ~35 km southeast of the Point Dume-Paradise Cove section, although tectonic reconstructions suggest that both settings have shifted many tens of kilometers since initial deposition. The Monterey in the Palos Verdes Hills is part of a sedimentary and volcanic sequence (Woodring et al., 1946; Conrad, 1983; Conrad and Ehlig, 1987) of rocks that rests unconformably on the Catalina Schist deposited coincidently with the upper Topanga, Modelo, Puente and San Onofre Breccia (Behl and Morita, 2007) during the Relizian, Luisian and Mohnian stages. This is similar to the stages assigned to the unit of the Monterey Shale in the Point Dume-Paradise Cove area. Therefore, Palos Verdes offers an excellent reference section for comparison of lithofacies and depositional environment with the Point Dume-Paradise Cove section.

Depositional Environment and Sediment Distribution Patterns

Remarkably little published work has been done on the fine-grained depositional environments of the Miocene Los Angeles basin, with sediment distribution patterns and provenance mapped only for the sandstone facies. Such reconstructions are made difficult by the tectonically

complex history of the basin and the separate movement of fault blocks over time.

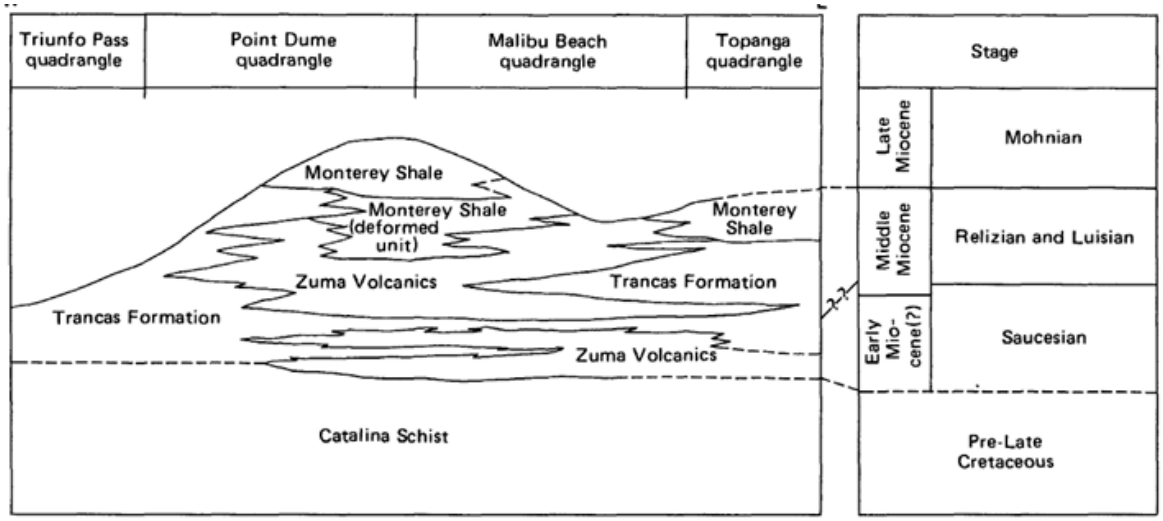

FIGURE 2.4. Stratigraphic distribution of rocks south of the Malibu Coast Fault (Yerkes and Campbell, 1979).

However, key studies have been completed by Wright (1991), Redin (1991) and Rummelhart and Ingersoll (1997) but with respect to source and depositional environment, the questions have been left somewhat unanswered by previous works. Redin (1991) (Figure 2.5) does not identify a source terrane for the Topanga Formation but suggests that the sediment source was north and/or east of the Los Angeles basin. Rummelhart and Ingersoll (1997) examined sandstone composition and provenance of the Tarzana, Puente and Simi fans and established the sediment source from the San Gabriel block. This confirmed the difference between the nearby Ventura basin and the Los Angeles basin in terms of sediment distribution pathways and depositional environment.

The Point Dume-Paradise Cove area is located near the border between the Ventura and Los Angeles basins and the origins of its sediments are one of the key questions this study proposes to answer. The source of the Miocene Trancas Formation located in the Point Dume- Paradise Cove area is not addressed specifically in any of the models by Wright

(1991), Redin (1991) and Rummelhart and Ingersoll (1997). Differences between Palos Verdes Hills and Paradise Cove sections might be related to their relative positions during deposition where the former was possibly a bathymetric high and the latter a slope on its northwestern flank.

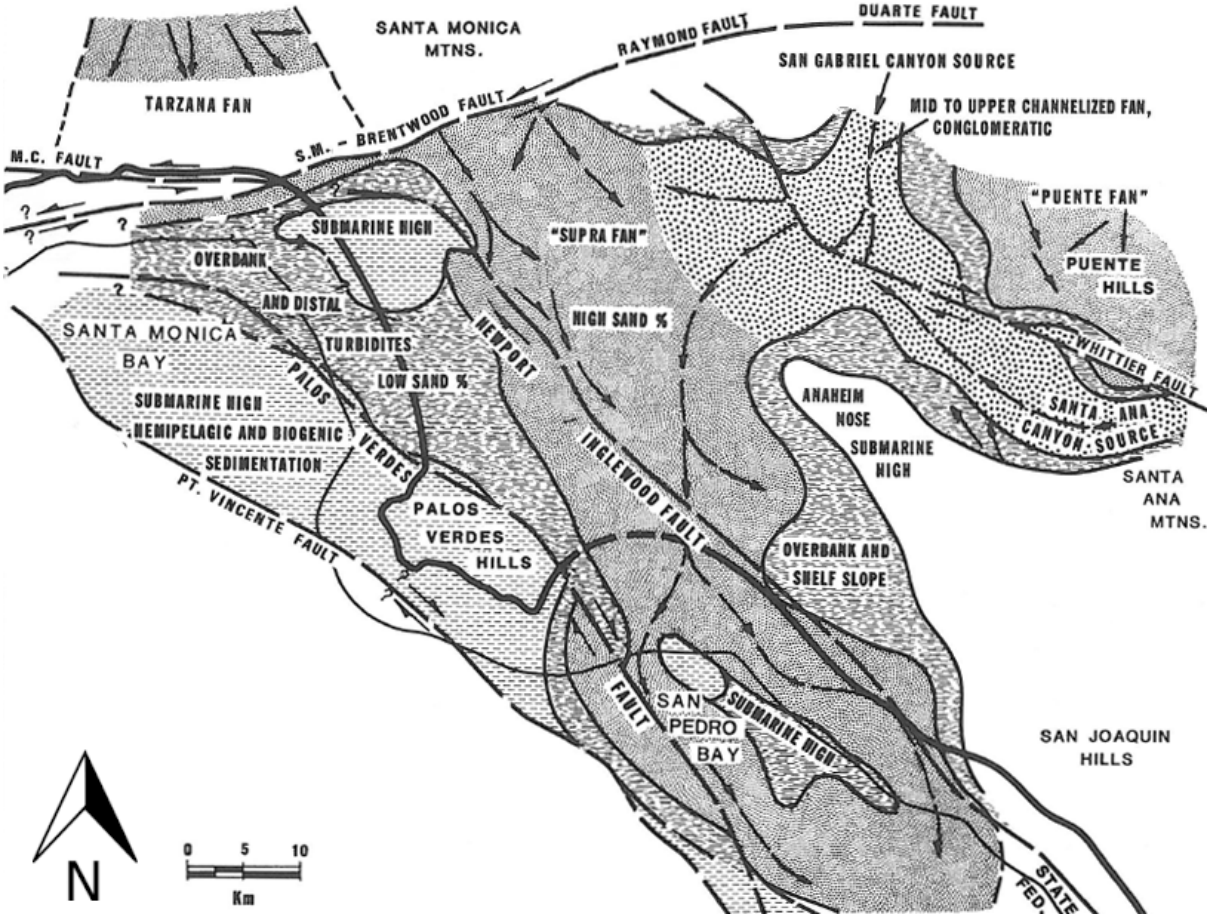

FIGURE 2.5. Upper Mohnian submarine-fan facies map. Present-day Los Angeles basin modified from Redin (1991).

Wright's (1991) reconstruction of the Los Angeles region during the Middle Miocene (Figure 2.6) suggests that source material for the area exposed in present day Paradise Cove might have come from the uplifted area of Palos Verdes. Analysis of sandstone composition of the Paradise Cove-Point Dume area in comparison with the lithology of the Palos Verdes area

could shed some light on the sediment transport direction for the study area. Alternately (not shown on figure), the sediment may have been derived from the Tarzana fan to the north and routed southwestward in a structural trough between the moving southwestern and northwestern blocks of the LA Basin as suggested by Redin (1991).

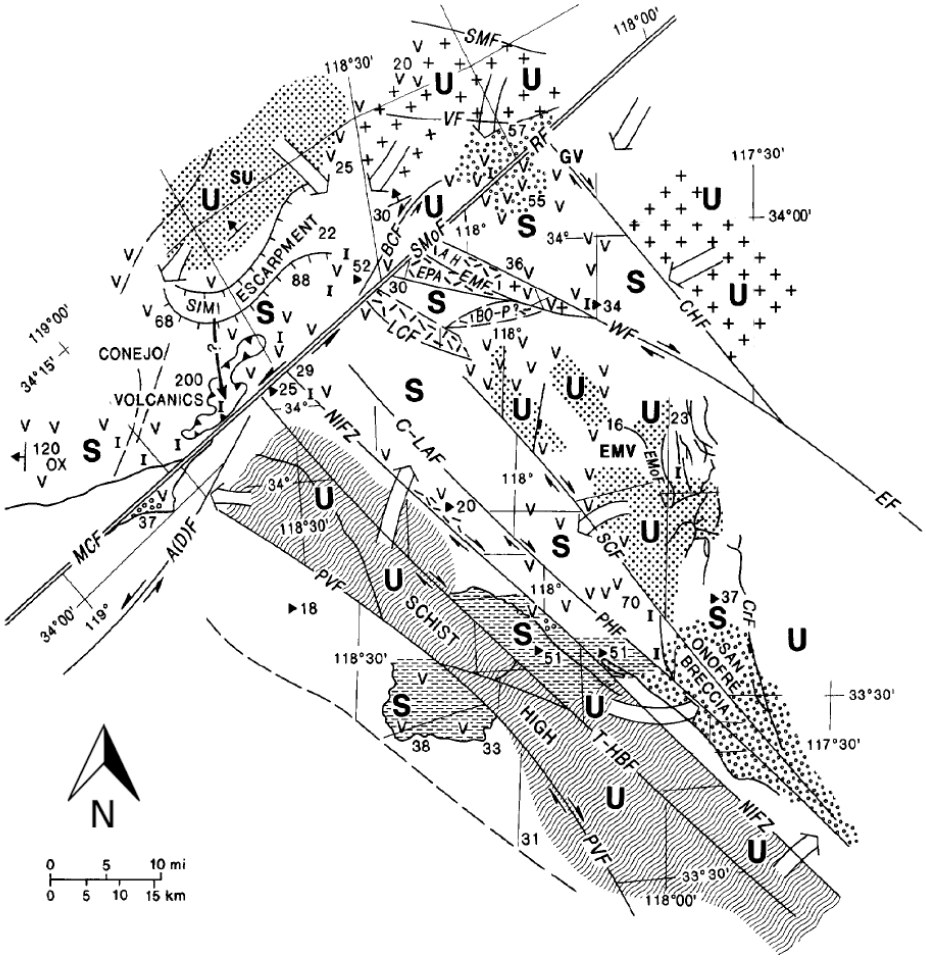

FIGURE 2.6. Reconstruction of the Los Angeles region during Middle Miocene (ca. 14 Ma) Showing possible direction of sediment transport to Paradise Cove area. From the east off uplifted area near Palos Verdes; modified from Wright (1991).

CHAPTER 3

METHODOLOGY

Fourteen high-resolution, oblique aerial photographs of the coastline between Point Dume and Paradise Cove, Malibu Beach, from the California Coastal Records Project (Copyright © 2002-2015 Kenneth & Gabrielle Adelman, California Coastal Records Project, www.californiacoastline.org) were studied to identify large structural features and major sedimentary units and to document locations of rock samples during fieldwork. The base of the section was established at the first continuous exposure of sedimentary rocks of the Monterey Formation stratigraphically above a short covered section abutting the Zuma Volcanics at Point Dume.

Geologic maps (Dibblee and Ehrenspeck, 1993; Yerkes and Campbell, 1980) were used for initial interpretations of structural and sedimentary geology. Bedding orientation was measured through the section with a Brunton compass. The section was measured using a Jacob's Staff oriented perpendicular to local average stratigraphic strike and dip. The stratigraphic interval measured, including covered or inaccessible sections, is approximately 752 meters. This is an approximation due to the inability to continuously measure covered, inaccessible and faulted sections of the succession.

The majority of the field visits and data collection occurred in the winter months, December and January 2014-2015. A few storms provided ephemeral, sand-scrubbed beach platforms, but on the whole, bed-to-bed lithology was described in the lightly to moderately weathered outcrops in the sea cliffs. Identification of rock types can be difficult in these fine-grained, easily weathered rocks, so an iterative training process was employed. Lithology was first identified by macroscopic and microscopic field appearance, including color, texture,

fracture style and carbonate composition determined by application of dilute hydrochloric acid. Field determinations were then confirmed or modified after X-ray diffraction analysis at CSULB. These preliminary analyses improved the accuracy of lithologic identification in subsequent field visits. Estimates of stratigraphic percent rock type and descriptions of the rock characteristics were made over 1-meter increments. XY scatter charts were made using Microsoft Excel to display the percent sandstone versus position in section per one-meter interval. The percent rock types and field descriptions were used to categorize the section into four primary lithostratigraphic members and a stratigraphic column with a weathering profile was generated starting from the base of the section at 0 meters to the top of the section at 752 meters.

A spectral gamma-ray log of the section was recorded using a portable handheld spectrometer (BGO SuperSpec RS 230 scintillometer) that measured potassium (%), and uranium and thorium at the parts per million levels. Measurements were taken for 180 seconds (3 minutes) each every 1m through accessible portions of the stratigraphic succession. Total gamma ray (API) was derived from the potassium, uranium and thorium data using the formula: total gamma = [8×uranium (ppm) + 4×thorium (ppm) + 16×potassium (%)] (Ellis, 1987). XY scatter charts were made of the spectral gamma ray data and the total gamma ray data per 1-meter interval for the height in the stratigraphic column. Cross-plots of the thorium and potassium from the spectral gamma ray measurements were made and were used to determine what clay species are present in the different lithologic members according to the relationships described in Schlumberger's Log Interpretation Charts (2009).

Attitude measurements of bedding (5), cross-lamination (17) data were collected using a Brunton compass and plotted in Stereonet 9 (Allmendinger et. al., 2013) to construct a rose-

diagram and determine paleocurrent directions (see Appendix B).

Roughly 100 samples were collected over the entire section, assigned an initial field description and then used for a laboratory analysis. Twenty-nine mudstones and organic-rich rocks were analyzed for weight percent total carbon (TC), inorganic carbon (IC) and total organic carbon (TOC) (lab work performed by Antonio Sandoval, Spring 2015). Ground samples were analyzed in a UIC CO_2 Coulometer where the samples were combusted in the furnace at 950º and dissolved in 5 ml of 10% perchloric acid in order to obtain the Total Carbon (TC wt %) and Inorganic Carbon (IC wt %). From these values, Total Inorganic Carbon (TOC wt %) and Total Carbonate ($CaCO_3$ wt %) were calculated by the following equations:

$$TOC = TC - IC$$

$$CaCO_3 = IC * 8.33$$

Six diatomaceous samples were analyzed by Diane Winter of Algal Analysis, Missoula, Montana, for diatom species and their abundances. Last and first appearances and ages were determined and zones were assigned. Using the data zone assignments from Diane Winter, the ages of the diatom zones was determined following Barron and Isaacs (2001). Benthic foraminiferal stages for the outcrops were obtained from assignments archived in the USGS/Chevron dataset (Brabb and Parker, 2003).

Seventeen thin-sections of sandstone samples were made by National Petrographic of Houston, Texas. Samples were stained for potassium feldspar and were analyzed using a polarizing microscope for mineral and rock fragment identification and sandstone classification. The abundance of grains were semiquantitatively classified as: trace (1 to few grains), minor (<10%), common (10-25%) and abundant (main component > 25%). The categories identified were volcanic rock fragments (VRF), mafic rock

fragments (MRF), sedimentary rock fragments (SRF), polycrystalline quartz, monocrystalline quartz, potassium feldspar and plagioclase, glaucophane, kerogen and bioclasts (sponge spicules, radiolarian, diatoms).

Ninety four samples (17 of which were sandstone) were analyzed by X-ray diffractometer (XRD) to determine silica phase and mineral composition. The samples were scanned from 5° to 45° 2θ at 0.02° steps for 1 second/step using a Rigaku MiniFlex X-ray diffractometer, operated at 30 kV and 15 mA with X-rays generated from a copper anode target

CHAPTER 4

RESULTS

The exposed succession of the Monterey Formation in the Point Dume to Paradise Cove area has been subdivided into four lithostratigraphic units using a variety of qualitative and quantitative methods. Meter-by-meter field descriptions, sandstone analysis and thin-section petrographic analysis, TOC (total organic carbon), spectral gamma-ray data, XRD (x-ray diffraction), and biostratigraphic analysis were used to define and characterize the different members. The members, in ascending order, are the Dolomitic Phosphatic Shale, Porcelanite and Shale, Mixed Clastics, and Cherty Diatomite. A simplified stratigraphic section was generated (Figure 4.1), and a detailed description of the members is discussed in this chapter.

The meter by meter descriptions of the lithologic units is determined by choosing a dominant rock type for each meter, based on the most abundant lithology present in these generally thinly interbedded rocks (Appendix A). Rocks are described and portrayed in figures chiefly as they appear in the lightly weathered cliff exposures (Figure 4.2) rather than the sand-blasted and fresh, but unpredictably exposed intertidal zone.

Lithostratigraphic Succession

Dolomitic-Phosphatic Shale Member

The Dolomitic-Phosphatic Shale member is approximately 87 meters thick. The base of the member is in contact with the Zuma Volcanics, dated at 15.0 ± 1.0 Ma (Berry et al., 1976; corrected by Stanley et al., 2000). This contact is abrupt and it is possible that it is a fault, rather than a depositional contact. This member is composed of medium to thick beds (.5 - 1 m), nodules and stratiform horizons of dolostone interbedded with very thick beds (1-3 m) of organic-rich and phosphatic mudstone that are locally cherty-porcelaneous (Figure 4.3A and

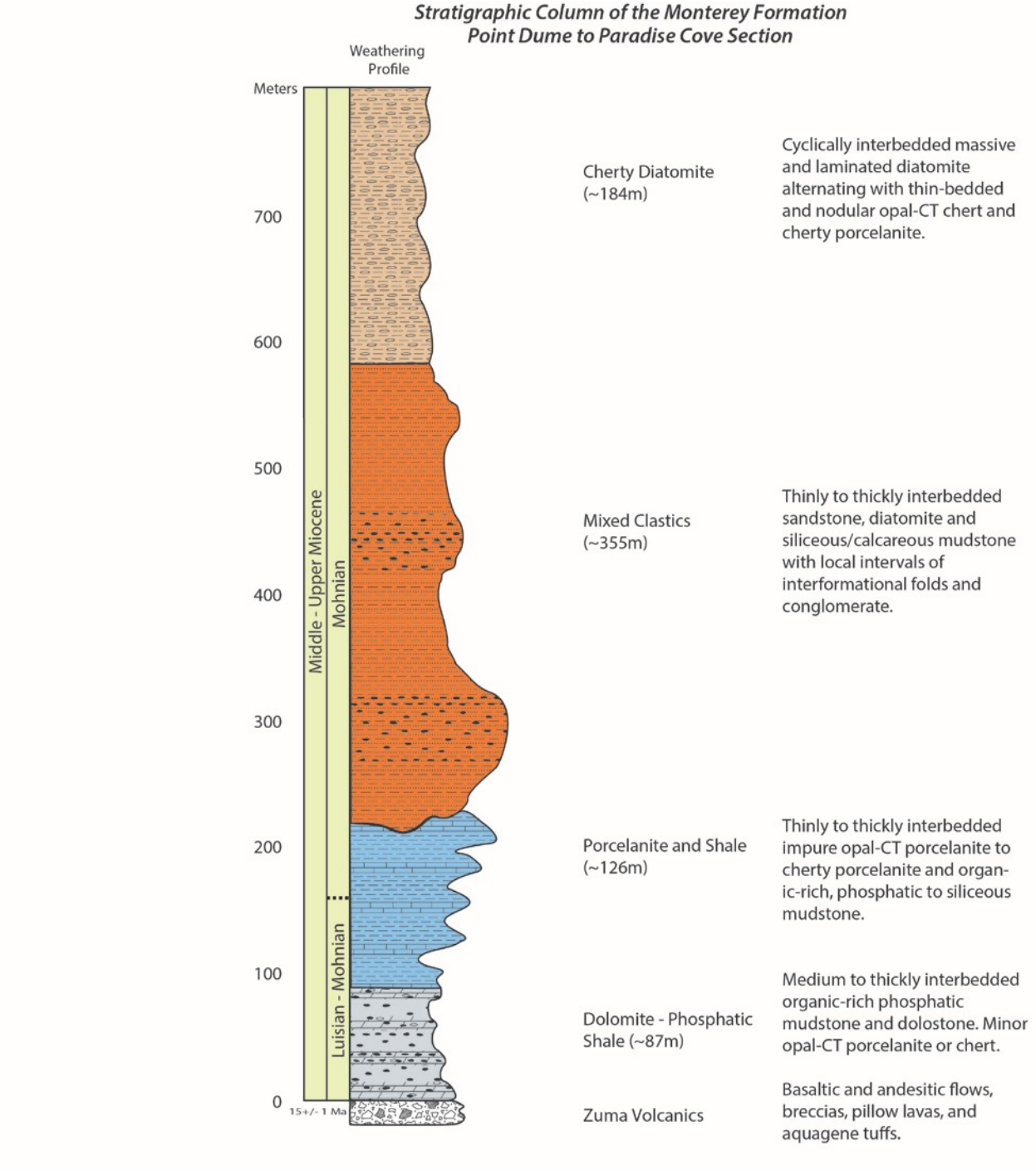

FIGURE 4.1. Stratigraphic column for Point Dume Paradise Cove section. Four lithostratigraphic members have been defined.

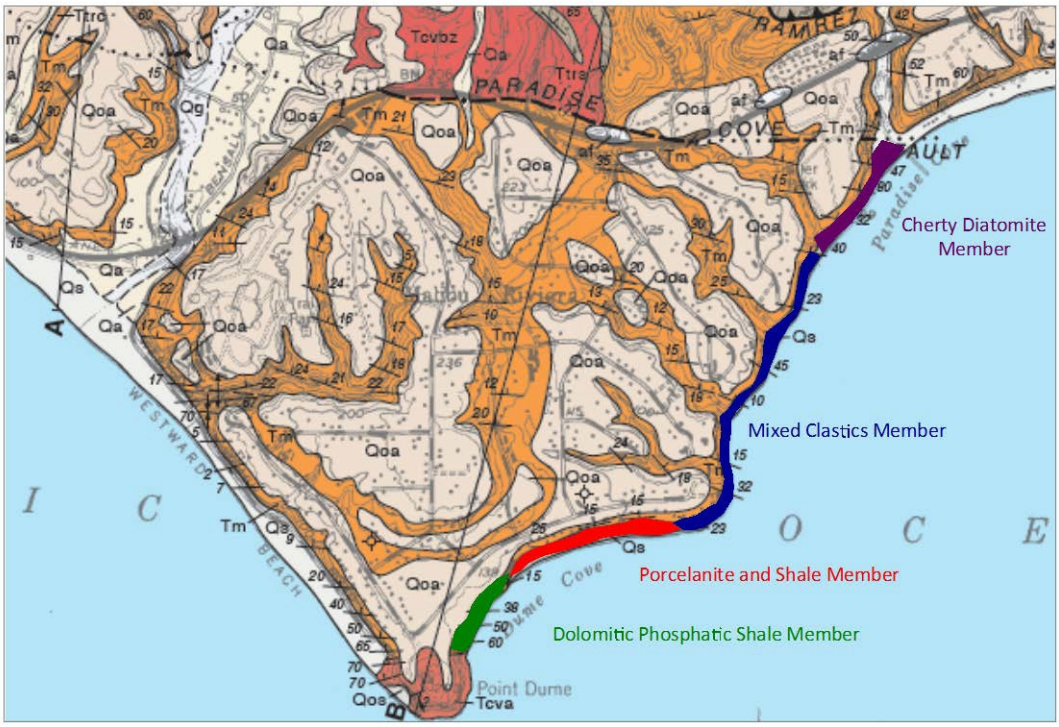

FIGURE 4.2. Extent of the four members of the stratigraphic column. Reflecting the Monterey Formation along the coastal cliffs between Point Dume and Paradise Cove. Displayed on geologic map modified from Dibblee and Ehrenspeck (1993).

Figure 4.3B). The mudstone is thinly to thickly interlaminated with light-colored phosphate (Figure 4.3C).The mudstone exposed on the weathered beach cliffs is light brown whereas the sandblasted beach platform exposures are black. The contacts between dolostone and mudstone beds are generally sharp. Some laminations are inversely graded in phosphate concentration. The phosphate content in the mudstone decreases upward in the member and fewer and thinner pale-grey laminations are present within the upper mudstone. Appendix A presents the meter-by-meter description of lithologic units and the member boundaries.

A portion of these organic-rich mudstones that were folded or faulted out of sequence into the overlying member have been altered by natural combustion. The exothermic oxidation of pyrite and marcasite is thought to trigger *in situ* pyrolysis of the organic-rich mudrocks (Mariner et al., 2008; Boles et al., 2010). These are located in the up-thrown, hanging wall side of a fault in the middle of the Porcelanite and Shale member and the underlying, now repeated mudstone and porcelanite beds of the Dolomitic Shale member have been naturally burnt to form a locally black (Figure 4.3D) or pink (Figure 4.3E) clinker texture.

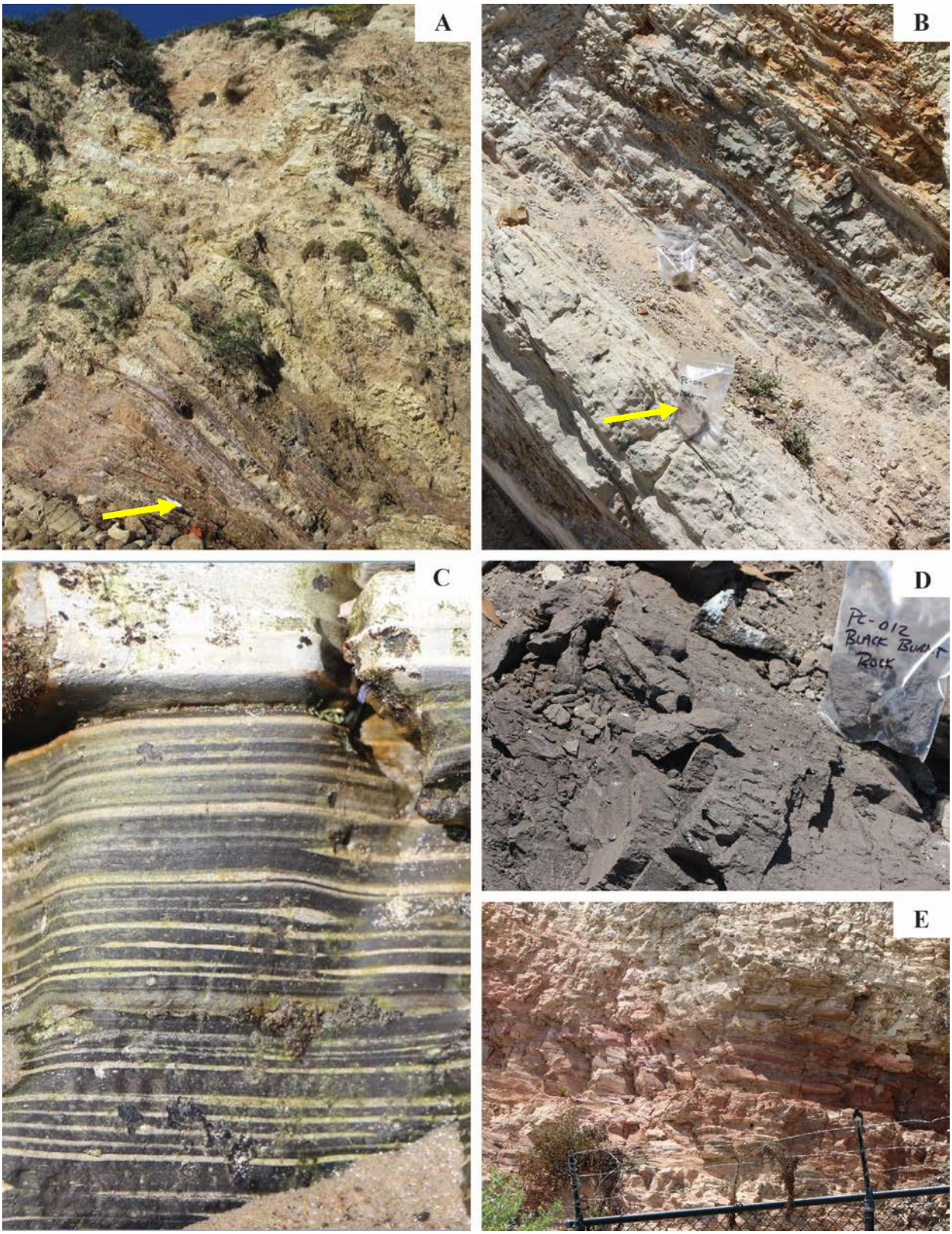
A
B
C
D
E
PC-012
BLACK BURNT
ROCK

FIGURE 4.3. Sedimentologic and stratigraphic features of the Dolomitic Phosphatic Shale member. (A) Medium to thick beds (.5 - 1 m) of dolostone and thick to massive (1 - 2 m) beds of mudstone. White notebook (yellow arrow) for scale. Vertical view ~10 m. (B) Weathered cliff exposure of dolostone bed in lower third and more recessed layer of siliceous-porcelaneous mudstone overlain by porcelanite. Scale: plastic ziplock bag 14.5 cm long (yellow arrow). (C) Fresh exposure in surf zone. White portion at the top is a siliceous (porcelanite) or calcareous mudstone. The lower organic-rich mudstone is dark grey to black with abundant light grey phosphatic laminations and lenses visible on its freshly abraded surface. Vertical view: ~15 cm. (D) Black/dark gray burnt mudrock that was likely organic-rich prior to combustion and is part of the faulted, repeated section of this member. (E) Red/pink areas of burnt porcelanite and mudstone are part of the faulted, repeated section of the underlying Dolomitic-Phosphatic Shale member faulted into the Porcelanite and Shale member.

Porcelanite and Shale Member

The Porcelanite and Shale member is approximately 126 meters thick. The contact with the Dolomitic Phosphatic Shale is gradational and determined by the transition between sections that are dominated by fissile mudstone and muddy porcelanites below and those that contain more siliceous lithologies, i.e., porcelanite and chert, above. This member contains beds of highly siliceous mudrock, opal-CT porcelanite and dolostone that have different fracture patterns due to their different lithologies and bed thickness. The abundant, thick dolostone beds that are a regular occurrence in the underlying Dolomitic Phosphatic Shale member are nearly absent. Structural deformation complicates the stratigraphic relationships between the underlying Dolomitic-Phosphatic member and the Porcelanite and Shale Member. A notable reverse fault with associated complex folding appears to have inserted an interval of pink to burnt black shale (described below), likely associated with the underlying member, into this section in the deformed hanging wall.

The section could not be continuously measured or described due to the deformation (Figure 4.5B) plus four intervals were covered by thick scree and vegetation (Figure 4.5C). The reverse fault and folds that span the entire cliff exposure divide the member into two stratigraphic intervals. The lower (southern) section (Figure 4.5B), contains cherty porcelanite (opal-CT) whereas the upper section, north of the disrupted zone, is less cherty, and consists largely of porcelaneous to clayey mudstone.

This member is chiefly composed of thinly (>1 cm to 10 cm) interbedded impure to cherty porcelanite interbedded at a large scale with organic-rich, phosphatic to siliceous mudstone (Figure 4.4A and Figure 4.4B) and occasional dolostone. The cleaner/purer porcelanite is light yellow-orange on the weathered surface and brown on a freshly exposed surface. Muddy porcelanite is brown and lacks the characteristic blocky fracture and matte

texture that a more pure porcelanite has on a freshly exposed surface. Short intervals are cherty (Figure 4.4C) with beds showing straight blocky fractures and joints whose close spacing is controlled by bed thickness and rock type (Figure 4.4D and Figure 4.4E).

Vein structures or “intrastratal microfaulted zones” (IMZ) occur within some of the most siliceous beds in the upper portion of this member. Veins are filled with fine-grained sediment (Figure 4.5A).

Dolostone beds are rare in this member. However, at approximately meter 130, a dolostone and porcelanite bed forms a distinct marker horizon and is folded nearly vertically (Figure 4.5B) near where the underlying Dolomitic-Phosphatic member is folded and faulted up into the stretch of cliff where the Porcelanite-Shale member is otherwise exposed. Stratigraphically above this zone, the porcelanite becomes muddier and the section is relatively unfolded permitting continuous meter-by-meter measurement and description. The overlying boundary between the Porcelanite-Shale and the Mixed Clastics member is close to several normal faults that disrupt beds of muddy porcelanite and underlie the lowermost thick sandstone bed.

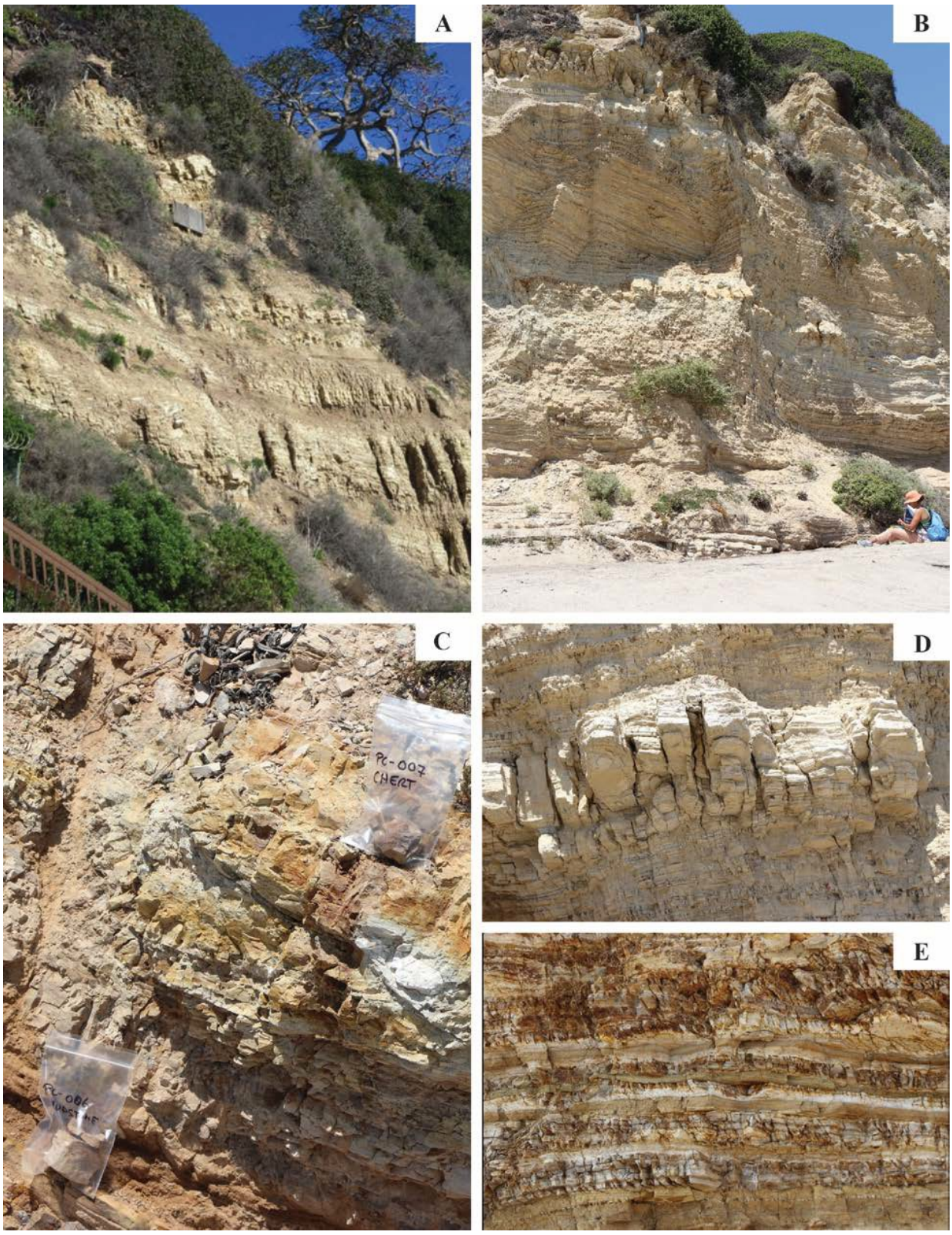
A
B
C
PC-007
CHERT
D
E

FIGURE 4.4. Sedimentologic and stratigraphic features of the Porcelanite and Shale member (A) Brown recessed beds of mudstone interbedded with ~meter-thick packages of thin-bedded, fractured porcelanite. (B) Thinly interbedded porcelanite and siliceous mudstones. (C) Upward transition from recessed brown mudstone to muddy porcelanite to blocky fractured yellow and light brown chert to cherty porcelanite beds. Scale: ziplock bag 14.5 centimeters long. (D) Thin- bedded porcelanite and mudstone with one medium thick, fractured dolostone bed. Scale: prominent dolostone bed at the center of the photograph is approximately 40 cm thick. (E) Bedding-confined joints occur primarily in porcelanite (white with orange stain), not in the interbedded mudstone (light tan). Scale: bedding <10 cm thick.

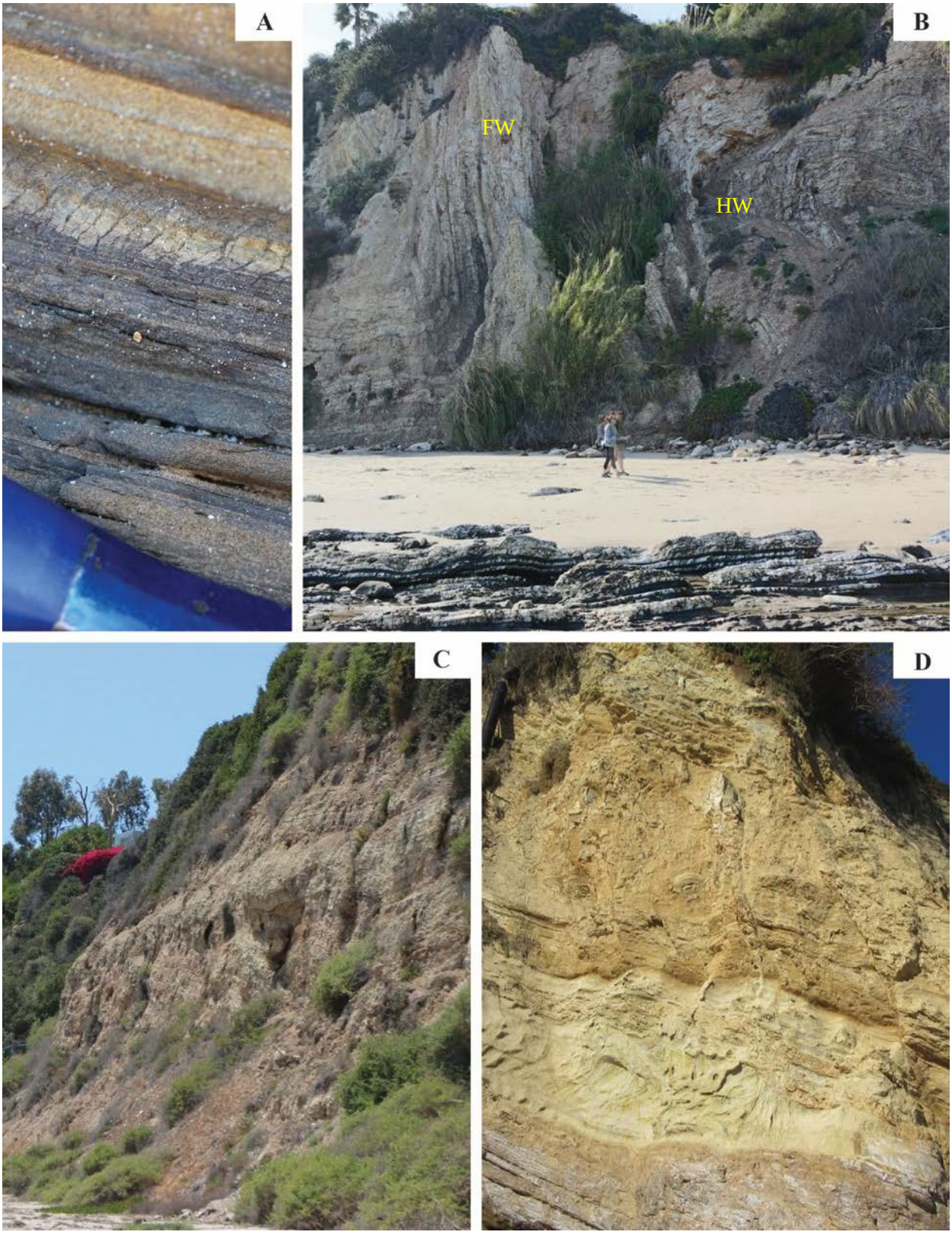
A
B
FW
HW
C
D

FIGURE 4.5. Sedimentologic and stratigraphic features of the Porcelanite and Shale member. Intrastratal microfaulted zones (IMZ) within light siliceous mudstone bounded by sandstones above and a darker, sandy mudstone below. Scale: portion of a geologic hammer ~2 cm wide. Vertically upturned light-colored dolostone and porcelanite beds in the foot wall (left and foreground) and down-folded mudstone beds in the hanging wall (right) separated by thick vegetation likely concealing a reverse fault trace. (C) Discontinuous direct exposure and access to outcrop due to covering vegetation or talus. (D) Boundary between the Porcelanite and Shale and overlying Mixed Clastic member at the lowermost thick sandstone shown in the center of the photograph. The mudstone bedding is planar whereas the ~1-m-thick sandstone bed has wavy, undulated lower contact in this area and deformed internal structure.

Mixed Clastics Member

The Mixed Clastics member is defined on the basis of significant occurrence of sandstone in the interval, along with other rock types present in underlying or overlying members (Figure 4.6A). The 355-meter-thick unit is the thickest member of the succession. It contains thin to very thick (1 cm – 3m) layers of interbedded sandstone, diatomite, siliceous and calcareous mudstone with some conglomeratic zones. The difference between the Porcelanite and Shale member and the Mixed Clastics member is not only the abundance of sand and conglomerate and the absence of porcelanite in the latter; but that its base marks the diagenetic boundary between opal-A diatomaceous sediments above and opal-CT phase sediments below. Additionally, the abundance of diatomite generally increases from the lower portion of the unit to the top of the member.

The base of the section is marked by an increase in sandstone and conglomerate, including thin lenticular or pinch-and-swell sandstone beds, thick coarse-grained massive to graded or laminated sandstone beds, highly deformed beds of intra- and extra formational conglomerates and breccias, plus intervening mudstone, diatomite and diatomaceous mudstone, and dolostone (Figure 4.6B and Figure 4.6C). The sedimentary structures suggest many episodes of high-energy transport and rapid deposition by downslope gravity flows in a slope setting.

The Mixed Clastics member can be subdivided into 3 sub-members. The lower sub-member contains about 173 meters of sandy mudstone, thin and lenticular sandstone, and medium to thick-bedded dolostone, conglomerate and breccia with thin-bedded siliceous mudstone and minor amounts of porcelanite. The approximately 102 meter-thick middle sub-member include siliceous and calcareous mudstone, sandstone, siltstone and diatomite. There are some intervals within this sub-member that are covered and inaccessible for measuring.


A
B
C
Canon
D

FIGURE 4.6. Sedimentologic and stratigraphic features of the Mixed Clastic member. (A) Thick to very thick sandstone beds with calcite cemented, spherical concretions with thinner beds of brown calcareous and siliceous mudstone and diatomite. (B) Well-stratified, thin-bedded mudstone with a sharp bedding-parallel contact with overlying conglomerate. The conglomerate is poorly sorted and contains intraformational mudstone clasts. Notebook is approximately 20 cm long. (C) Close up of the conglomerate showing clasts of sandstone, mudstone and various granitic and metamorphic rocks. (D) Interbedded sandstone, siliceous-calcareous mudstone and diatomite. For scale: a kayak 2 meters long at the base of the cliffs.

Sandstone beds that range from centimeter to meter thick are interbedded with sandy mudstones and diatomite on the meter to decimeter scale (Figure 4.6D).

The upper sub-member, approximately 80 meters thick, is composed primarily of calcareous mudstone and sandstone, sandstone with large concretions and dolostone beds that form prominent ledges exposed on the beach during low tide and especially after a sand-removing storm event (Figure 4.7A). Both the dolomitized sandstone beds and the prominent ledge forming dolostone are ~1-meter thick. Thinly bedded to laminated mudstone also form stratigraphic packages that are approximately meter-thick.

The lower sub-member contains evidence that the sediments were deposited in a high energy, mass-transport-dominated, steep slope environment. Folded and contorted beds of mudstone and sandstone with mud rip-up clasts are common (Figure 4.7B and Figure 4.7C). Scoured surfaces and flame structures (Figure 4.7D) occur between sandstone and mudrocks. Some sandstone beds also contain low-angle trough, planar and wavy cross-lamination (Figure 4.8B). Large mass-transport deposits in this member include a 5-8 meter thick, tabular olistostrome (Figure 4.7E) containing intraformational boulder- to cobble-size slabs of mudstone, that is bounded above and below by continuous planar beds. A meter-thick conglomerate (Figure 4.8A) containing extraformational clasts (e.g., blueschist) is another type of mass- transport deposit present in this part of the Mixed Clastics member.

Within this member, diatomite is interbedded with sandstone and mudstone in a variety of bed thickness, bedsets and lithofacies combinations. These range from thick (.5 m to 1 m) beds of interbedded diatomite and massive sandstones to thinly interbedded associations (Figure 4.8B).

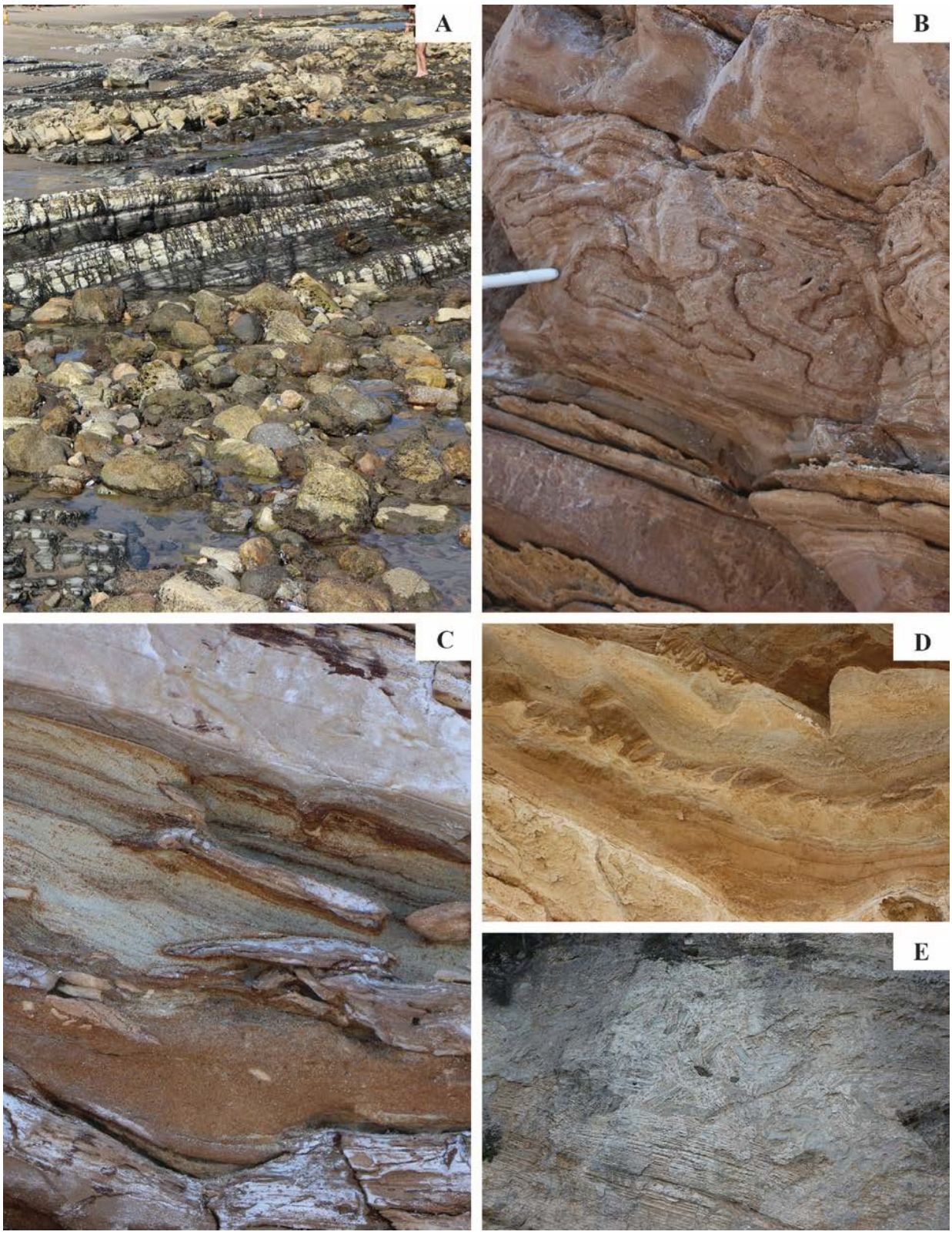
A
B
C
D
E

FIGURE 4.7. Sedimentologic and stratigraphic features of the Mixed Clastic member. (A) Prominent beds of pale yellow dolostone (30-50 cm thick) and dark grey siliceous mudstone interbedded with light grey calcareous mudstone. (B) Highly folded, sandy mudstone bed with tabular massive to laminated beds of sandstone above and below. (C) Cross-bedded sandstone bed with mudstone rip-up clasts and scoured basal surface. White surface reflects salt precipitated on weathered surface of the mudstone. Vertical scale 20-30 cm. (D) Flame structures formed at base of sandstone bed (orange) from underlying laminated diatomite.(E) Olistostrome near the base of the Mixed Clastics member indicating high-energy mass transport in a slope setting. Vertical field of view 8-10 meters.

A particularly common and distinctive lithofacies consists of a three-part series of thinly interbedded (decimeter to centimeter) medium to coarse grained sandstone, massive mudstone containing white specks of diatomite, interbedded with finely laminated muddy to pure diatomite (Figure 4.8C and Figure 4.8D). Contacts between the lithologies vary from sharp to disrupted with flame structures, detached and ripped-up clasts (Figure 4.8E).

Cherty Diatomite Member

The Cherty Diatomite member is 184 meters thick and is made up of cyclically interbedded massive and laminated diatomite that is interbedded with thin-bedded nodular opal-CT chert and cherty porcelanite (Figure 4.9A). The Mixed Clastics member and the Cherty Diatomite member are distinguished by increased abundance of opal-CT chert and diatomite and a near absence of sandstone in the upper member except for one isolated interval near its base. A 57-meter section in between the two members is covered with thick vegetation, thus the contact is obscured. The first measurable unit is a discontinuous 4-meter-thick section of chert, siliceous mudstone, diatomite and sandstone. Two more sections (98 meters combined) were unmeasured due to vegetation cover, a wide gully/road and hostile property owners. Estimates of lithology spanning these are made based on observations made from a distance of the inaccessible overhanging cliffs. The uppermost 25 meters are well-exposed and meter by meter lithologic observations are possible.

Thinly bedded (1 cm to 10 cm) opal-CT chert is interbedded with calcareous mudstone, massive and laminated diatomite and occasional thicker (.1m to .5 m) dolostone beds. The diatomite beds have a two or three part coupling of thinly laminated pure diatomite, “speckled” bed diatomite with visible flecks of purer white diatomite within a less pure diatomite and a muddier, brown diatomite or siliceous/calcareous mudstone (Figure 4.9B and Figure 4.9C).

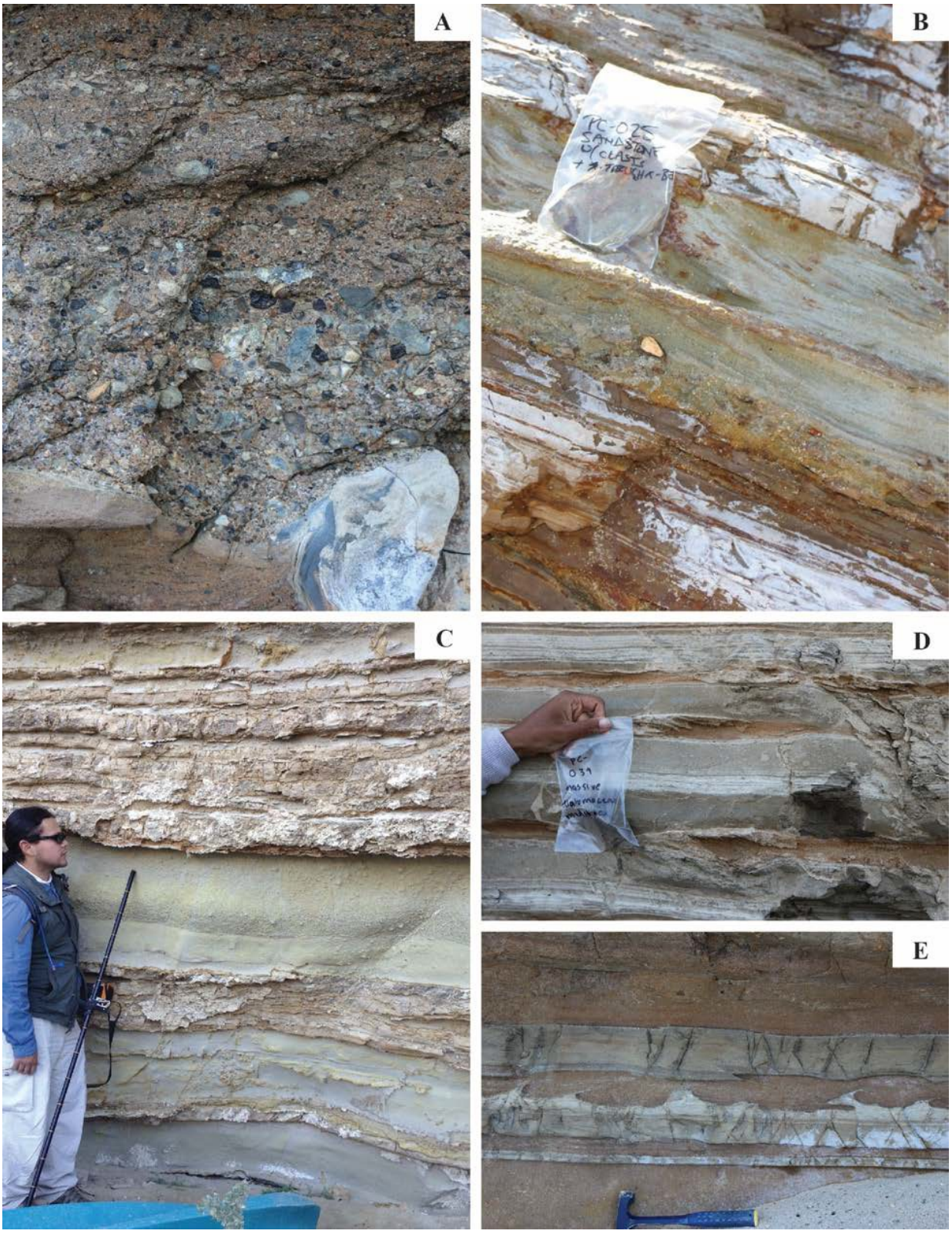
A
B
C
D
E

FIGURE 4.8. Sedimentologic and stratigraphic features of the Mixed Clastic member (A) Conglomerate in Mixed Clastics member containing blueschist clasts grading upwards from clast-supported to matrix-supported fabric. Vertical scale 50 cm. (B) Massive sandstone and thick units of diatomite beds made up of bed-sets consisting of ~10 cm-thick thin beds of diatomite. (C) Common three-part lithological units. Brown lenticular and cross-laminated sandstone interbedded with tabular grey diatomaceous mudstone and generally thinner laminated white diatomite (D) Contacts between the calcareous mudstones, muddy diatomite and sandstones Planar bedding, cross-lamination and wavy lamination in sandstone interbedded with mudstones. Scale ziplock bag is 14.5 cm (E) Flame structures and almost detached fragments of muddy diatomite caused by injection by sand.

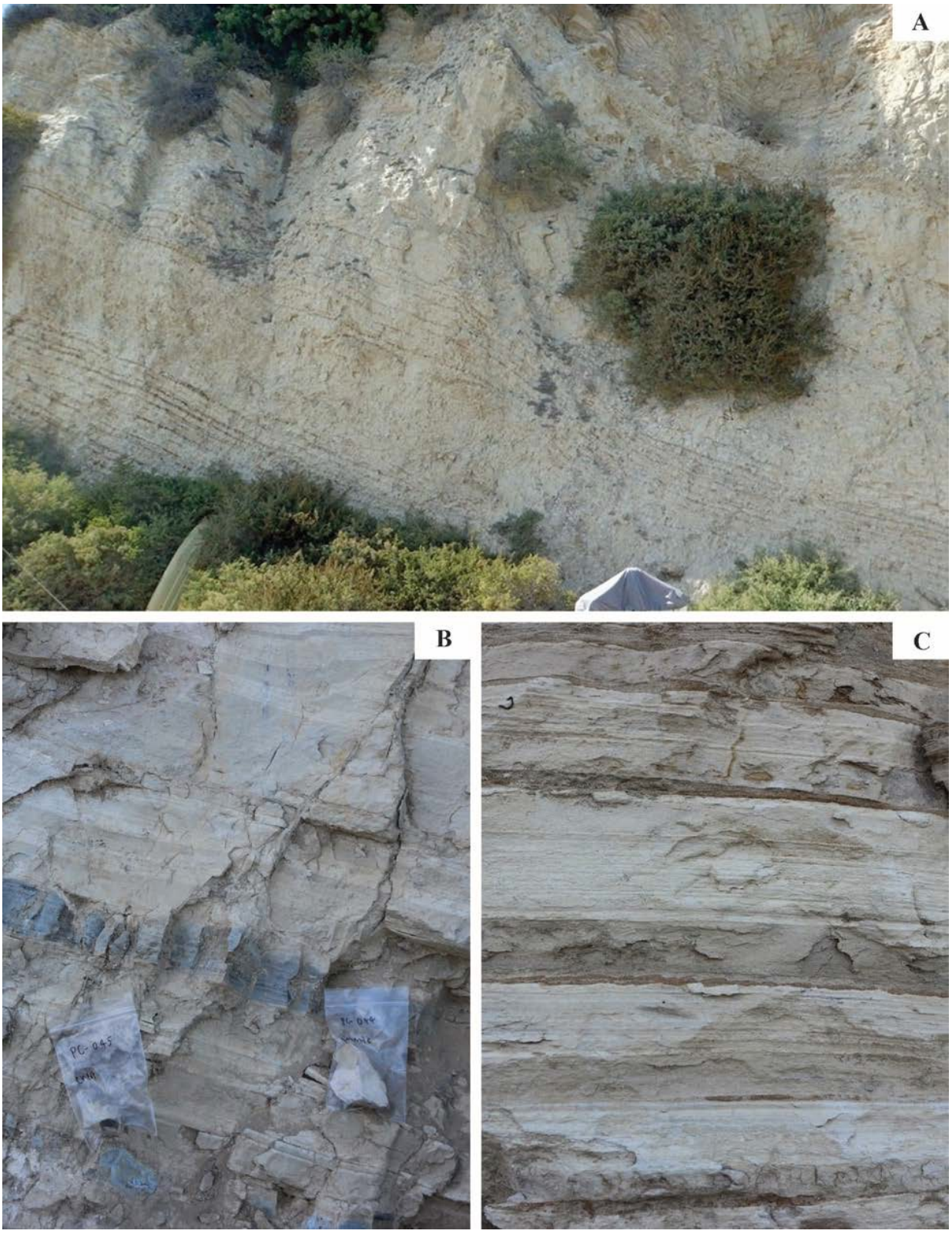
A
B
C

FIGURE 4.9. Sedimentologic and stratigraphic features of the Cherty Diatomite member (A) Thick beds of massive diatomite interbedded with very thick bedsets of thin-bedded diatomite, muddy diatomite and chert. Scale: surf board about 2 meters (B) Dark grey opal-CT chert beds with thinly laminated pure diatomite, and muddier diatomite (C) Interbedded laminated diatomite, speckled and muddy diatomite with lenticular laminations of sandstone (Scale: thickest mudstone bed is ~20cm)

Sandstone analysis (% SS and thin section petrography)

Sandstone is almost exclusively present in the middle part of the succession, within the Mixed Clastics member and near the base of the overlying Cherty Diatomite member. The abundance of sandstone (stratigraphic % per 3-meter increment) is plotted in Figure 4.10 and shows that the lowest sandstone occurs near the contact between the Porcelanite and Shale member and the Mixed Clastics member and the uppermost sandstone bed is part of the Cherty Diatomite member, located near the contact between the two members. The contact of the Cherty Diatomite member is defined at the lowermost chert exposed and not where the uppermost sandstone occurs.

Sixteen sandstone samples were studied by thin section petrography to classify framework grain types and semi-quantitatively estimate their abundances (Table 4.1). The sandstone specimens are primarily feldspar and lithic-rich with 4 lithic arenites, 10 feldspathic arenites, a lithic-feldspathic arenite and a feldspathic lithic wacke. The lithic arenites are most frequent lower in the section, the feldspathic arenites are found in the middle and the lithic-feldspathic arenites and wacke found towards the top of the section.

The lithic arenites have abundant (> 25%) or common (10-25%) amounts of metamorphic rock fragments (MRF). Some of the metamorphic rock fragments include blueschist, glaucophane grains, quartz-mica schist and polycrystalline metaquartzite fragments. The feldspathic arenites contain abundant plagioclase (Plag) and volcanic rock fragments (VRF) and abundant or common. mono-crystalline quartz (Mono-qtz). There are also minor to common amounts of potassium feldspars (Kspar)..

TABLE 1. Sandstone Petrography

Sample Name	Sandstone classification	Provenance	VRF	MRF	SRF	Poly-qtz	Mono-qtz	Kspar	Plag	G-phane	Kerogen
PD-PC SS-06	sandy dolomite/subarkose	Granitic		m		c	a	m	m	t	c
PD-PC SS-05	lithic wacke	Schist mix		a	a	c	c	t	m		m
PD-PC SS-11	lithic arenite	Schist mix		a		a	a	m	c	m	
PD-PC SS-13	Lithic arenite	Shist mix	C	c	c	c	c	m	c		
PD-PC SS-02	Feldspathic arenite	Volcanic/granitic	m	t		m	a	c	c	t	
PD-PC SS-08	Feldspathic arenite	Granitic		c		m	a	c	c	t	
PD-PC SS-09	Feldspathic arenite	Volcanic/granitic	m	c		c	c	m	c		
PD-PC SS-10	Feldspathic arenite	Volcanic/granitic	c	m			a	c	a	t	
PD-PC SS-07	Lithic arenite	Schist/San Onofre breccia	c	a			m			m	
PD-PC SS-16	Feldspathic arenite	Granitic					m	m	m	t	m
PD-PC SS-14	Feldspathic arenite	Volcanics	a				c		a		
PD-PC SS-01	Feldspathic arenite	Volcanics	a				c		a		
PD-PC SS-04	Feldspathic arenite	Volcanics	a				c		a	t	
PD-PC SS-03	Feldspathic arenite	Too few grains					m	m	m		
PD-PC SS-12	Lithic-feldspathic arenite	Volcanics	a	m		m	m	m	a		
PD-PC SS-15	Feldspathic arenite	Volcanics	m	t			m	m	c		
PD-PC SS-17	Feldspathic-lithic wacke	Meta-volcanics	c	m	c	m	c		a	t	

trace	1 to few grains
minor	<10%
common	10-25%
abundant	main component >25%

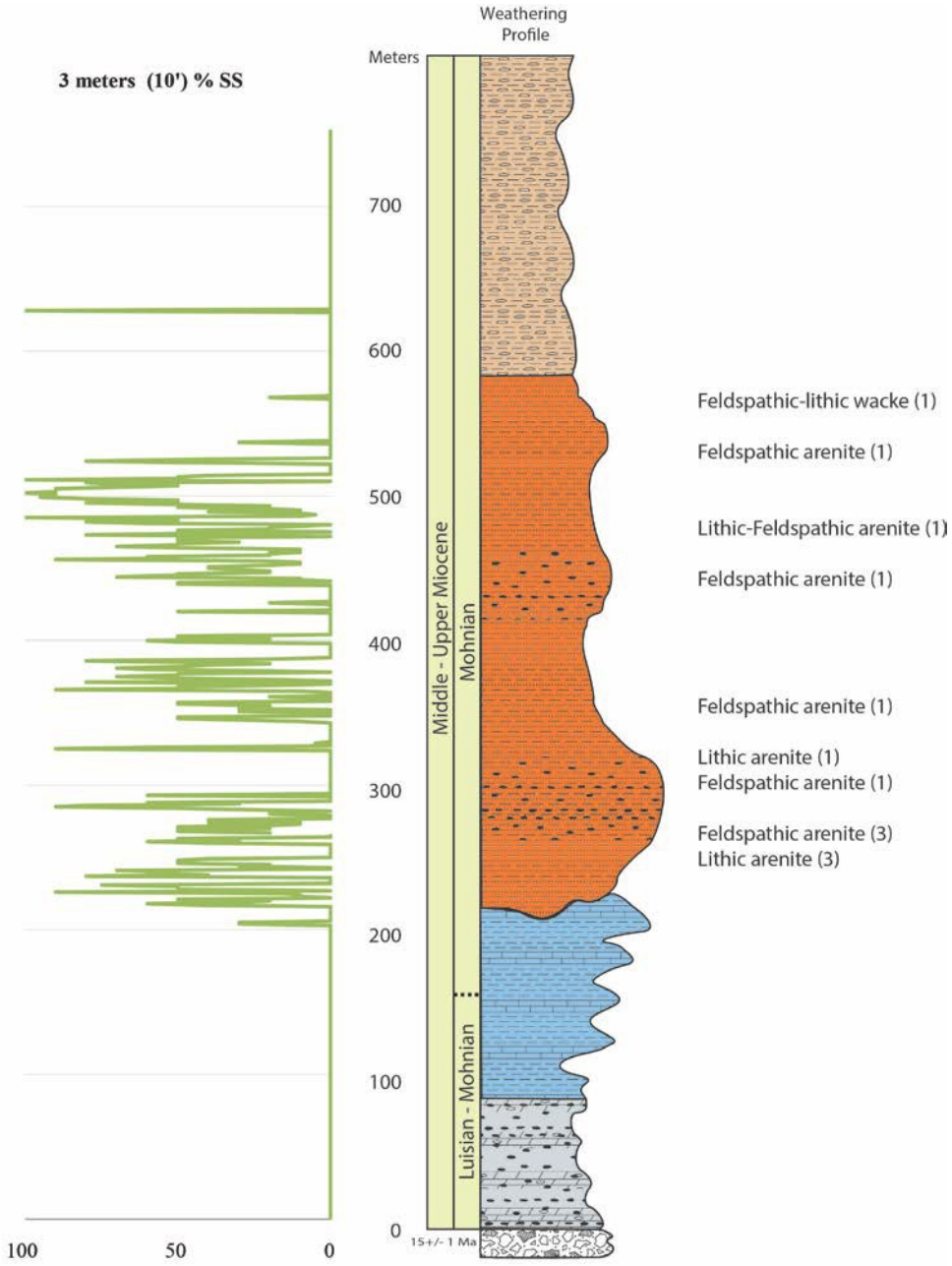

FIGURE 4.10. Stratigraphic sandstone abundance graph. Approximate locations and number of sandstone samples used for thin section petrography.

Total Organic Carbon (TOC)

Twenty-nine samples were analyzed for weight % total organic carbon (TOC). The results for each member and their relative stratigraphic positions are shown (Figure 4.11 and Table 4.2). The values ranged from less than 1% to greater than 14%. The Cherty Diatomite member had 5 analyzed samples that contained the lowest amount of total organic carbon. The Porcelanite and Shale member had 9 samples that were analyzed and contained the highest total organic carbon readings in the succession.

Dolomitic Phosphatic Shale Member

Four samples were obtained from this member and were analyzed for the percent total organic carbon content by weight. TOC in this section ranges from 0.4 and 7.0 %, averaging 3.12 %.

Porcelanite and Shale Member

TOC of ten samples analyzed in this member range from a maximum of 14.6 % to a low of 1.4%, with an average value of 5.99 %. The highest value is found towards the bottom of the member.

Mixed Clastics Member

Thirteen samples were analyzed for total organic carbon content. TOC values range from 0% to 4.7 % by weight, averaging 1.53 %. Overall, TOC content is this member is lower than in the Porcelanite-Shale and the Dolomitic-Shale members.

Cherty Diatomite Member

Two samples were analyzed and their TOC values are 2.1% and 1.06 % by weight, averaging 1.61 %. This unit is the least organic-carbon-rich of the four members.

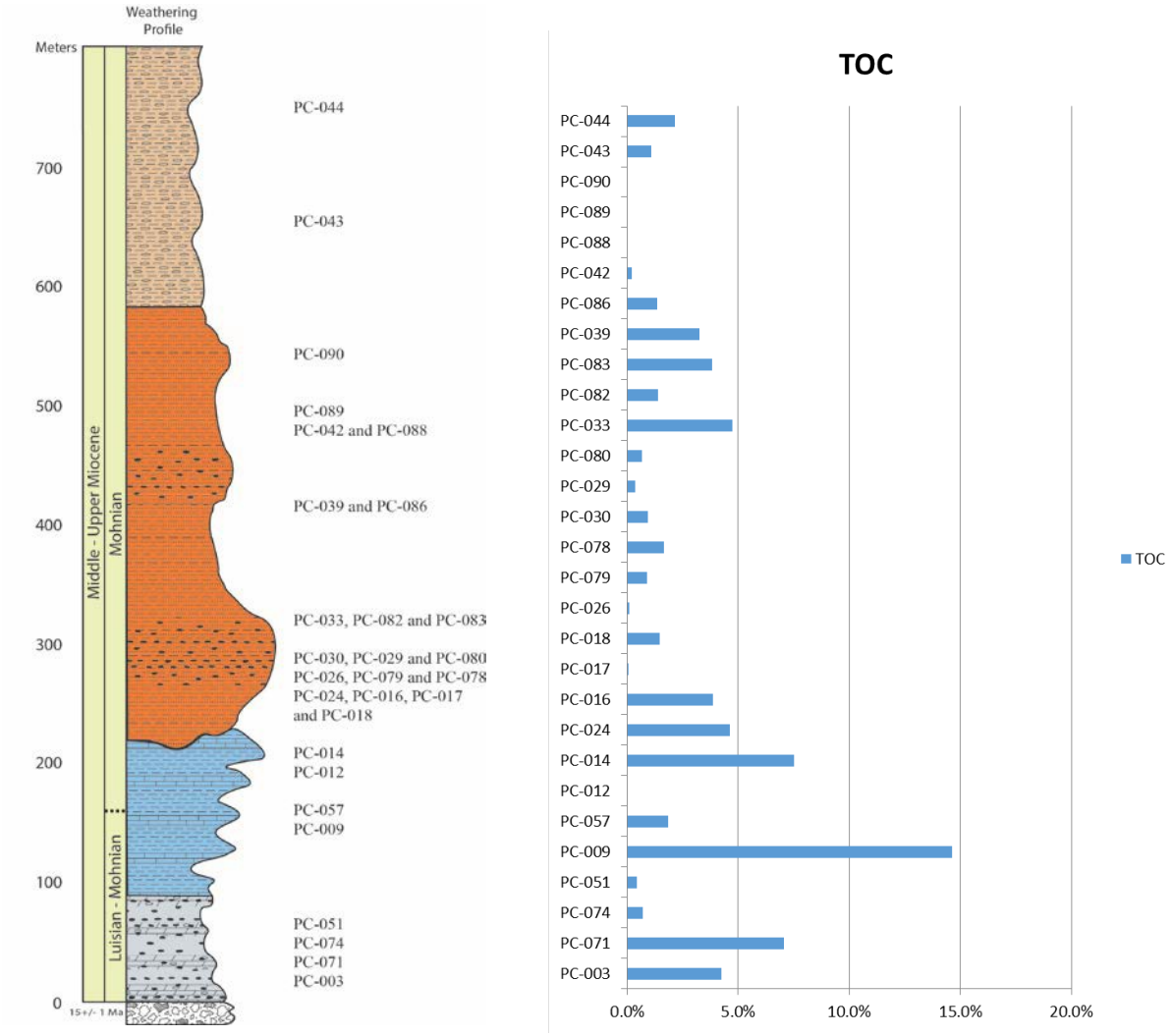

FIGURE 4.11. Total Organic Carbon (weight %). In mudrocks found in each member and their relative stratigraphic height in the member.

TABLE 2. Total Organic Carbon (%) Results

Stratigraphic Column	Sample	TOC
Dolomite-Phosphatic Shale Member	PC-003	4.25%
Dolomite-Phosphatic Shale Member	PC-071	7.05%
Dolomite-Phosphatic Shale Member	PC-074	0.71%
Dolomite-Phosphatic Shale Member	PC-051	0.42%
Porcelanite and Shale Member	PC-009	14.63%
Porcelanite and Shale Member	PC-057	1.86%
Porcelanite and Shale Member	PC-012	0.00%
Porcelanite and Shale Member	PC-014	7.50%
Mixed Clastics	PC-024	4.64%
Mixed Clastics	PC-016	3.84%
Mixed Clastics	PC-017	0.01%
Mixed Clastics	PC-018	1.48%
Mixed Clastics	PC-026	0.09%
Mixed Clastics	PC-079	0.88%
Mixed Clastics	PC-078	1.63%
Mixed Clastics	PC-030	0.92%
Mixed Clastics	PC-029	0.37%
Mixed Clastics	PC-080	0.64%
Mixed Clastics	PC-033	4.74%
Mixed Clastics	PC-082	1.37%
Mixed Clastics	PC-083	3.81%
Mixed Clastics	PC-039	3.23%
Mixed Clastics	PC-086	1.34%
Mixed Clastics	PC-042	0.22%
Mixed Clastics	PC-088	0.00%
Mixed Clastics	PC-089	0.00%
Mixed Clastics	PC-090	0.00%
Cherty Diatomite	PC-043	1.06%
Cherty Diatomite	PC-044	2.15%

Spectral Gamma Ray Data

Three hundred thirty Spectral Gamma Ray measurements were collected at a 1-meter spacing through all accessible intervals of the succession. Gaps in the data occur where vegetation or talus covered the outcrop or where sections were otherwise inaccessible. Results are presented in Figures 7, 9 and 9 for uranium (ppm), potassium (wt %) and thorium (wt %). Overall results show significant stratigraphic trends in uranium. Smaller scale variation in potassium and thorium concentration occurs, showing elevation in the lower section – Dolomitic-Phosphatic and Porcelanite-Shale members – compared to the overlying Mixed-Clastic and Cherty Diatomite members (Figure 4.12). Potassium (Figure 4.13) has values between 0.5 – 1.5% and also shows rough ~50- to 100-meter-thick cycles throughout the section. The lowest potassium (%) is in the Dolomitic-Phosphatic Shale member and the highest potassium peak is in the Mixed-Clastic member. Fluctuations within the thorium (ppm) data (Figure 4.14) are between 1- 5 ppm and show several high peaks. Peaks of high thorium abundance occur in the Mixed-Clastic member and in the Dolomitic-Phosphatic member. The total gamma ray (API units) curve shows high values in the Dolomitic-Phosphatic and Porcelanite-Shale members at the base of the section and then significantly lower values in the upper Mixed-Clastic and Cherty Diatomite members.

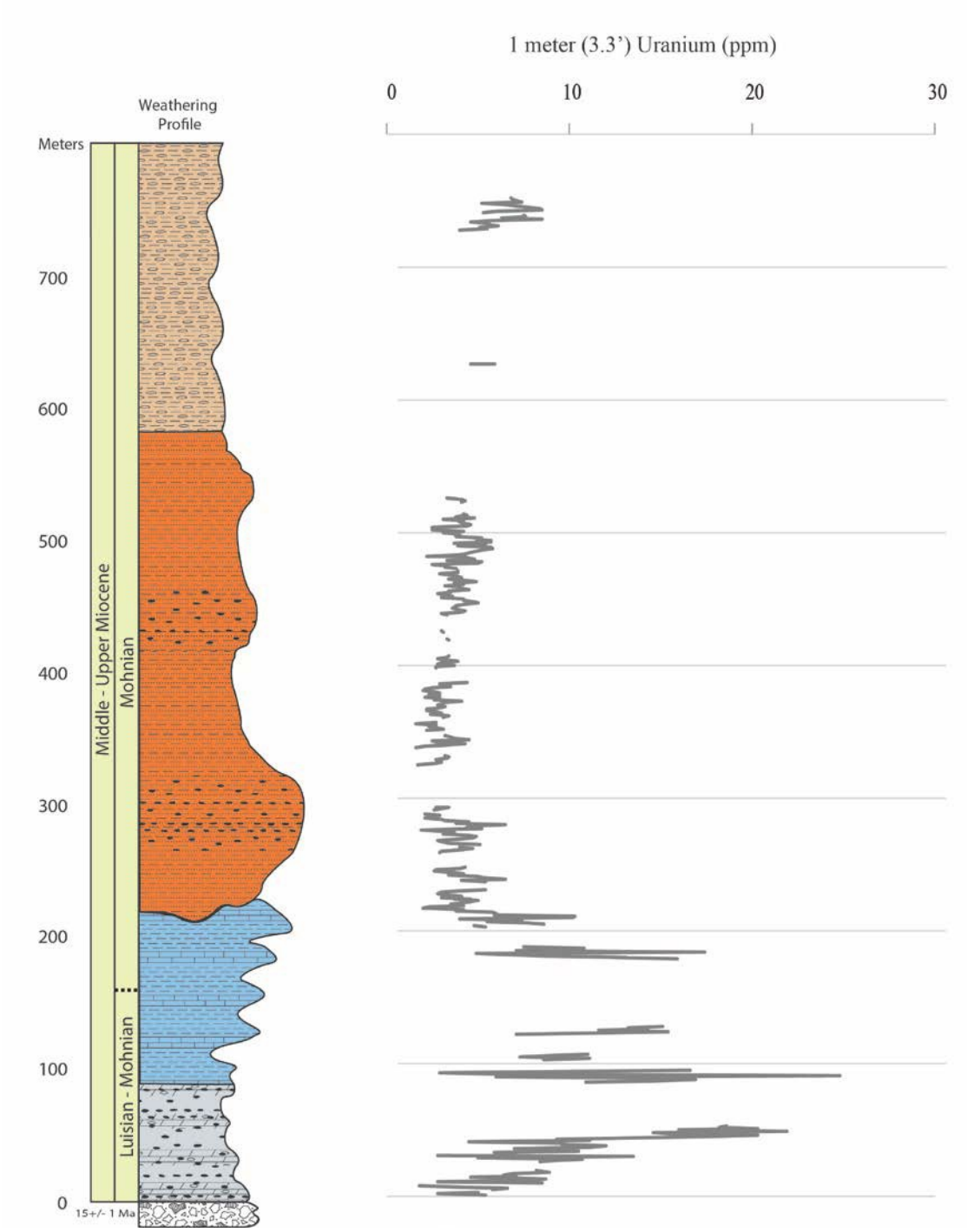

FIGURE 4.12. Uranium concentration (ppm) through the stratigraphic section. Note significantly higher concentrations in the lower section than in the upper portion of the section.

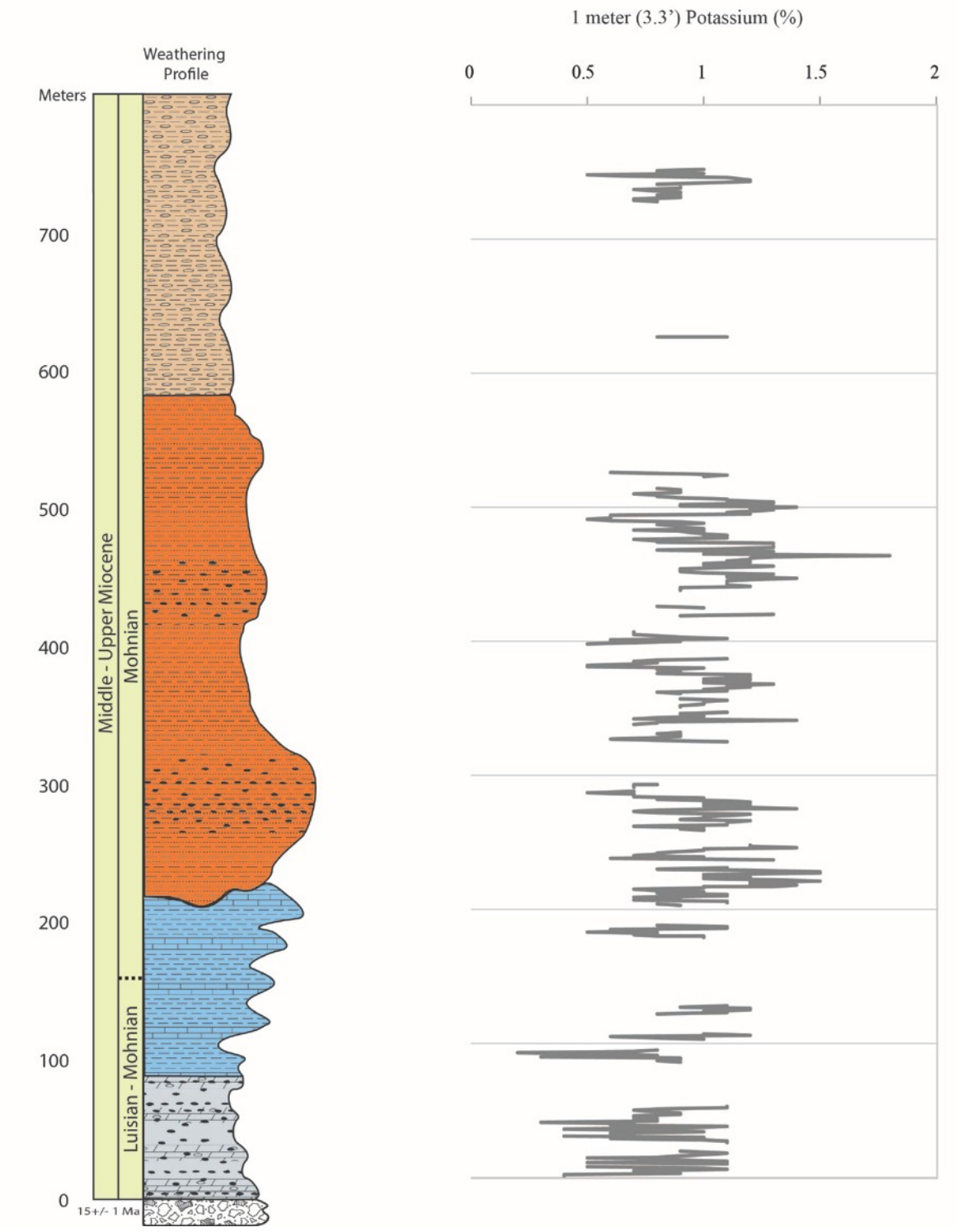

FIGURE 4.13. Potassium (%) has lower concentration in the Dolomitic-Phosphatic shale member.

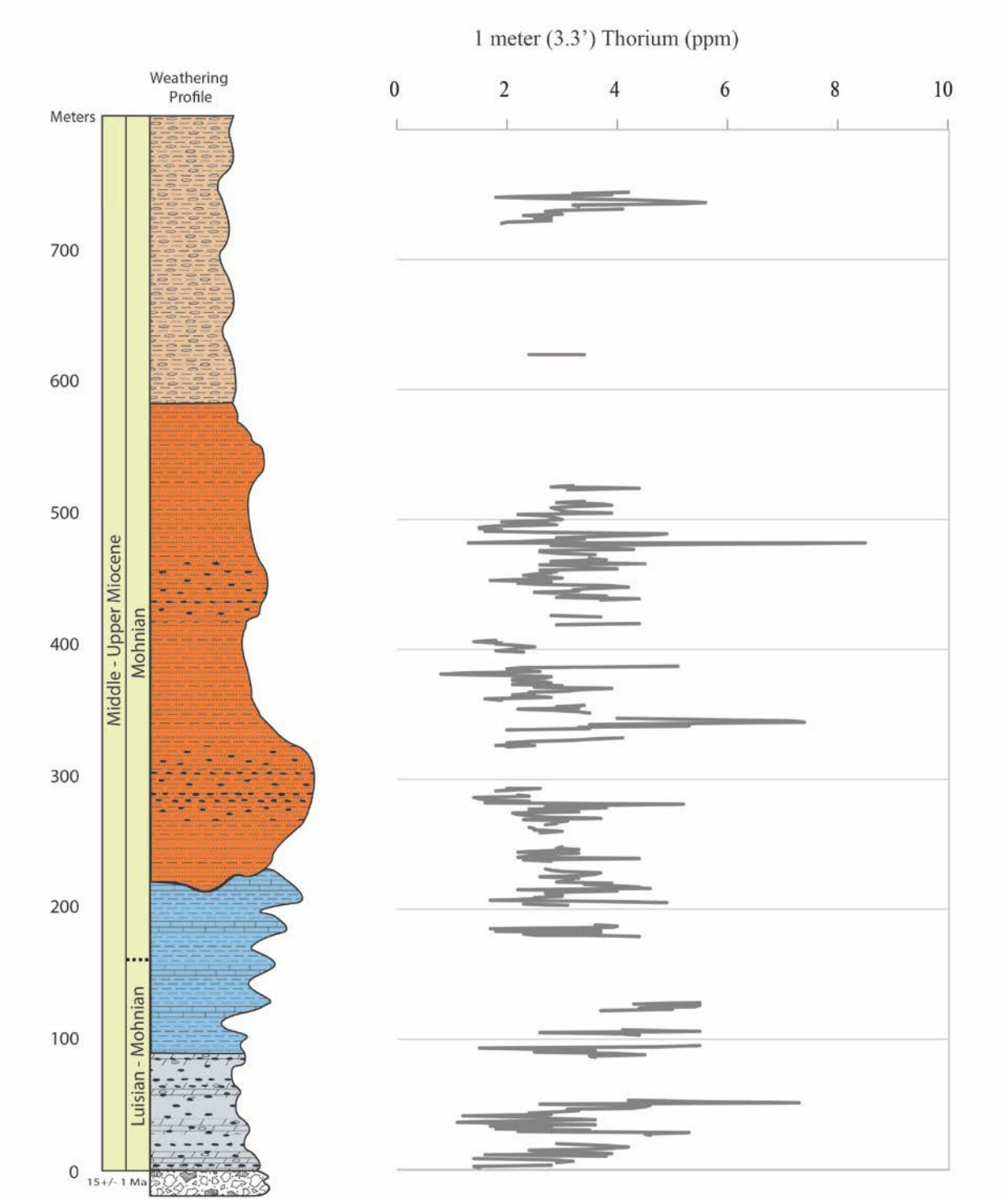

FIGURE 4.14. Thorium concentration (ppm) shows sharp peaks in the Dolomitic-Phosphatic member and the Mixed-Clastics member.

Dolomitic-Phosphatic Shale Member (Spectral GR)

The meter-by-meter measurements of percent (%) potassium, parts per million (ppm) of uranium and thorium plots are displayed in Appendix A.

The potassium (%) does not vary significantly in this member. The lowest value is 0.3 % and the highest value is 1.1 %: the average is 0.79 %.

The uranium (ppm) varies widely in this member. The lowest value is 1.8 and the highest value is 21.9. At the bottom of the member the values were lower (bottom 26 meters in the stratigraphic column, average 6 ppm for 20 data points), and increased in amount as the height in the member increased (27 – 87 meters stratigraphically, average 11.77 ppm for 30 data points).

The thorium (ppm) varies from 1.1 to 7.3, the average is 3.11. Meters 51 through 53 are where the highest values are found.

The total gamma ray (API) varies from 28 to 204 and the average is 100.8. The general trend is from low API values (55.6) at the top of the member and increasing with depth in the section (143.6), with some fluctuations in between.

Porcelanite and Shale Member (Spectral GR)

The spectral gamma ray results in this member share some similarities with the underlying Dolomitic and Phosphatic Shale member. Similarly, the potassium (%) values do not vary significantly (lowest point is 0.2 % and the highest is 1.2 %, average, 0.87 % for 43 data points). Generally, the potassium is relatively low at the base of the member and then gradually increases with upward progression in the member. In contrast to the trend seen in the Dolomitic-Phosphatic member, the uranium (ppm) values (lowest value 2.9 and highest value 24.8, average 10.2) in the Porcelanite and Shale Member are high (16.9) at the bottom of the member and then decrease (6) at the top of the member. The thorium (ppm) values (lowest value 1.5 and highest value 5.5, average 3.6) show a gradual increase from bottom to top of the member and continue

an overall trend of increasing that is seen in the Dolomitic Phosphatic Shale member. There are two large spikes in the Total Gamma Ray data. The high value (meter 91, Assay #547, Total GR is 225.6 API) is associated with a fissile mudstone and porcelanite bed and is driven by a layer rich in Uranium (24.8). On the low end (meter 93, Assay #549, Total GR is 32.4) the spike is associated with a cherty porcelanite. With the exception of the two contrasting data spikes, the Total GR shows a gradual increase in the values with increase in height in the member.

Mixed Clastics Member (Spectral GR)

In terms of Spectral Gamma Ray, the boundary between the Mixed Clastics member and the underlying Porcelanite and Shale member is the most noticeable in terms of contrast. The potassium (%) values in this member are overall higher (low value 0.5 % and high value 1.8 %, average .97 %) than in the two underlying members. There are cyclic fluctuations that occur within the potassium values and appear to occur every 30-50 meters. Uranium values are significantly lower (lowest value 1.6 and highest 6.5 value, average 3.6) in this member compared to the other members, and, within the member, the values do not vary widely. The thorium values (lowest value 0.8 and highest value 8.5, average 2.9) in this member have overall similar ranges compared to the underlying two members. However, there are two fluctuations of very high thorium values (7.4 ppm at 344 meters and 8.5 ppm at 482 meters) associated with a dominantly diatomite and sandstone bed and a sandstone bed respectively. The total gamma ray values are low (average 56 API, lowest 27.2 and highest is 86.4) and match the uranium curves closely.

Cherty Diatomite Member (Spectral GR)

The Spectral Gamma Ray Data in the Cherty Diatomite member is comparatively sparse due to the inaccessible and unmeasured sections. The data that do exist are located in the top of

the member and show data that closely resemble the trends seen in the Mixed Clastic member. The uranium (ppm), potassium (%) and the total gamma ray (API) values are overall slightly higher in this member than in the Mixed Clastic Member and do not vary widely within the member. The lack of many meters of continuous data makes it difficult to comment on general trends over the whole 184 meter of section. However there are interesting peaks that occur. The thorium peak is at 654 meters and is 9.2 (ppm) and correlates with a dolostone bed. The uranium (ppm) peaks at 736 meters, 8.5 (ppm) 743 meters, 8.5 (ppm) and 744 meters, 8.4 (ppm) correlate with a "hot" calcareous mudstone with some chert lenses, a siliceous mudstone and a "hot" calcareous mud rock and dolostone respectively.

Biostratigraphic Analysis

There are 6 locations in the Point Dume-Paradise Cove section that contain foram data based on benthic foraminifera assignments from the USGS/Chevron dataset (Brabb, 2011). The location data in latitude and longitude and the ages of the foraminifer samples were obtained by Chevron Petroleum Company paleontologists for more than 2,500 oil test wells in California (U.S. Geological Survey Open-File Report 2011-1263, 4 p. and data files http://pubs.usgs.gov /of/2011/1262. The benthic foraminifera assignments from the USGS/Chevron dataset from the Point Dume-Paradise Cove are all of Mohnian age (13.5 – 7.5 Ma) and are found at the top of the Porcelanite and Shale Member, in the upper half of the Mixed Clastics member and at the lower portion of the Cherty Diatomite member (Figure 4.15).Diatom biostratigraphy analysis was done by Diane Winter (2015) on samples from Point Dume and Paradise Cove and this helped refine the age of the upper half of the section to *D. hustedtii-D lauta* zone, subzone D (~9.2 – 9.9 Ma). Middle upper Miocene is also indicated by the presence of *Thalassionema schraderi*. The lower part of the section is only roughly dated as middle to upper Miocene.

Specifically, there are 4 samples containing diatoms from the early late Miocene and 2 samples contain diatoms from the middle late Miocene (Appendix C). Most of the samples (5) are from the Mixed Clastic member and contain diatoms from both of the time periods (Figure 4.15). 1 sample is from the Cherty-Diatomite member and is from the early late Miocene member.

Yerkes and Campbell (1979) describe numerous collections of Foraminifera that are found in the Monterey section of Point Dume and that are assigned to the Luisian and Mohnian Stages of Kleinpell (1938). The USGS/Chevron dataset and the diatom biostratigraphic analysis provide age constraints on the Porcelanite and Shale, Mixed Clastics and Cherty Diatomite members of the section, and for the undated Dolomitic-Phosphatic Shale member it may be inferred infer that it is between Luisian and Mohnian age.

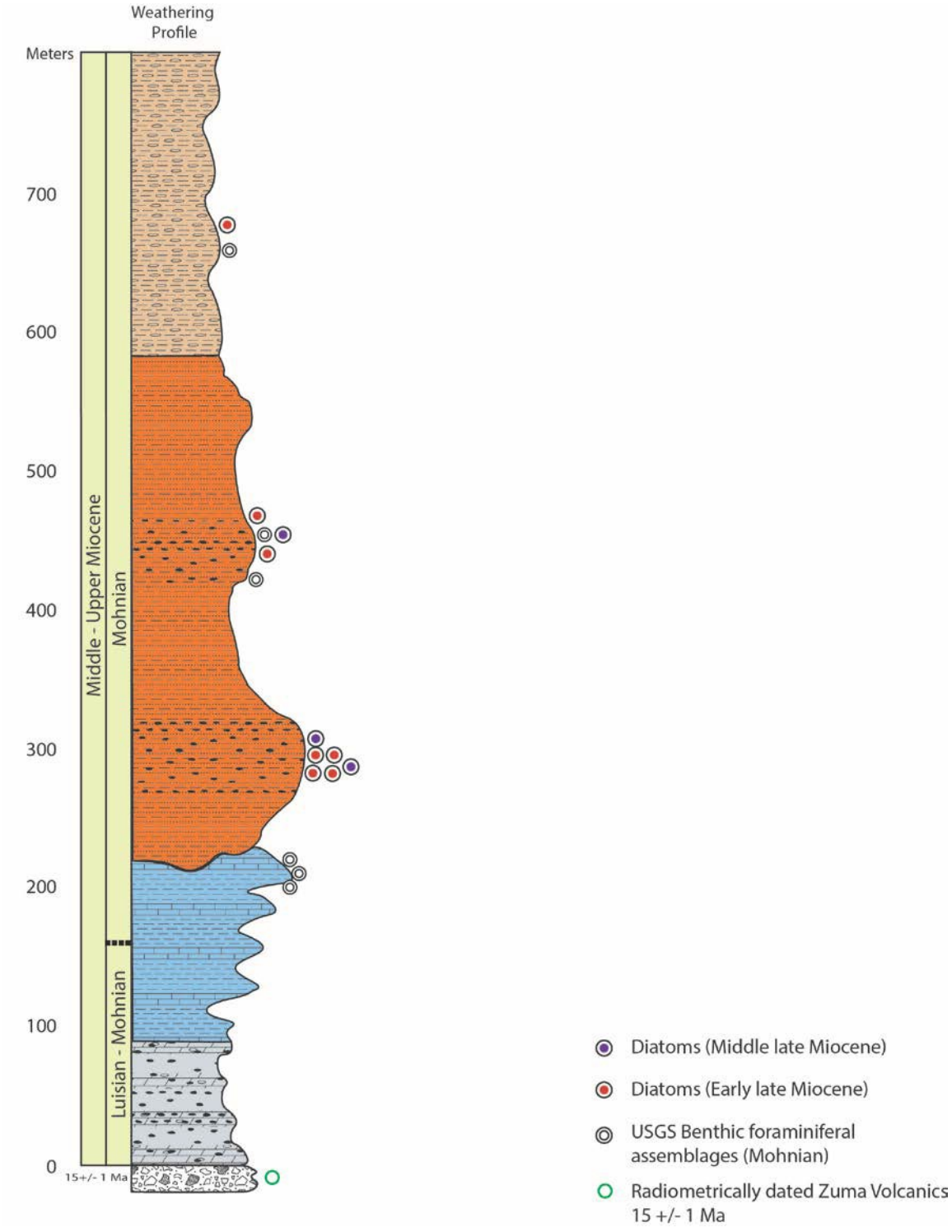

FIGURE 4.15. Locations for radiometrically dated Zuma Volcanics. USGS Benthic Foraminifera data and Diatom Zones.

CHAPTER 5

DISCUSSION

The Monterey Formation exposures in the Point Dume-Paradise Cove area of Malibu are important to study, in part because they are located in a significant tectonic location for southern California. Kamerling and Luyendyk (1979) and other workers showed that this area was the boundary between the rifting and rotating Western Transverse Ranges and the Los Angeles basin. Reconstructions suggest that the Point Dume-Paradise Cove study area was outboard of the Los Angeles basin, the Schist Ridge and Palos Verdes (Wright, 1991; McCulloh and Beyer, 2003). It is also most likely that the area has moved in a left-lateral sense along the Malibu Coast and the Anacapa-Dume faults during the last 20 million years (McCulloh and Beyer, 2003).

Furthermore, the stratigraphy south of the Malibu Coast fault has been described as having noteworthy differences from nearby successions to the north in the western Santa Monica Mountains (Yerkes and Campbell, 1979). The Modelo Formation in the eastern Santa Monica Mountains and Ventura basin is distinguished from the Monterey Formation of the central California coast by containing massive sandstone units deposited within Miocene submarine fans and channels (Hoots, 1931). These Modelo sandstones can be compared with the sandstones found in Point Dume-Paradise Cove sequence.

Having characteristics of both classic hemipelagic Monterey Formation and Modelo Formation strata makes understanding the sediment source, depositional environment and relationships to other Monterey Formation locations important study issues for this area. This chapter examines the lithostratigraphic succession from Point Dume to Paradise Cove, characterizes and interprets the sequence of lithostratigraphic members and relates them to other

Monterey Formation successions. Finally, constraints on the source of sediments and depositional environment are evaluated.

Lithostratigraphic Members of Point Dume-Paradise Cove Sequence

The Monterey Formation exposures located south of the Malibu Coast fault and between Point Dume and Paradise Cove can be subdivided into distinct lithologic members (see Figure 4.1 in Results). The base of the section is at Point Dume and is marked by the sharp contact with the Zuma Volcanics 15 +/-1 Ma (Berry et. al., 1976) and overlain by what Yerkes and Campbell (1979) describe as the Monterey Shale that they describe as being intertongued with the Trancas Formation in the area south of the Malibu Coast fault. This study describes the sequence of sedimentary rocks in the area south of the Malibu Coast fault in greater detail and divides the succession of rocks into four lithostratigraphic members. These are the Dolomitic Phosphatic Shale member, the Porcelanite and Shale member, the Mixed Clastics member and the Cherty Diatomite member.

Base of Section

The base of the section at Point Dume to Paradise Cove lies unconformably over the Zuma Volcanics but it is possible that this is a fault-contact and likely that the true depositional basement rock in the study area is the Catalina Schist. Yerkes et. al. (1965) describe the results from the Sovereign Oil Company, Malibu 1 oil well that drilled through the Trancas Formation (correlative in part, with the San Onofre Breccia – also a Catalina Schist-derived clastic unit), which locally underlies and intertongues with the Monterey and the Zuma Volcanics. This relationship is similar to that of Palos Verdes where the Catalina Schist underlies the Altamira Shale member of the Monterey Formation separated locally by a thin schist-bearing conglomerate (Conrad and Ehlig, 1987). The Catalina Schist, overlain by schist conglomerate

and sand in turn overlain by Monterey Formation is also characteristic of the subsurface in Venice Beach, Playa del Rey and Hyperion fields along the coast north of Palos Verdes (DOGGR, 1992) The Zuma Volcanics have been radiometrically dated at 15.0 +/- 1 Ma (Berry et. al., 1976, updated by Stanley et. al, 2000).

Dolomitic Phosphatic Shale Member

The Dolomitic Phosphatic Shale member is characterized by medium to thick beds of organic rich phosphatic shales interbedded with medium beds of dolostone. On the weathered cliffs, the mudstone is light brown, however it is black on the freshly sand-blasted beach platform. The mudstones are very organic-rich, containing between 4.2 and 7.5% by weight of total organic carbon (Sandoval, pers. comm., 2015). The phosphate layers within the mudstone occur as mm- to cm-thick laminations, light-colored lenses, small nodules and coprolites. The phosphate is an authigenic precipitate that is formed during shallow burial diagenesis (Garrison et al., 1994). In some parts of the member, the phosphatic laminations display an inverse grading that is reflective of the varying intensity of winnowing and sedimentation rates along the sea floor that ultimately affect phosphatization (Föllmi, 1996). The pale grey, dolostone beds occur as 0.2-0.5-meter-thick nodules and medium thick beds that, like the phosphate, are also reflective of periods of very slow sedimentation rates in a dysoxic setting.

In this section are black and pink “burnt shales” that are stratigraphically part of the Dolomitic Phosphatic Shale member but have structurally been emplaced to the overlying Porcelanite and Shale member. These are evidence of a process of exothermic oxidation of marcasite and pyrite in the organic-rich mudrocks in this member that, in some locations, has been shown to trigger pyrolysis and hydrocarbon generation (Mariner et al., 2008; Boles et al., 2001). Burnt shales are a relatively common feature in similar outcrops where organic-rich

sediments like Monterey Formation are exposed along cliffs and unstable hillsides. The process has been recently observed while occurring and is believed responsible for not only altering the chemistry and mineralogy of sedimentary deposits, but also for triggering forest fires (Mariner et al., 2008) and disrupting landfill operations (Boles et al., 2010)

The Dolomitic Phosphatic Shale member in the Point Dume to the Paradise Cove section shares similar characteristics to lower members of the Modelo and Monterey rocks found in the Los Angeles, Ventura, Santa Maria and Santa Barbara basins. Yerkes (1965) describes the Monterey Shale in the area south of the Malibu Coast fault as consisting of marine clay shale that is interbedded with phosphatic and bituminous (i.e., organic-rich) rocks. Pisciotto and Garrison (1981) describe a Phosphatic Facies of the Monterey that contains phosphatic shales and mudstones that contain phosphatic layers that are light tan and may be cyclic and graded. Föllmi et al. (2005), describe a section of the Naples Beach (Santa Barbara) Monterey Formation as having a middle part that is composed of an organic-rich mudstone that is interstratified with phosphatic laminae. The similarities with the Point Dume to Paradise Cove section also include similar total organic carbon (TOC) values of 7% in the study area and 8.5% in Naples Beach.

The organic-rich phosphatic mudrocks are composed of mostly F-phosphates that occur as friable, light-colored laminate, nodules and lenses within the organic-rich mudstones and diatomaceous muds and some well lithified, dense nodules or hard grounds of the darker D-phosphates (Garrison et al., 1994). F-phosphates and D-phosphates represent early stage diagenesis versus multiple stages of sediment reworking and diagenesis respectively (Garrison et. al, 1990). Precipitation of phosphate occurs close to the sea floor and at a very shallow burial depth. Slow sedimentation rates and some winnowing and erosion lead to the concentration of the phosphatic rich laminae and nodules that are present in this member (Garrison et. al., 1994).

The dolostone that is formed in this environment is due to the diffusion of magnesium and calcium cations from the seawater and methane or bicarbonate from below during a period of paused sedimentation that favors pore-filling dolomitization (Garrison et. al., 1994). The cyclicity of alternating phosphate and dolostone at Point Dume-Paradise Cove and other sections of the Monterey Formation has been linked to Milankovitch cycles (Garrison et. al., 1994; Meister et al., 2008).

Other workers who have studied the Monterey Formation observe the relationship between carbonate and phosphate-rich organic rocks. Isaacs (1981) describes the Monterey Formation along the Santa Barbara coast as being organic-rich calcareous shale that is "abundant in the middle of the carbonate-bearing sequence." Furthermore, in a description of the outcrops at Gaviota Beach, Isaacs (1981) refers to "nodular dolomite layers in organic-rich phosphatic calcareous shale" that is found in the Organic Shale member (later termed the Carbonaceous Marl member). In the Santa Maria Basin, Compton and Siever (1984) described the Phosphatic member that contains dolostone, porcelanite and phosphatic organic-rich mudstone. Closer to the study area is the Palos Verdes Hills, whose sequence of Monterey Formation Conrad and Ehlig (1981) described as having a Phosphatic Lithofacies that contains meter-thick ledge-forming dolostone beds. The depositional setting and environment for this member is likely a bank-top or sediment-starved slope to basin floor in an isolated basin distant from the outer continental shelf (Garrison, 1994) and within or at the edge of a well-developed oxygen minimum zone.

Porcelanite and Shale Member

The Porcelanite and Shale member is characterized by thinly bedded opal-CT porcelanite to cherty porcelanite alternating with generally more thickly bedded siliceous mudstone to

muddy opal-CT porcelanite and organic-rich phosphatic mudstone. Whereas the underlying member contains a predominance of phosphatic mudrocks, this member is marked by an abundance of highly siliceous rocks of varying levels of purity and diagenesis that weather more purely white. The relatively few beds of organic-rich mudstone (black on fresh sand-scrubbed surfaces) contain fewer phosphate nodules and white laminations of phosphate that are more broadly spaced compared to the narrower, more frequently occurring laminations in the Dolomitic Phosphatic Shale member. This member contains stratiform horizons of dolostone nodules, but this lithology is much less abundant than the somewhat regularly spaced dolostone beds present in the lowest member. Bed-confined joint sets are well-developed in this member due to the predominance of brittle, highly siliceous rocks. Fracture spacing varies with the lithology of the beds, with closest spacing occurring in opal-CT porcelanite beds.

The Porcelanite and Shale member of the Point Dume to Paradise Cove succession is very similar to portions of other Monterey stratigraphic sections. Yerkes and Campbell (1979) describe the Monterey exposures of Palos Verdes as being made up of “cherty and porcelaneous shale”. Conrad and Ehlig (1981) describe the Monterey Formation of the Palos Verdes Peninsula as having a cherty lithofacies subdivision, whose dominant lithology is porcelanite and chert.

The increased abundance of siliceous rocks, and decreased dolostone and organic-rich phosphatic shale indicate a somewhat higher overall sedimentation rate that is also confirmed by more-widely spaced laminations in the mudrocks. The depositional environment for this member is likely a slope to basin floor setting in a basin proximal or distal to the continental outer shelf.

Mixed Clastics Member

The Mixed Clastics member of Point Dume-Paradise Cove succession is comparable to coarse-grained portions of the upper Miocene Modelo Formation. This member marks an

important boundary between the opal-A diatomaceous sediments within and above and the opal-CT phase siliceous sediments in the underlying members. The Modelo Formation is the more sandstone-rich, upper Miocene age unit that is identified north of the Malibu Coast fault (Yerkes et. al, 1965) and on the north flank of the Santa Monica mountains (Hoots, 1931) and in its type area north of the Santa Clara Valley. However, Dibblee and Ehrenspeck (1991) considered these same rocks in the Santa Monica Mountains to be Monterey Formation, just with significant intraformational sandstone lenses and bodies.

This study of the Point Dume to Paradise Cove section identifies a thick (355 meter) clastic-rich member with conglomerate, siliceous/calcareous mudstone, and interbedded sandstone and diatomite that is not unlike the coarse clastic units of the Modelo in the rest of the Santa Monica Mountains. Nonetheless, there are two significant differences between the Monterey succession south of the Malibu fault and the Modelo succession north of it. First, there are no massive, map-scale sandstone bodies in the Point Dume to Paradise Cove section and second, there are compositional differences in the sandstone. Most of the sandstones from the Point Dume to Paradise Cove section are feldspathic arenites, although some are volcanic or metamorphic (schist) lithic arenites/wackes, and many contain metamorphic rock fragments in the framework grains. Sullwold (1960) describes the sandstones in the Modelo Formation as being arkosic wackes and sharing many of the same attributes like angular grains, high silt content, and poor cementation as the sandstones in this study area.

Hoots (1931) also described the Modelo Formation in the eastern Santa Monica Mountains as containing many similar rock types as the Mixed Clastic member. These include medium-coarse grained arkosic sandstone, light brown and gray siliceous and calcareous mudstone, a basal conglomerate and lenticular, well-indurated sandstone beds. Neither Hoots

(1931) nor Sullwold (1960) identified schist or volcanic grains in their petrographic analyses, however, they are minor components in approximately half of the sandstones studied in the Point Dume-Paradise Cove section. In particular, sandstones in the study area contain fragments of glaucophane and glaucophane schist known to be associated with the Catalina Schist and San Onofre Breccia. (Stuart, 1976). These minerals are absent in the Modelo Formation on the Northern flank of the Santa Monica Mountains (Rummelhart and Ingersoll, 1997), suggesting a local sediment contribution to the Point Dume-Paradise Cove deposits.

There is abundant evidence for turbidity currents being the primary mechanism for deposition of the sandstones in the Mixed Clastic member. Sullwold (1960) categorizes depositional features created by turbidity currents within Modelo sandstones into non-oriented and oriented features. The Mixed Clastic member contains many of the non-oriented features described by Sullwold, such as rhythmically interbedded sandstone and shale and sharp basal contacts of many of the sandstones indicating an erosional surface by a turbidity current. Additionally, shale inclusions and rip up clasts are common features in the sandstones in the Mixed Clastic unit and suggest scour by high-energy gravity flows. Among the non-oriented features in the Mixed Clastic member, there are scoured surfaces, flame structures, load casts, cross-laminations and few folds whose measurements were noted for paleocurrent direction data. Slump beds and intraformational folds are also abundant in some parts of the member, indicating gravity-driven movement.

The lower portion of the Mixed Clastics member contains thick to very thick intra- and extraformational conglomerate beds or olistostromes near the base of the member. The intra-formational conglomerates contain rip-up clasts of diatomaceous mudstones, diatomite or siliceous mudstone which suggest a high energy, downslope depositional environment

responsible for the upheaval and disruption of the overlying beds. The extraformational conglomerates contain blueschist clasts that suggest a provenance from the basement material like the Trancas Formation/San Onofre Breccia or Catalina Schist. In the upper portion of the Mixed Clastics member, there is a marked increase in thick beds of interstratified diatomaceous mudstone, white diatomite and lenticular sandstone. These three lithologies are also described in the Modelo (Sullwold, 1960).

The depositional environment for the Mixed Clastic Member was likely on a slope or base-of-slope setting where mass wasting, turbidity currents and hemipelagic sedimentation could co-occur with a local supply of eroded Catalina Schist grains and clasts from an upslope location. With the abundance of thin and ripple-bedded sandstones, this setting may also have been adjacent to a submarine channel-levee environment.

Cherty Diatomite Member

The Cherty Diatomite member is the uppermost lithostratigraphic unit exposed in the Point Dume-Paradise Cove sequence. It is composed chiefly of cyclically interbedded massive diatomite and laminated diatomite alternating with lesser amounts of opal-CT cherty porcelanite and nodular or thin-bedded opal-CT chert. The porcelanite tends to form thin planar beds, whereas the chert forms continuous thin beds or lenticular nodules. The nodules preserve primary laminations from the diatomite that do not show evidence of differential compaction. This suggests that they formed by pore-filling silicification of diatomite after reaching maximum burial depth.

Scales of cyclicity in this member range from several-meter-thick alternations between massive beds of diatomite and thin-bedded packages of cherty porcelanite and chert. Within these meter-scale alternations, smaller cycles involve <10 cm-thick interbedding of laminated

pure diatomite, muddy diatomite "speckled bed" diatomite and porcelanite. As in the Mixed Clastics member, the Cherty Diatomite member contains evidence for turbulent flow, but involving fine-grained sediment deposited at lower energy levels that are identical to those described as "speckled beds" by Chang and Grimm (1999) – massive to graded beds of mixed diatomaceous mud and white flecks of pure diatomite, ripped up and mixed by an erosive turbulent flow. The resulting interbedded lithofacies of laminated pure diatomite, "speckled" bed diatomite, muddy diatomite and cherty porcelanite is characteristic of the fine-grained deposits in this member.

Chert forms with burial only in the purest diatomite, sometimes with minor carbonate content, but with little to no clay (Behl and Garrison, 1994). Such purely biogenic calcareous-siliceous proto-sediments generally accumulate only in the most distal, outboard basins of the continental borderland (e.g., ancient Santa Barbara or Santa Maria basins, or modern Tanner basin). Accumulation of pure enough pelagic sediment that could form chert is rare in the more proximal, terrigenous-rich basins such as the Los Angeles or San Joaquin (Behl and Garrison, 1994) except for during intervals of restricted sedimentation during relative transgressions due to tectonics or eustacy (Garrison, 1992).

With diagenesis, highly diatomaceous deposits may become porcelanitic or cherty, therefore correlative sections may have different lithologic character if buried to different depths. The fact that opal-A and opal-CT phase rocks are interbedded in this member limit the burial depth and maximum burial temperature to < 45°C, but more likely <30°C (Behl and Garrison, 1994). Within the Monterey Formation, cherts appear to be best developed, or have greatest potential to develop, in certain stratigraphic intervals such as the Upper Miocene Upper Calcareous-Siliceous member of the Santa Barbara and Santa Maria coast (Isaacs, 1981; Behl

and Garrison, 1994) or the Valmonte Diatomite member or Cherty Lithofacies of the Monterey in the Palos Verdes Hills (Conrad and Ehlig, 1987; Behl and Morita, 2007). Like these other locations, the Cherty Diatomite member in the Point Dume to Paradise Cove section is also Upper Miocene/Mohnian and consists of interbedded chert, calcareous mudstones, siliceous mudstones, diatomite and occasional dolostones.

The depositional environment for the highly biosiliceous sediments that could be diagenetically altered to chert are likely distal or sediment-starved settings under a strong upwelling zone, however, they could be on bathymetric highs that were isolated from any bottom-seeking, detritus-transporting currents. The thick alternations between massive diatomite and laminated to thin-bedded diatomite and chert/porcelanite suggest that the depositional environment fluctuated between well-oxygenated and dysoxic conditions, perhaps near the boundary of the oxygen minimum zone.

Age of the Point Dume to Paradise Cove Succession

Yerkes and Campbell (1979) describe the Monterey Formation in the Point Dume, Malibu area as being Luisian and Mohnian (15.7 Ma to 7.1 Ma) based on Kleinpell's Miocene Stages (1938) of benthic foraminifera assemblages. However, the Luisian biostratigraphic designation is not confirmed by samples included in the USGS/Chevron benthic foraminiferal dataset (Brabb and Parker, 2005; Malmblorg et al., 2008) nor by diatom zones obtained for this study (pers. comm., Diane Winter). Unfortunately, the available biostratigraphic data throughout the succession is so overlapping that distinction in age between members is not possible, nor is calculation of sediment accumulation rates.

The ages of the Dolomitic Phosphatic Shale member and the Porcelanite and Shale member are only constrained by the radiometrically dated Zuma Volcanics (15 +/-1 Ma) at the

base and a sample containing diatoms from the base of the Mixed Clastics Member (Figure 5.1. The diatom assemblages are indicative of the *D. hustedtii* zone or top of *D. hustedtii-D lauta* subzone d which is early late Miocene, between 8.5 to ~9.2 Ma (Barron and Isaacs, 2001). The benthic foraminiferal assemblages reported by Brabb and Parker (2005) and Malmborg et al. (2008) are upper Mohnian Stage (~ 9.4 Ma to 7.1 Ma, according to Barron and Isaacs, 2001). Consequently, the ages of the Dolomitic Phosphatic Shale and the Porcelanite and Shale members are younger than 15 Ma and older than 8.5 Ma.

The age of the Mixed Clastic member is well documented by the presence of diatoms throughout its entire stratigraphic extent. The section includes microfossils indicative of deposition between the top of the *D. hustedtii-D lauta* subzone d (~9.2 Ma) and the *Thalassiosira antigua* zone (8.4 to 7.6 Ma) (ibid). The few USGS Benthic Foraminiferal samples are upper Mohnian Stage (~ 9.4 to 7.1 Ma). Consequently, the Mixed Clastics member was likely deposited between ~9.2 and 7.6 Ma.

The Cherty Diatomite member contains a sample from diatom zone *D. hustedtii* or the top of *D. hustedtii -D lauta* subzone d which is from the early late Miocene and between ~9.2 to Ma. The USGS benthic foraminiferal dataset samples in this member are upper Mohnian Stage (~ 9.4 to 7.1 Ma). Consequently, the Mixed Clastics member was likely deposited between 9.2 to 8.5 Ma.

Sediment Source and Depositional Environment

The depositional environment, energy regime and diagenetic history vary for each of the members in the Point Dume-Paradise Cove section. The interplay between these factors has resulted in a stratigraphically heterogeneous sequence of the Monterey Formation.

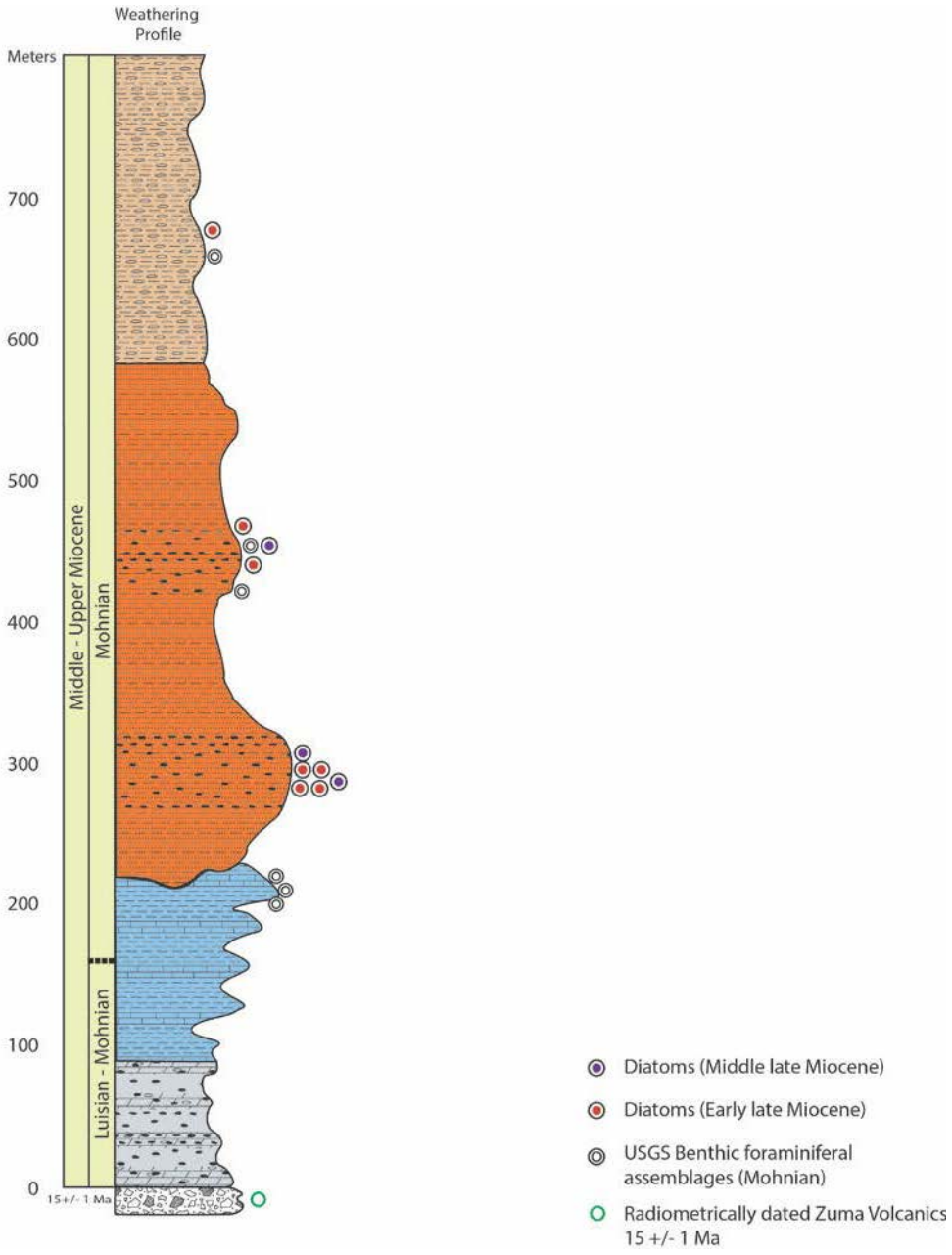

FIGURE 5.1. Stratigraphic column with locations of radiometric and biostratigraphic samples

The sequence of the environments for the section goes from a sediment-starved deep marine banktop or basin where the Dolomitic Phosphatic Shale member was deposited, next to the basin floor environment where higher productivity accumulation of biosiliceous sediments formed the Porcelanite and Shale Member, to the higher energy slope setting of the lower portion of the Mixed Clastic Member followed by an off-channel / levee environment where the upper portion of the Mixed Clastic member was deposited. The final portion of this sequence is the Cherty-Diatomite member that was deposited in a high-productivity setting, most likely a bathyal bathymetric high or other environment isolated from coarse siliciclastic sediments (Ingle, 1981) within a fluctuating oxygen minimum zone.

While the deep basin was likely the depositional setting for deposition of the hemipelagic, biogenic sediments, there were links to the mainland continental shelf and terrigenous clastics (Schwalbach, et. al, 2007) that contributed large amounts of sediments in the Mixed Clastic member. The bulk of the sand, silt and cobbles seen in the slumps, conglomerate and sandstone beds that comprise the lower part of the Mixed Clastic member were deposited by high-energy turbidity currents or by mass wasting on a relatively steep slope setting adjacent to a distal channel of the Tarzana fan (Sullwold, 1960) as it spread southwestward around a proto- Santa Monica Mountain high, possibly related to the Conejo Volcanics. As the Tarzana fan moved south and south westward, it incorporated glaucophane/metamorphic rock fragments from San Onofre Breccia / Catalina Schist that were eroded from the Schist High. (Figure 2.5 in Background Chapter, Redin, 1991; Figure 2.6 in Background Chapter, Wright, 1991). Local paleocurrent indications from ripple cross-bedded sandstone show transport from the east (in Miocene coordinates) (Figure 5.3).

In addition to finely laminated diatomite and chert layers that are rhythmically layered and

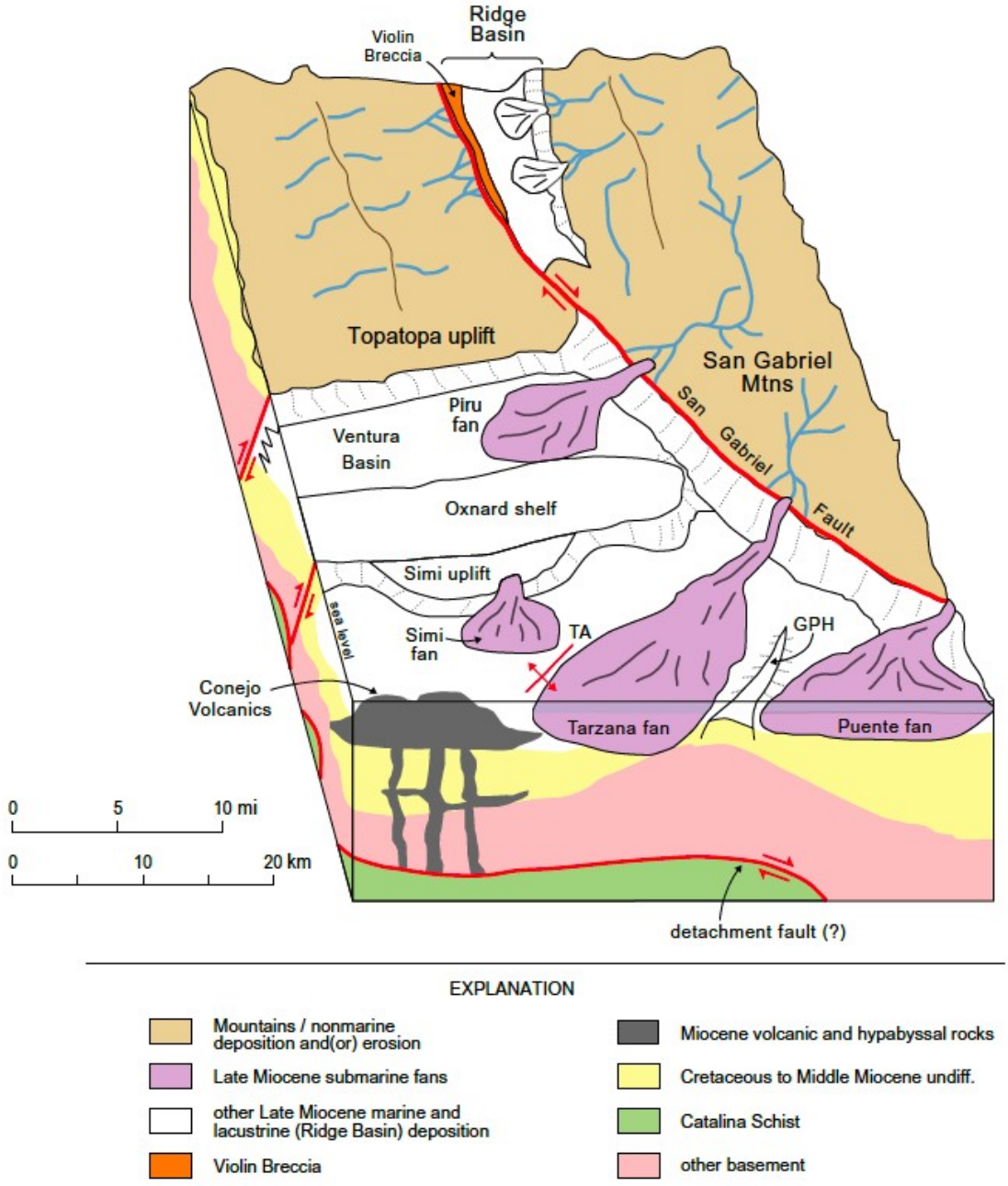

FIGURE 5.2. Possible pathway for Tarzana fan. Relative to Point Dume and Paradise Cove (Rummelhart and Ingersoll, 1997). The paleogeographic location of Point Dume-Paradise Cove would have been just south of the extent of this block diagram.

undisrupted, the Cherty-Diatomite member also contains speckled beds that are likely formed when the finely laminated diatomite is eroded, disrupted and becomes a gravity flow which holds the small flecks of diatomite in suspension (Chang et. al, 1999).

A comparison between the models proposed by Redin (1991, Figure 2.5 in Background Chapter), Wright (1991, Figure 2.6 in Background Chapter) and Rummelhart and Ingersoll (1997, Figure 5.2) suggests that the Tarzana Fan may have been the primary source of the coarse clastics that accumulated in the Point Dume-Paradise Cove section during the late Miocene. Redin (1991) discusses the input from three coalescing fans into the Los Angeles basin. The Santa Ana and the San Gabriel fans are sourced from the eastern and north central portion of the basin respectively and the Tarzana fan from the northwestern Los Angeles basin. For the area by the Malibu Coast fault near Point Dume and Paradise Cove, Redin (1991) suggests a possible source as being a westward branch of the Mohnian Tarzana fan that flowed westward of Santa Monica and down approximately south of Malibu (Figure 2.5).

The tectonic history of this area complicates the story of tracing the direction of sediment supply since there was both rotation and lateral movement occurring near the Point Dume-Paradise Cove area. The palinspastic map of Redin (1991), Figure 2.5 in Background Chapter shows the fan going to the west but this does not account for tectonic rotation. Accounting for rotation would result in the sediment supply direction towards the southwest (from the southeast) during deposition of the Point-Dume and Paradise Cove sequence. Wright (1991) describes the Point Dume-Paradise Cove area as being outboard of the Los Angeles Basin and since 20 Ma, then rotated in a clockwise direction and moved in a left-lateral direction along the Malibu Coast and Anacapa-Dume faults.

Additionally, Wright (Figure 2.6 in Background Chapter) depicts uplifted areas or

"schist highs" bounded by the Newport Inglewood Fault Zone and the Palos Verdes Fault during the Middle Miocene (14 Ma) which suggests a likely path way for Catalina Schist and/or San Onofre Breccia sediment towards Point-Dume and Paradise Cove to the west.

The upper Mohnian Rancho and Hauser sandstones are the petroleum reservoirs in the LA Basin found at Sawtelle, Cheviot Hills, East Beverly Hills, West Beverly Hills and Inglewood fields and represent sediments that were deposited near the channel of the westernmost branch of the Tarzana fan. The branch of the Tarzana fan supplied much of the sediments into the Los Angles base during the Upper Mohnian and these sandstones may have stratigraphic equivalents that extend to the west of the basin to near the Point Dume-Paradise Cove area. A correlation (Figure 5.3) from west to east from Sovereign Well Malibu 1 (037-05937) to Beverly Hills East (Type Log) shows the presence of sands in the Malibu 1 (037-05937) well and the Mixed Clastic Member of Point Dume-Paradise Cove, but these are fewer and thinner in this part of the LA Basin than the massive units seen in the Beverly Hills East (Type Log). This suggests that the section at Point Dume-Paradise Cove is located on the possible upslope fringes of the channel carrying clastic sediment from the Tarzana fan.

The sandstone analysis of the composition of the framework grains sheds some light on the question of provenance and transport direction. Twelve of the seventeen analyzed sandstones contain some metamorphic rock fragments such as glaucophane and glaucophane schist. These are almost certainly derived from the Catalina Schist or San Onofre Breccia (Table 1 in Appendix). The Trancas Formation that interfingers with the Monterey Formation in the area south of the Malibu Coast Fault (Yerkes and Campbell, 1979) contains sedimentary breccias with glaucophane schist detritus from Catalina Schist or San Onofre Breccia as well as sandstones, mudstones and siltstones.

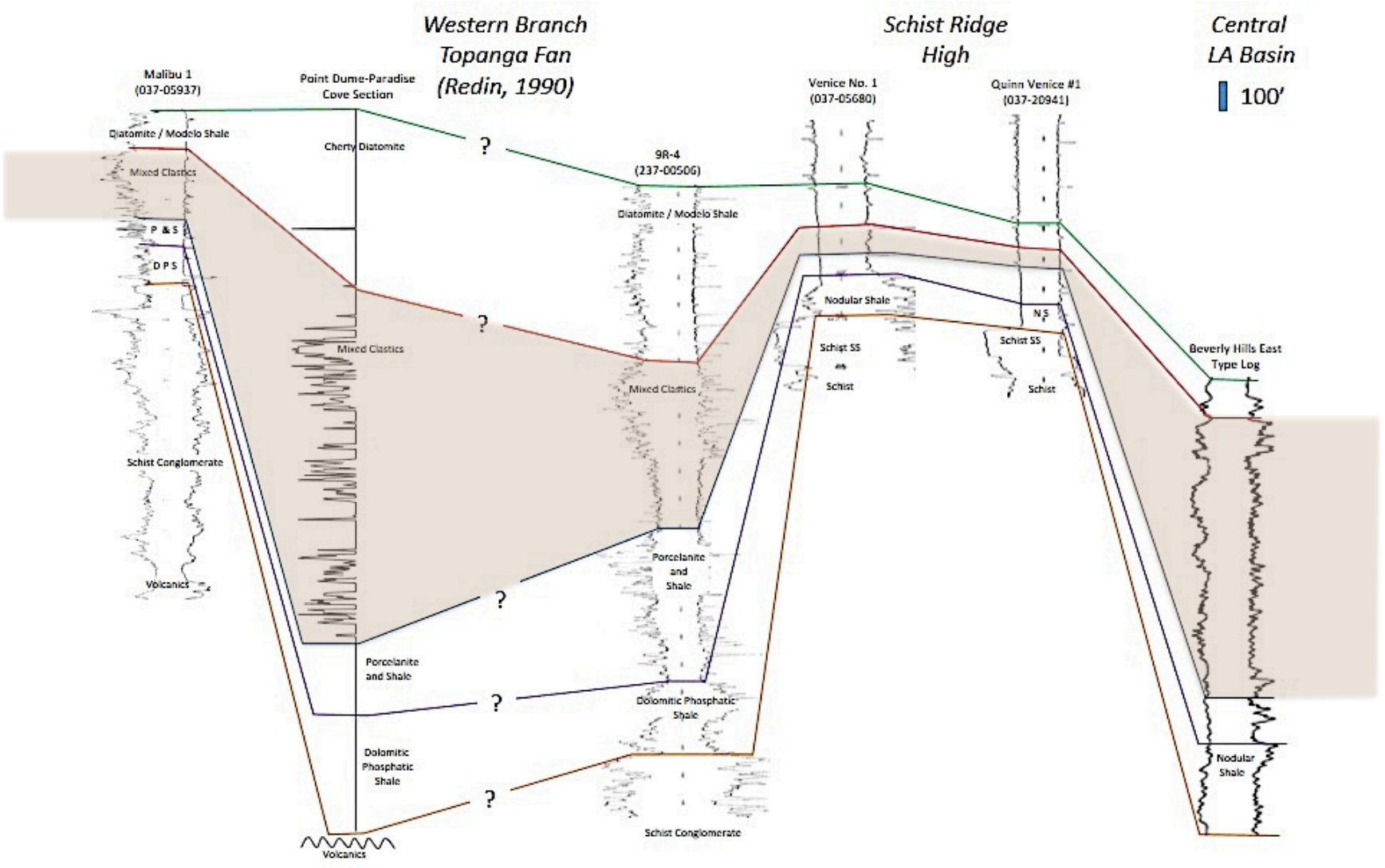

FIGURE 5.3. West to east correlation from Malibu and the Point Dume-Paradise Cove section to Beverly Hills East field showing overall changes in thickness in sandstones suggesting different locations relative to the westernmost branch of the Tarzana fan (logs are not shown on equal scales).

Rummelhart and Ingersoll (1997) and Sullwold (1960) did not report any glaucophane schist in their petrographic analyses of the age-equivalent Modelo Formation of the Santa Monica Mountains (north of the Malibu Coast fault), although they do document some metamorphic rock fragments in the lowermost Modelo. However, these are fine-grained metasediments locally derived from the Santa Monica Slate, not the Catalina Schist with its characteristic glaucophane. The fact that the lowermost Modelo Sandstone contains Santa Monica Slate that is not found in the sediments in the Point Dume-Paradise Cove section is an important one as it clarifies the location with respect to the Western Transverse Ranges, the Santa Monica Mountains and the Los Angeles Basin blocks (Figures 2.1 and 2.2 in the Background Chapter).

The study area is demonstrated to be part of the Southwestern block of the Los Angeles Basin and is separated from the Northwestern block by faults related to the Santa Monica-Raymond Hill Fault system. The area not only shares the same basement material as the Palos Verdes area (see Figure 2.3 in Background) but there is evidence that suggests that the clastic sediments found in Point Dume-Paradise Cove contain contribution from much more local sources such as the Schist Ridge high described by Wright (1991) and Redin (1991).

Wright's Middle Miocene (14 Ma) reconstruction of the Los Angeles region back-rotates the Malibu Coast fault to a SW-NE trend and places Malibu relatively south of its present day orientation and more directly outboard (west) of the Schist Ridge high and the Los Angeles basin proper. Accounting for left-lateral strike slip with clock-wise rotation, the Schist High and Palos Verdes become more directly east of Point Dume-Paradise Cove area. There is positive evidence that the clastic sediment was jointly sourced from the San Gabriel granitics (feldspathic arenites found in the Tarzana Fan) (Sullwold, 1960), the Catalina Schist (metamorphic grains like glaucophane and glaucophane schist) (Stuart, 1976 and Conrad and Ehlig, 1987) and some

volcanics (Yerkes and Campbell, 1979), but not specifically from the central or eastern Santa Monica Mountain terrane where slate/phyllite formed the basement (Yerkes and Campbell, 1979).

Finally, the ripple cross-lamination-derived paleocurrent data (Figure 5.4) that is corrected for rotation and bedding orientation, suggests that flow direction was from east to west or from southeast to northwest in modern coordinates. This transport direction from the Schist Ridge high is consistent with the inclusion of metamorphic rock fragments in the conglomerates and sand grains, including the mineral glaucophane that is characteristic of the Catalina Schist (Stuart, 1976). Unfortunately, the only paleocurrent indicators in the Point Dume-Paradise Cove succession are small-scale ripple cross-lamination, which may indicate local, or even overbank transport laterally outward from a submarine channel, rather than the main regional transport direction.

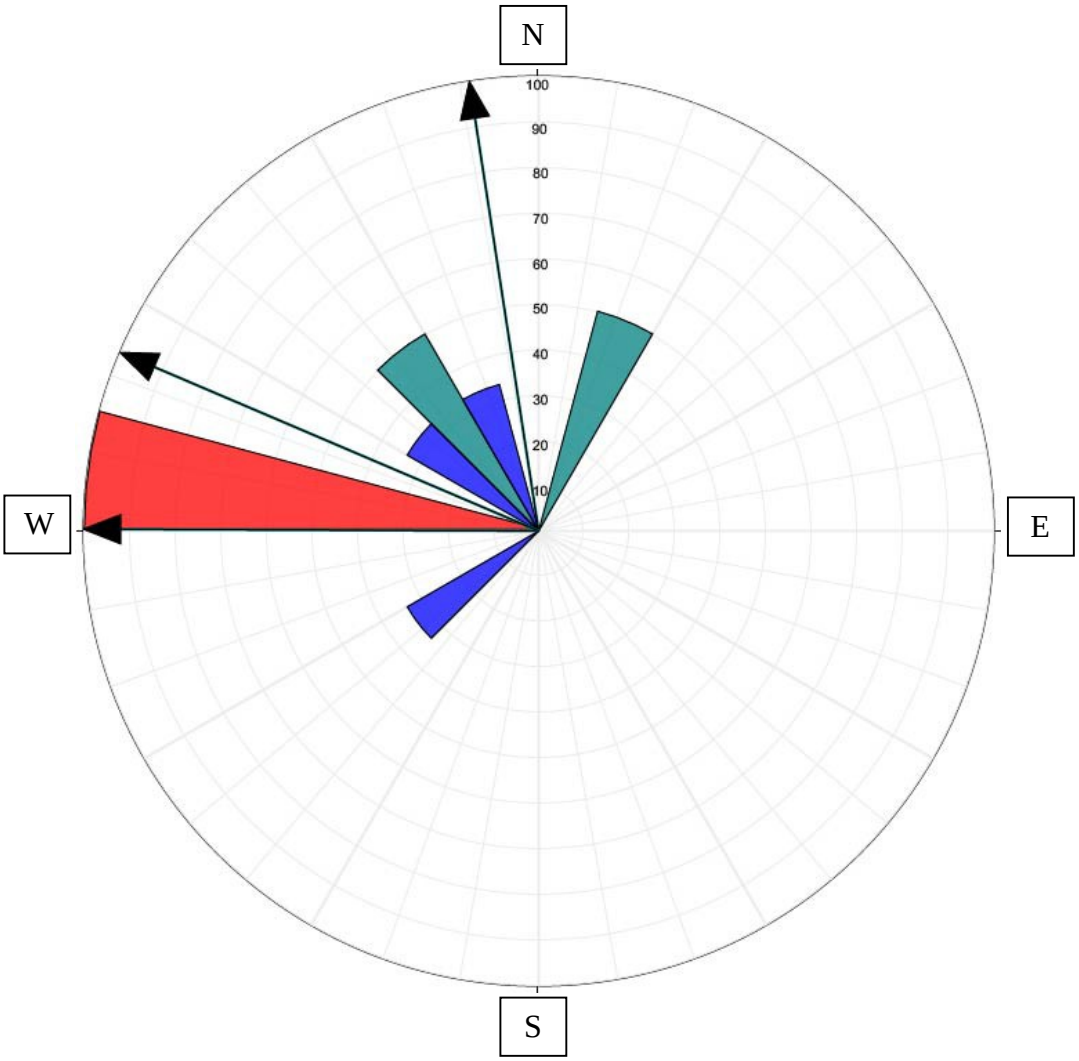

FIGURE 5.4. Paleocurrent data from ripple cross-laminations. In sandstones in the Mixed Clastics member, Point Dume to Paradise Cove. N=3. The different colors are the three attitudes and different beds (within 5 meters of each other) data for which cross-lamination data exists. The 3 mean vector arrows indicate average paleocurrent direction based on cross-laminations.

CHAPTER 6

CONCLUSION

This research project documented and interpreted the lithostratigraphy of the Monterey Formation exposed in Malibu, California between Point Dume and Paradise Cove. A detailed stratigraphic study of this area had not previously been completed even though the Monterey Formation – an important hydrocarbon source and reservoir rock in California - has long been of key interest and focus in the Los Angeles Basin and the other Neogene basins of California.

The significant findings and contributions of this study are:

1) the >700-meter thick stratigraphic succession south of the Malibu Coast fault between Point Dume and Paradise Cove can be subdivided into four lithostratigraphic members that consist, from bottom to top, of: the Dolomitic Phosphatic Shale, the Porcelanite and Shale, the Mixed Clastics and Cherty Diatomite units. These units have some similarities to informal members of both the Miocene Modelo and Monterey formations in the Los Angeles, Ventura, Santa Barbara and Santa Maria basins.

2) percent sandstone for the section and sandstone petrographic analysis revels that sandstone is almost exclusively present in the middle part of the succession within the Mixed Clastics member and near the base of the overlying Cherty Diatomite member. The lowest sandstone is near the contact between the Porcelanite and Shale member and the Mixed Clastics member. The uppermost sandstone bed is part of the Cherty Diatomite member, located near the contact between the two members. Thin section petrography shows that most sandstones are feldspar and lithic-rich. The lithic arenites are mostly located lower in the section and the arenites and arenites containing feldspars are found in the middle to upper portions of the section.

3) siliceous sedimentary rocks are composed of opal-CT in the lower portion of the section and opal-A phase silica is found in the diatomites in the upper portion of the section and is interbedded with opal-CT phase silica in chert layers of the Cherty Diatomite member.

4) spectral gamma ray (potassium, uranium and thorium) data was collected through the succession. Potassium has a lower concentration in the lowermost Dolomitic Phosphatic Shale member and uranium concentration is significantly higher in the lower members of the section. Thorium concentrations show sharp peaks in the Dolomitic Phosphatic member and the Mixed Clastic member. The total gamma ray values show a general trend going from high (143.6 API) at the base of the section to low (55.6 API) at the top of the section. Total organic carbon (TOC) is highest in the Porcelanite and Shale member and the Dolomite Phosphatic Shale member, reaching values as high as 14.63 %. The upper member (Cherty Diatomite) contains few mudrocks and TOC content is low.

5) diatoms and benthic foraminifera biostratigraphic data show some overlap and between ages. The base of the section is constrained by the radiometrically dated Zuma Volcanics (15 +/- 1 Ma). The USGS benthic foraminiferal samples are Mohnian in the upper three members. Diatoms provide a range of ages from Middle late Miocene and Early late Miocene that overlap throughout the section so do not constrain the ages of particular members.

6) a west to east correlation linking a western point of the Los Angeles Basin at Malibu (Point Dume-Paradise Cove) to prolific oil fields like Beverly Hills to the east shows overall changes in sandstone thickness, likely due to position relative to the westernmost branch of the Tarzana fan or deposition on the Schist Ridge high. The Point Dume-Paradise Cove succession appears to have been deposited at the edge of the channel of the southwest-

flowing submarine fan.

7) The Dolomitic Phosphatic shale member was deposited in a sediment starved deep marine bank top or basin and the Porcelanite and Shale member was also deposited in a basin environment. The high energy deposits found in the Mixed Clastics member are indicative of slope settings at the bottom of the member and then off-channel / levee environments at the top of the member. The bulk of the sand, silt and cobbles in the Mixed Clastics were likely derived from the Tarzana fan and transported southward, but incorporated glaucophane / metamorphic rock fragments from San Onofre Breccia / Catalina Schist that were eroded from the Schist High. Local paleocurrent indications from ripple cross-bedded sandstone show transport from the east (in Miocene coordinates). The Cherty Diatomite member was deposited in a bathyal / bathymetric high / high productivity area with a fluctuating oxygen minimum zone where it was isolated from input of coarse siliciclastic sediments.

CHAPTER 7

FUTURE WORK

This study provides a framework for understanding Monterey Formation exposures between Point Dume and Paradise Cove in Malibu, California. The preliminary findings suggest that the clastic input into the section was from a secondary branch of the Tarzana Fan. Detailed correlations of logs from the Point Dume area to Los Angeles Basin would help delineate the extent and thicknesses of the submarine fans and provide a better understanding of lateral facies variations across this area.

The biostratigraphic data available to or produced by this study were useful, but as there was overlap in the ages of the diatoms, it was not sufficient to date the individual members or determine rates of sedimentation. Additional sampling and analysis for diatom, calcareous nannofossil, or planktonic foraminiferal zonations throughout the section would be very useful to provide more refined dating and for basin wide correlation across the rest of the Los Angeles basin.

The spectral gamma ray data (uranium-potassium) could be used in conjunction with knowledge of volcanic activity in the area to identify any volcanic ash beds by high thorium content that may be used for tephrochronology.

Qualitative sandstone petrology was completed on 17 samples in this thesis research, however a much more rigorous quantitative petrographic analysis of detrital modes would permit better understanding of lateral and vertical variations of the sandstones and better document the provenance history.

Understanding the paleotectonic history of the section would benefit from an in-depth structural study of the Malibu Coast Anacapa-Dume fault system and the larger Santa Monica-

Raymond fault system that was responsible for tectonic translation of the study area through and after its deposition, and may be responsible for the repeated section of the Dolomitic Phosphatic Shale member. Furthermore, as the heterogeneous and thin-bedded rocks in this area have been strained by the Malibu Coast-Anacapa-Dume fault system, this location would provide an excellent site for a study of mechanical stratigraphy and strain partitioning between different rock types and at different scales within an active fault system.

APPENDICES

APPENDIX A

SPECTRAL GAMMA RAY AND ROCK TYPE DESCRIPTIONS

APPENDIX A: Spectral Gamma Ray Data and Rock Type Descriptions

Meter	Assay #	% Potassium	Uranium ppm	Thorium ppm	% Rock type per meter
1	494#	0.4	5.4	1.5	30 % dolostone 30% mudstone 30% porcelanite
2	495#	0.4	2.8	1.4	35% dolostone 65% siliceous mudstone
3	covered				
4	covered				
5	497#	0.7	5.8	2.9	60% mudstone 40% siliceous flaky fissile mudrock with phosphatic laminations
6	498#	1.1	6.6	3.2	100% deformed beds of siliceous mudrocks
7	499#	1	4	2.9	100% deformed beds of siliceous mudrocks with porcelanite (?)
8	500#	0.5	1.8	1.4	30% mudrock 60% dolostone
9	covered				Some fissile mudstone seen
10	501#	1.1	8.5	3.9	100% fissile mudstone
11	502#	0.5	2.8	1.6	70% dolostone 30% mudstone
12	503#	1.1	7.2	3.9	10% dolostone

					70% very organic rich, "hot" mudstone
13	504#	0.9	8.7	3.3	100% thinly bedded grey mudstone, interbedded with fissile mudstone
14	505#	0.8	6.6	2.5	100% highly weathered pale grey porcelanite? Siliceous mudstone?
14.5	506#	0.5	4.6	2.4	45% dolostone, 55% porcelanite
15	507#	6.8	7.1	3.2	25% mudstone 75% dolostone
16	508#	0.9	6.9	4.2	100% phosphatic mudrock
17	509#	1	6.9	4.2	100% phosphatic mudrock
18	510#	1.1	8.9	3.8	70% phosphatic mudrock with fissile beds 30% dolostone
19.5	511#	0.9	8.2	2.9	Mostly covered but there is dolostone at the base of the section and a phosphatic mudrock. Measurement taken at the mudrock.
20	covered				
21	covered				
22	covered				
23	512#	0.5	4.4	2	Mostly covered but measurement taken on dolostone bed
24	covered				
25	covered				

26	513#	1.1	8.4	4.6	10% mudstone and 90% covered with vegetation
27	514#	1.1	9.1	4.5	100% phosphatic rich mudstone
28	515#	1	10.7	5.3	100% fissile phosphatic rich mudstone
29	516#	0.6	5	2.2	80% nodular dolomite and 20% phosphatic mudrock
30	517#	1	13.5	3.5	100% phosphatic rich mudstone with lenses and blebs
30.8	518#	0.4	2.8	1.8	50% dolostone, 50% phosphatic mudstone
32	519#	0.7	7	2.8	60% brittle, hard, cherty mudstone
33	520#	0.6	1.9	1.7	40% very organic rich mudstone 20% brown, waxy mudrock interbedded
34	521#	1	10.5	3.6	80% cherty mudstone 30% mudstone
35	522#	0.8	8.8	2.3	40% cherty mudstone 30% dolostone stratoform 40% mudstone
36	523#	0.4	7	1.1	60% dolostone 30% dolostone
37	524#	0.9	11.1	2.1	70% organic rich phosphatic mudstone 30% fissile mudstone, very phosphatic rich 70% dolostone

38	525#	1.1	12	3.6	90% fissile mudstone with phosphatic lenses
39	526#	0.6	9.6	2.8	10% opal-CT porcelanite 50% muddy porcelanite
40	527#	0.7	9.7	2.6	50% dolostone 60% mudstone
41	528#	0.3	4.5	1.2	40% dolostone 80% dolostone
42	529#	0.8	11.1	2.8	20% mudstone 100% light grey, organic rich, phosphatic rich dolostone?
43	530#	0.7	9.3	2.4	80% dolostone and 20% mudstone
44	531#	0.8	13.5	2.9	70% fissile, "hot", organic rich mudstone
45	532#	0.7	17.5	3.3	30% porcelanite 100% "hot" and muddy porcelanite
46	533#	0.7	20.3	3.1	50% "hot" fissile mudstone
47	534#	0.9	15.7	4.3	50% muddy porcelanite 50% organic rich, phosphatic mudstone
48	535#	0.9	14.6	4.5	50% muddy porcelanite 50% mudstone
49	536#	0.8	21.9	4.6	50% cherty (?) porcelanite 60% "hot" mudstone
50	537#	0.7	16	2.6	40% porcelanite 60% porcelanite
					40% porcelaneous mudstone

51	538#	0.8	20.3	7.3	40% "hot" mudstone 60% cherty lenses in mudstone
52	539#	1.1	18.2	5.8	50% phosphatic rich mudstone 50% cherty (?) porcelaneous mudstone
53	540#	1.1	18.6	4.2	50% fissile mudstone 50% muddy porcelanite
54 - 83	covered				
84	541#	0.6	3.5	1.9	95% dolostone 5% chert
85	covered				
86	542#	0.9	10.9	3.6	45% Dolostone 55% Cherty mudstone
87	543#	0.8	14.6	3.5	80% porcelanite 20% chert
88	544#	0.9	16.9	4.5	90% porcelanite 10% lenses of chert
89	545#	0.9	15.2	3.9	60% siliceous porcelanite
90	546#	0.3	6	2.5	80% siliceous mudstone 20% chert lenses
91	547#	0.8	24.8	3.6	40% blocky porcelanite with opal-CT (?) 60% fissile mudstone
92	548#	0.6	6.3	2.8	50% highly deformed chert 50% very pure porcelanite
93	549#	0.2	2.9	1.5	10% chert 70% porcelanite 20% dolostone stratoforms
94	550#	0.7	10.2	4.7	80% muddy porcelanite

					20% mudstone
95	551#	0.8	16.6	5.5	80% porcelanite
					20% highly weathered mudstone
96 - 102	covered				
103	552#	1	8.6	4.4	80% muddy porcelanite
					20% laminated mudstone
104	553#	0.8	11.1	4.1	100% porcelanite
105	554#	0.6	7.3	2.6	10% chert
					90% muddy porcelanite
106	555#	1.2	9.1	5.5	100% muddy porcelanite
107	556#	1	11	4.1	100% chert porcelanite
108	covered				
109	covered				
110	covered				
111	covered				
112	covered				
113	557#	1.1	14.9	4.6	60% porcelanite
					40% organic rich porcelanite
114 - 121	covered				
122	558#	0.8	7.1	3.7	100% muddy porcelanite
123	559#	1.1	11.1	5	80% fissile mudstone
					20% muddy porcelanite
124	560#	1	15.4	4.4	50% porcelanite
					50% cherty porcelanite
125	561#	1.2	11.6	5.4	65% organic rich mudstone
					35% porcelanite
126	562#	1.2	14.2	5.5	60% organic rich mudstone
					40% muddy porcelanite
127	563#	0.9	13.2	4.3	50% muddy porcelanite

					50% fissile phosphatic rich mudstone
128	564#	1.1	15.1	5.5	50% organic rich porcelanite
					50% fissile phosphatic rich mudstone
129	565#	0.6	12.5	2.6	80% dolostone and 20% mudstone
130 - 178	fault / burnt shale section				
179	565# (check assay #)	1	15.9	4.4	60% muddy porcelanite
					40% fissile mudstone
180	566#	1	12.4	3.3	80% porcelanite
					20% fissile mudstone
181	568# (skipped 567#)	0.7	8.7	2.3	10% cherty layers
					60% muddy porcelanite
					30% fissile mudstone
182	569#	0.8	6.8	3.7	70% muddy porcelanite
					30% fissile mudstone
183	570#	0.5	4.9	1.8	60% muddy porcelanite
					40% fissile mudstone
184	571#	0.8	17.4	3.7	10% organic rich, fissile mudstone
					90% organic rich porcelanite
185	572#	0.6	7.1	1.7	100% cherty porcelanite
186	573#	1.1	10	3.9	70% muddy porcelanite
					30% fissile mudstone
187	574#	1.1	10.8	4	80% fissile mudstone
					20% muddy porcelanite

188	575#	0.8	7.5	3.6	90% muddy porcelanite 10% fissile mudstone
189 - 202	covered section				
203	576#	0.9	5.4	3.1	95% porcelanite 5% fissile mudstone
204	577#	0.8	4.8	2.3	60% clean porcelanite 30% sandstone 10% fissile mudstone
205	578#	1.1	8.6	4.9	30% sandstone 30% muddy porcelanite 40% fissile mudstone
206	579#	1.1	7.6	3.7	50% siltstone 30% muddy porcelanite 20% fissile mudstone
207	580#	0.7	5.5	1.7	40% porcelanite 60% siliceous mudstone
208	581#	0.9	7.4	2.5	50% fissile, highly siliceous mudstone 50% siltstone
209	582#	0.7	4	2.5	80% dolostone 10% siliceous mudstone 10% siltstone
210	583#	1.1	10.2	3.2	45% muddy porcelanite 45% siltstone 10% dolostone
211	584#	1.1	10.3	3	50% muddy porcelanite 50% siltstone
212	585#	0.8	5.9	2.7	80% porcelanite 20% siliceous rich siltstone

213	586#	1	6	2.7	25% mudstone 25% cherty porcelanite 25% dolostone 25% porcelanite
214	584#	0.8	5.8	4	100% mudstone
215	588#	0.7	3.8	2.2	50% soft mudstone 45% siliceous rich mudstone 5% dolostone
216	589#	1	4.2	4.6	30% mudstone 30% chert 30% dolostone 10% sandy lenses/conglomerate
217	590#	1	2.4	3.9	40% sandstone 60% organic rich mudstone
218	592# (skipped assay 591#)	1.4	2.3	3.9	60% sandstone 40% mudstone
219	593#	1.1	4.2	3.4	70% dolostone 30% sandstone 10% mudstone
220	594#	1.2	3.5	3.9	80% mudstone 20% sandstone
221	595#	1.5	4.1	2.9	50% sandstone 50% mudstone
222	596#	1.3	4.6	3.1	60% mudstone 30% dolostone
223	597#	1	5	3.2	90% mudstone 10% sandstone
224	599# (skip 598#)	1.2	4.6	3.3	80% mudstone

					10% sandstone
					10% dolostone
225	600#	1.2	3	2.6	50% dolostone
					5% cherty conglomerate
					15% sandstone
					30% mudstone
226	601#	1	4.1	3.4	80% mudstone
					90% coarse grained sandstone
227	602#	1.5	3.3	3.6	10% sandstone
228	603#	1.5	2.8	3.7	50% mudstone
					50% sandstone
229	604#	1.2	3	3	50% sandstone
					50% mudstone
230	605#	0.8	3.9	2.8	50% sandstone
					50% mudstone
231	606#	1.1	5.4	2.7	75% sandstone
					25% mudstone
232	brecciated zone / covered				
233	brecciated zone / covered				
234	brecciated zone / covered				
235	brecciated zone / covered				
236	brecciated zone / covered				
237	607#	1.3	5.4	2.8	80% sandstone
					20% mudstone
238	608#	0.6	4.1	2.3	50% mudstone

					40% sandstone
					10% dolostone
239	609#	1	6.5	4.4	60% sandstone
					30% mudstone
					10% dolostone
240	610#	0.7	5.3	2.2	50% sandstone
					50% mudstone
241	611#	0.8	5	2.4	70% sandstone
					30% mudstone
242	612#	0.8	3.4	2.6	100% mudstone
243	613#	0.9	4.2	3.3	100% mudstone
244	614#	1	3.7	2.2	70% mudstone
					30% sandstone
245	615#	1	2.6	2.7	80% mudstone
					20% sandstone
246	616#	1.4	2.7	3.3	50% sandstone
					50% mudstone
247	617#	1.2	4	2.9	50% sandstone
					50% mudstone
248	618#	1.2	4.3	3	50% sandstone
					40% mudstone
249 - 258	unmeasured				
259	619#	1	2.9	2.6	60% mudstone
					40% sandstone
260	620#	0.9	3	3	60% mudstone
					40% sandstone
261	621#	1	4	2.5	60% sandstone
					40% mudstone
262	622#	0.7	4.7	2.5	40% mudstone

					30% dolostone
					30% sandstone
263	623#	1.1	4	2.4	50% mudstone
					50% sandstone
264	covered				
265	624#	1.1	5.1	2.7	100% mudstone
266	625#	1.2	3.4	2.9	60% conglomerate
					40% mudstone
267	626#	0.9	3	2.9	80% mudstone
					20% sandstone lenses
268	627#	1	2.8	3.1	50% mudstone
					50% sandstone
269	628#	1	3.8	2.3	50% mudstone
					50% sandstone
270	629#	1.1	4.7	3.7	20% sandstone
					80% mudstone with white flecks
271	630#	1.2	4.9	2.7	50% sandstone
					50% mudstone
272	631#	0.8	4.5	2.4	80% mudstone with white flecks
					20% sandstone
273	632#	0.7	3.1	2.2	90% mudstone
					10% sandstone
274	633#	0.8	3.7	2.1	60% mudstone
					40% sandstone lenses
275	635#	1.4	2.9	2.4	80% conglomerate
					10% sandstone with dolomite
					10% highly deformed dolomite
276	636#	1.2	1.9	2.7	20% mudstone
					20% chert

					20% dolostone
					40% sandstone with dolostone and carbonate cement/veins
277	637#	1	5.2	2.4	80% mudstone
					20% dolostone
278	638#	1.2	4.4	3.8	90% mudstone
					10%% sandstone as clasts in mudstone
279	639#	1	4.9	2.7	60% lighter colored mudstone with laminations
					40% very organic rich mudstone
280	640#	1.2	6.5	3.8	80% mudstone
					20% siltstone with sandstone clasts
281	641#	1.1	3.8	5.2	90% organic rich mudstone
					10% sandstone in lenses/ripples
282	642#	0.8	4.5	1.6	60% mudstone
					40% dolostone
283	643#	1	3.2	2.4	30% muddy conglomerate
					30% sandstone
					20% mudstone
					10% dolostone
284	644#	0.7	3	1.7	50% sandstone
					50% mudstone
285	645#	0.7	2.1	1.5	90% sandstone
					10% mudstone
286	646#	0.7	2.7	1.4	80% sandstone
					20% mudstone
287	647#	0.5	2.9	2.4	70% mudstone

						30% sandstone
	288	648#	0.7	2.1	2.2	60% sandstone
						40% siltstone
	289	very deformed sandstone				
	290	very deformed sandstone				
	291	649#	0.7	2.6	1.8	50% mudstone
						50% siltstone
	292	650#	0.7	3.4	2.6	50% SS
						40% siltstone
						10% diatomite, white, low density
	293	651#	0.8	2.7	2	60% coarse grained sandstone
						30% "fluffy" diatomite
	294 - 324	rough estimate of covered section				
	325	652#	1.1	1.7	2	90% sandstone
						10% diatomite, white, low density
	325.5	653#	0.8	2.5	2.5	100% diatomite
	326	654#	0.8	2.6	1.8	60% coarse grained sandstone
						40% finer grained sandstone
	327	655#	0.6	3	2.4	80% diatomite
						20% dolomitic diatomite
	328	656#	0.8	2.8	2.7	55% diatomite
						45% dolomitic diatomite
	329	657#	0.8	2.8	2	80% diatomite
						15% dolomitic diatomite
						5% sandstone
	330	658#	0.9	3.3	3.2	90% diatomite

					10% muddy diatomite
331	659#	0.8	3.4	3.5	100% diatomite
332	660#	0.9	3.2	4.1	100% diatomite
333	covered / inaccessible				
334	covered / inaccessible				
335	covered / inaccessible				
336	covered / inaccessible				
337	covered / inaccessible				
338	661#	0.7	1.6	2	100% dolostone
339	662#	0.8	2.1	3.5	80% mudstone
					20% dolostone
340	663#	0.8	3.3	3.3	80% siliceous mudstone
					20% sandstone lenses
341	664#	1.4	4.3	5.3	60% muddy diatomite
					40% siltstone
342	665#	0.7	2.8	3.5	50% dolomitic diatomite
					50% muddy diatomite
343	666#	0.8	2.5	5	60% siliceous mudstone
					40% chert
344	667#	1	4.5	7	70% diatomite
					10% sandstone
					10% cherty, siliceous mudstone
					10% muddy diatomite
345	668#	1	3.7	7.2	40% diatomite
					30% muddy diatomite

					30% sandstone
346	669#	0.9	3.5	5.6	50% muddy diatomite
					50% sandstone
347	670#	1.1	3.2	4	50% muddy diatomite
					50% sandstone
348	unmeasured				
349	unmeasured				
350	unmeasured				
351	671#	0.9	2.2	3.5	70% muddy diatomite/carbonate
					30% sandstone
352	672#	0.9	3.1	3.3	50% dolomitized diatomite
					50% muddy diatomite
353	673#	1	2.7	2.9	60% dark mudstone
					30% sandstone
					10% siliceous mudstone
354	674#	1	2.3	2.2	60% dolomitic diatomite
					30% siltstone and sandstone
					10% mudstone
355	675#	1	2.7	3.3	80% dolomitic diatomite
					20% sandstone/siltstone
356	676#	1.1	1.6	2.9	50% sandstone
					50% dolomitic diatomite
357	677#	0.9	2.7	3.7	50% sandstone
					50% muddy dolomitic diatomite
358	covered				
359	covered				
360	covered				
361	678#	0.9	3.1	1.9	80% dolomitic diatomite
					20% sandstone

362	679#	0.8	3.4	1.6	70% siliceous mudstone 30% dolomitic diatomite
363	680#	1.1	2.4	2.8	80% siliceous mudrock 20% diatomitic mudrock
364	681#	1	3	2.4	90% siliceous mudstone 10% dolomitized diatomite
365	682#	1.1	2.7	2.1	90% siliceous mudstone 10% sandstone lenses
366	683#	1.2	2.2	2.5	90% sandstone with carbonate cement 10% mudstone
367	684#	1.1	2.2	2.4	50% mudstone, possibly a conglomerate? 50% sandstone with carbonate cement
368	685#	1.3	2.9	3.1	50% sandstone 50% conglomerate/mudstone?
369	686#	1	3.2	3.3	80% mudstone 20% sandstone
370	687#	1	2.8	3.8	80% siliceous mudrock 20% organic rich mudstone
371	688#	1.2	3	2.5	80% sandstone with carbonate cement 20% mudstone
372	689#	1	3.1	3	100% organic rich mudstone
373	690#	1.2	4.1	2.1	20% sandstone 80% mudstone
374	691#	1.1	2.6	2.8	50% sandstone 50% mudstone

375	692#	1.2	2.9	2.7	70% sandstone with carbonate concretions 30% organic rich mudstone
376	693#	0.8	2.1	2.1	50% ripped up, highly deformed mudstone with sandstone 50% sandstone with carbonate concretions
377	694#	0.9	2.9	2.1	50% sandstone 50% mudstone
378	695#	0.9	2.3	2.7	50% siltstone 50% mudstone
379	696#	0.8	2.9	2.8	80% siliceous mudrock 20% sandstone
380	697#	1	2.7	2.1	60% sandstone 20% dolostone 20% mudstone
381	698#	0.5	2	0.8	70% sandstone 30% dolostone
382	699#	0.5	2.1	1.3	50% highly carbonaceous sandstone 50% fissile mudstone
383	700#	0.7	2.5	2.6	60% mudstone 40% sandstone
384	701#	0.8	3.5	2.2	80% siliceous mudstone 20% sandstone
385	702#	0.7	3.1	2	50% carbonaceous mudstone 50% carbonaceous sandstone
386	703#	0.8	2.9	2.3	80% sandstone 20% diatomaceous mudstone

387	704#	1.1	4.4	5.1	60% diatomaceous mudstone 20% sandstone 20% diatomite
388 - 397	covered section				
398	705#	0.5	2.7	2.3	reading taken on dolostone bed, partially exposed
399	706#	0.7	2.7	1.8	50% grey carbonaceous sandstone
400	707#	0.9	3.7	2.1	60% sandstone 40% deformed mudstone
401	708#	0.6	2.8	2.2	80% porcelanite 20% sandstone
402	709#	1.1	3	2.5	50% sandstone 50% siliceous mudstone
403	710#	0.9	3.9	2.2	100% organic rich mudstone
404	711#	0.8	3.3	1.8	100% interbedded sandy organic rich mudstone
405	712#	0.7	2.8	1.9	100% interbedded organic rich mudstone with sand clasts
406	713#	0.7	3.3	1.4	60% white, fluffy diatomite
407	714#	0.7	3.4	1.8	50% diatomite 50% muddy diatomite
408 - 418	covered section				
419	715#	0.9	3.4	2.9	100% mudstone bed
420	716#	1.3	3.3	4.4	50% sandstone 50% mudstone
421 - 424	covered section				

425	717#	1	3.1	3.7	100% mudstone
426	718#	1	3.1	3.4	80% mudstone
					20% sandstone
427 to 437	across creek				
438	719#	0.9	3.3	3.7	100% organic rich mudstone
439	720#	0.9	3	4.4	50% mudstone
					50% sandstone
440	721#	0.9	4	2.9	50% sandstone in lenses
					50% mudstone
441	722#	1.2	4.3	3.8	100% mudstone
442	723#	1.1	3.9	3	90% mudstone
					10% sandstone
443	724#	1.1	3.6	3.1	90% mudstone
					10% sandstone
444	725#	1.1	3.8	2.5	70% sandstone
					30% mudstone
445	726#	1.1	3.8	3.3	50% sandstone
					50% mudstone
446	727#	1.2	4.3	3.2	50% mudstone
					50% sandstone
447	728#	1.4	5	3.6	80% mudstone
					20% sandstone
448	729#	1.1	4.7	4.2	80% mudstone
					20% sandstone
449	730#	1.1	4.2	3.9	70% mudstone
					30% sandstone
450	731#	1.3	4.2	2.6	60% mudstone
					40% sandstone
451	732#	1	3	2.2	60% mudstone

					40% sandstone
452	733#	0.9	3.6	2.8	80% mudstone
					20% sandstone
453	734#	0.9	3.2	1.7	90% mudstone
					10% sandstone
454	735#	0.9	2.8	2.4	90% mudstone
					10% sandstone
455	736#	1.1	3.5	3	80% mudstone
					20% sandstone
456	737#	1.3	3.4	2.7	90% sandstone
					10% mudstone
457	738#	1	4.5	2.3	50% sandstone
					50% mudstone
458	739#	1	4.1	2.5	60% sandstone
					55% mudstone
459	740#	1.2	3.9	2.8	80% mudstone
					20% sandstone
460	741#	1.1	3.2	2.9	80% mudstone
					20% sandstone
461	742#	1.2	4.2	2.6	90% mudstone
					10% sandstone
462	743#	1.2	3.7	4	80% mudstone
					20% sandstone
463	744#	1.3	4.9	3.3	90% mudstone
					10% sandstone
464	745#	1.8	4.4	3.5	50% sandstone
					50% mudstone
465	746#	1	3.4	2.6	70% sandstone with calcareous cement

					30% mudstone
466	747#	1.1	4.1	4.5	50% mudstone
					50% sandstone with calcareous cement
467	748#	1.3	3.9	2.8	50% sandstone
					50% sandstone with calcareous cement
468	749#	0.8	3.5	2.8	70% mudstone
					30% sandstone
469	750#	1.1	2.9	3	50% calcareous mudstone
					50% sandstone
470	751#	1.3	3.9	3.5	50% mudstone
					50% sandstone
471	752#	1.3	3.9	3.5	50% mudstone
					50% sandstone
472	753#	1.7	4.7	10	100% mudstone with calcareous cement
473	glitch with assay number	1.3	3.8	3.6	80% organic rich sandstone
					20% mudstone
474	754#	0.8	3.2	2.9	50% detrital rich sandstone
					50% calcareous mudstone
476	756#	0.7	2.5	2.6	50% calcareous mudstone
					50% sandstone
477	757#	1	5	4.3	80% organic rich mudstone
					20% sandstone
478	758#	1	5.2	3.6	80% organic rich mudstone
					20% sandstone

479	759#	1.1	3.3	4	90% mudstone 10% sandstone
480	760#	1	4.8	2.8	70% mudstone
481	761#	0.9	4.1	8.5	60% sandstone 30% chert 10% mudstone
482	762#	1	2.2	1.3	80% sandstone 20% mudstone
483	763#	0.7	3.9	2.2	50% sandstone 50% diatomaceous mudstone
484	764#	0.7	3		50% mudstone 50% sandstone
485	765#	0.9	4.6	3.4	100% deformed beds of mudstone with small amounts of sandstone
486	766#	0.9	4.8	2.9	90% deformed mudstone 10% sandstone
487	767#	0.8	5.3	3.7	95% deformed mudstone 5% sandstone
488	768#	1	5.8	4.6	90% mudstone 10% sandstone
489	769#	0.9	5.7	4.9	60% mudstone 40% sandstone
490	770#	0.6	3.9	2.8	90% dolostone ledge 10% sandstone
491	771#	0.5	5.4	1.6	30% mudstone 50% dolostone 20% sandstone
492	772#	0.6	3.7	1.9	50% dolomitized sandstone

					30% dolomitized mudstone 20% dolostone
493	773#	0.6	5.7	1.5	80% diatomaceous mudstone 20% dolomitized sandstone
494	774#	0.6	5.7	1.5	50% sandstone with calcite cement
495	775#	1.2	4.9	1.8	50% diatomaceous mudstone 80% sandstone 20% mudstone with calcite cement
496	776#	1.1	5.2	2.9	50% calcareous mudstone 50% sandstone
497	777#	1.2	3.8	2.6	50% sandstone 40% mudstone with calcite
498	778#	1.3	4	1.9	80% sandstone 20% mudstone
499	779#	1.2	3.7	2.6	95% sandstone 5% mudstone with dolomitic concretion
500	780#	1.4	3.1	3	90% sandstone 10% mudstone with concretions
501	781#	0.9	4.2	2.9	90% sandstone and dolostone concretion (reading taken on concretion).
502	803#	0.9	2.5	2.8	10% mudstone 100% sandstone with dolomitic concretions

503	804#	1.3	3	2.7	90% sandstone with mudstone
504	805#	1.3	2.5	2.2	90% sandstone with dolomitic concretions
505	806#	1.1	4.4	3.9	90% sandstone 10% mudstone
506	807#	1.1	4.6	3.1	70% calcareous sandstone and 30% calcareous mudstone
507	808#	0.9	4.2	3	50% calcareous mudstone 50% calcareous sandstone
508	809#	0.8	4	2.9	70% calcareous sandstone 30% calcareous mudstone
509	810#	0.8	4.2	2.8	80% calcareous sandstone 20% calcareous mudstone
510	811#	0.7	3.1	3.2	50% dolomite 50% fissile mudstone
511	812#	0.9	4.8	3.9	100% calcareous sandstone
512	813#	0.9	3.8	3.7	50% mudstone 50% calcareous sandstone
513	814#	0.9	4.4	2.9	50% calcareous sandstone 50% calcareous mudstone
514	815#	0.8	4.2	3.4	60% mudstone 40% calcareous sandstone
515	covered				
516	816#	0.5	3.8	2.8	50% dolomite 50% mudstone
517 - 518	covered				
519	817#	0.7	3.4	3.2	100% calcareous mudstone
520 - 522	covered				
523	818#	1	4.1	3.1	50% calcareous mudstone

					50% calcareous sandstone
524	819#	1.1	4.3	4.4	80% sandstone
					20% calcareous mudstone
525	820#	0.9	4.1	2.8	50% calcareous mudstone
					50% calcareous sandstone
526	821#	0.6	3.3	3.2	80% dolostone
					20% mudstone
527 - 536	covered section				
537	822#	1	4.8	3.5	70% mudstone
					30% sandstone
538 - 567	covered section				
568	823#	xx	xx	xx	80% calcareous mudstone
					20% sandstone
569 - 626	covered section				
627	824#	0.8	4.6	3.2	30% chert
					30% siliceous mudstone
					30% diatomite
628	825#	1.1	4.6	2.4	100% sandstone
629	826#	0.9	5.9	3.4	100% diatomite
630 - 653	covered section				
654	827#	1.2	4.5	9.2	100% dolostone
655 - 727	hostile home owner / no data gathered				
728	828#	0.8	4	1.9	50% chert
					50% dolostone
729	829#	0.7	5.5	7	50% calcareous mudstone
					50% chert

730	830#	0.7	5.1	2.8	80% calcareous mudstone 20% chert
731	831#	0.9	6.1	2.5	100% calcareous mudstone
732	832#	0.9	5.5	2.8	60% chert 40% mudstone
733	833#	0.8	5.6	2.8	80% calcareous mudstone 20% chert
734	834#	0.9	4.6	2.3	60% calcareous mudstone 40% chert
735	835#	0.9	5.7	3	90% calcareous mudstone 10% chert
736	836#	0.8	8.5	2.9	95% "hot" calcareous mudstone 5% chert lenses
737	837#	0.7	6.3	2.7	50% chert 50% calcareous mudstone
738	838#	0.9	7.6	2.9	10% chert lenses 90% calcareous mudstone
739	839#	0.9	7.5	4.1	80% calcareous mudstone 20% chert
740	covered				
741	840#	0.8	5.3	3.3	50% chert 50% muddy diatomite
742	841#	1.2	8.5	5.1	100% siliceous mudstone
743	842#	1.2	8.5	5.1	100% siliceous mudstone
744	843#	1.2	8.4	5.6	50% "hot" calcareous mudrock 50% dolostone
745	inaccessible due to overhanging rocks				
746	844#	1.1	7.1	4.3	80% calcareous mudrocks

					20% chert
747	845#	0.7	6.6	2.9	50% chert
					50% diatomaceous mudrock
748	846#	0.5	5.2	1.8	80% diatomite
					20% chert
749	847#	1	7.4	2.7	80% calcareous sandstone
					20% chert
750	848#	0.8	7.1	3.1	50% chert
					50% muddy diatomite
751	849#	0.8	6.9	3.2	50% chert
					50% muddy diatomite
752	850#	1	6.8	4.2	50% muddy diatomite
					50% chert

APPENDIX B

SPECTRAL GAMMA RAY DATA

APPENDIX B: Paleocurrent data

Data Points	Bedding	Cross Lamination	Azimuth Conversion	Perpendicular to Strike
1	N70W / 23E	335 / 29E	335	65
		305 / 44NE	305	45
2	338 / 30NE	N54W / NE	306	44
3	N32W / 20NE	N50W / 11NE	310	40
		N35E / 21E	35	125
		N56E / 20E	56	146
		N70W / 28NE	290	20
		N25E / 15E	25	115
		N10E / 6NE	10	100
		N15E / 20S	15	105
		N30E / 22N	30	120
		N42W / 25NE	318	48
		N65E / 10E	65	155
		N15W / 26E	345	78
4	N32W / 20NE	N30W / 33NE	330	60
		N55W / 39NE	315	45
		N70W / 26NE	280	10

APPENDIX C

DIATOM ANALYSIS

APPENDIX C: Diatom Analysis

Sample -- PC-032 223 meters			
Species	**Abundance**	**Notes**	**Age**
Actinocyclus ingens	r		
Actinocyclus oculatus	r		
Coscinodiscus marginatus	a		
Denticulopsis hyalina	r-f		
Denticulopsis simonsenii	r		middle to early late Miocene
Denticulopsis vulgaris	r	change to dominance by C marg and thalassiothrix frags	middle to early late Miocene
Thalassionema nitzschioides v. parva	x-r		
Thalassiothrix fragments (longissima?)	c-a		
Silicoflagellates	x		
sponge spicules	c-a		
Spores	r		
early late Miocene -D. hustedtii zone or top of D. hustedtii-D. lauta zone			
D. vulgaris, D. simonsenii, lack of T. schraderi			

Sample -- PC-035 273 meters		
Species	**Abundance**	**Age**
Actinocyclus ingens	x	
Actinocyclus oculatus	x	
Coscinodiscus marginatus	r	
Denticulopsis hyalina	r-f	
Denticulopsis kamtschatica?	x	
Denticulopsis simonsenii	r	middle to early late Miocene
Denticulopsis vulgaris	f	middle to early late Miocene
Paralia sulcata	r	
Rhizosolenia styliformis	x	
Rouxia california	r	late Miocene
Stephanopyxis spp.	r	
Thalassionema fragments	a	
Thalassionema nitzschioides	a	
Thalassionema nitzschioides v. parva	r-f	
Thalassionema robusta	f-c	late middle to early late Miocene (dsdp85)
Thalassiosira sp. 1 Barron	3	early late Miocene (dsdp86)
Distephanus pseudocrux	x	late Miocene
Distephanus speculum	x	
benthic/nearshore species	r-f	
sponge spicules	f	
spores	f	
early late Miocene -D. hustedtii zone or top of D. hustedtii-D. lauta zone		
D. vulgaris, D. simonsenii, R. californica, T. sp. 1 Barron, lack of T. schraderi		

Sample -- PC-084 285 meters		
Species	**Abundance**	**Age**
Actinocyclus ingens	f	
Actinocyclus oculatus	x-r	
Coscinodiscus marginatus	r	
Denticulopsis simonsenii	x	middle to early late Miocene
Hyalodiscus	x	
Stephanopyxis turris	r	
Thalassionema nitzschioides v. parva	x-r	
Thalassionema schraderi	f-c	late Miocene
Thalassiosira primalabiata	x	
Thalassiothrix	c	
Paradictyocha apiculata	x	late Miocene
sponge spicules	?	
spores	?	
Middle late Miocene - Thalasiosira antiqua zone		
Thalassionema schraderi present as well as Rouxia californica, few Denticulopsis		

Sample -- PC-088 440 meters					
Species	**Abundance**	**Age**	**LAD**	**FAD**	**(according to Cody, 2007)**
Actinocyclus ingens	r-f				
Actinocyclus oculatus	r-f				
Actinoptychus splendens	x				
Coscinodiscus nodulifer	x				
Denticulopsis katayamae (??)	x-r				
Nitzschia malinterpretaria	x				
Paralia	r				
Rhizosolenia curvirostris	x				
Rhizosolenia praebarboi	x				
Rhizosolenia styliformis	x				
Rouxia california	x-r	late Miocene	4.29-4.82	8.5-8.74	
Stephanopyxis turris	x				
Thalassionema hirosakiensis	f-c	middle to middle late Miocene (dsdp86)			
Thalassionema nitzschioides	f				
Thalassionema nitzschioides v. parva	f-c				
Thalassionema robusta	r-f	late middle to early late Miocene (dsdp85)			
Thalassionema schraderi	x-r	late Miocene			
Thalassiosira sp. 1 Barron		early late Miocene (dsdp86)			
Distephanus speculum	x				
sponge spicules	r-f				
spores	?				
Middle late Miocene - Thalasiosira antiqua zone					
Thalassionema schraderi present as well as Rouxia californica, few Denticulopsis					

Sample -- PC-042 450 meters				
Species	**Abundance**	**Age**		
Coscinodiscus fragments	c			
Coscinodiscus marginatus	f-c			
Coscinodiscus nodulifer	r-f			
Denticulopsis simonsenii	r-f	middle to early late Miocene	4.83-4.95	14.15-14.16
Denticulopsis vulgaris	x-r	middle to early late Miocene		
Hemidiscus cuneiformis	3			10.24-10.91
Nitzschia porteri?	x			
Rhizosolenia curvirostris	x			
Rouxia california	r-f	late Miocene	4.29-4.82	8.5-8.74
Stephanopyxis fragments	c			
Thalassionema hirosakiensis	f	middle to middle late Miocene (dsdp86)		
Thalassionema nitzschioides	a			
Thalassionema nitzschioides v. parva	f-c			
Thalassionema robusta	r	late middle to early late Miocene (dsdp85)		
Thalassiosira fragments	c			
benthic/nearshore species	r-f			
Dictyocha spp	r			
Distephanus crux scutulatus	x	middle Miocene		
Distephanus pseudofibula	x?	early to middle late Miocene		
Distephanus speculum	f-c			
sponge spicules	?			
spores	?			
e arly late Miocene -D. hustedtii zone or top of D. hustedtii-D. lauta zone				
D. vulgaris, D. simonsenii, R. californica, lack of T. schraderi				

Sample -- PC-044 728 meters		
Species	**Abundance**	**Age**
Actinocyclus oculatus	r	
Chaetoceros spp	f	
Denticulopsis simonsenii	x	middle to early late Miocene
Denticulopsis vulgaris	x	middle to early late Miocene
Paralia sulcata	x	
Rouxia californica	x	late Miocene
Stephanopyxis turris	r	
Thalassionema nitzschioides	c-a	
Thalassionema robusta	r-f	late middle to early late Miocene (dsdp85)
Thalassiosira sp. 1 Barron	r	early late Miocene (dsdp86)
Thalassiothrix	c-a	
Dictyocha	c	
Distephanus speculum	c	
Paradictyocha apiculata	x	late Miocene
sponge spicules	?	
spores	f-c	
C pelagicus		
C leptopus		
R asanoi		
R haqii >5		
R pseudoumbilicus		
R ampla		
e arly late Miocene -D. hustedtii zone or top of D.		
most biostratigraphically useful species rare or absent		
D. simonsenii, D. vulgaris and R. californica		

REFERENCES

REFERENCES

Adelman, K., and Adelman, G., 2002-2015, California Coastal Records Project: www.californiacoastline.org [Accessed November, 2016]

Allmendinger, R. W., Cardozo, N. C., and Fisher, D., 2013, Structural Geology Algorithms: Vectors & Tensors: Cambridge, England, Cambridge University Press, 289 pp.

Atwater, T., 1989, Plate tectonic history of the northeast Pacific and western North America, *in* Winterer, E. L., Hussong, D. M., and Decker, R. W., eds., The Eastern Pacific Ocean and Hawaii: Geological Society of America, Boulder, Colorado, The Geology of North America, v. N, pp. 21-72.

Barron, J.A. 1986. Paleoceanographic and tectonic controls on deposition of the Monterey Formation and related siliceous rocks in California. Palaeogeography, Palaeoclimatology, Palaeoecology, v. 53, p. 27-45

Barron, J.A., and Isaacs, C.M., 2001. Updated Chronostratigraphic framework for the California Miocene, *in* Isaacs, C. M., and Rullkötter, J., eds, The Monterey Formation: From Rocks to Molecules: New York, Columbia University Press, p. 393-395.

Behl, R.J., 1999, Since Bramlette (1946): The Miocene Monterey Formation of California revisited *in* Geological Society of America, Special Paper 338, Classic Cordilleran Concepts: A View from California, p. 301-313.

Behl, R. J., and Garrison, R. E., 1994, The origin of chert in the Monterey Formation of California (USA), *in* Iijima, A., Abed, A., and Garrison, R., eds., Siliceous, Phosphatic and Glauconitic Sediments of the Tertiary and Mesozoic: Utrecht, International Geological Congress Proceedings, Part C: p. 101–132.

Behl, R.J., and Morita, S. 2007. The Monterey Formation of the Palos Verdes Hills, California: Stratigraphy and diagenetic implications for burial and uplift history, *in* Brown, A.R.; Shlemon, R.J.; and Cooper, J.D., eds., Geology and Paleontology of the Palos Verdes Hills, California: A 60th Anniversary Revisit to Commemorate 1946 Publication of U. S. Geological Survey Professional Paper 207, ed. Pacific Section SEPM Book 103. p. 51-72.

Berry, A.L., Dalyrymple, G.B., Lanphere, M.A., and Von Essen, J.D., 1976, Summary of miscellaneous potassium-argon measurements, U.S. Geological Survey, Menlo Park, California, for the years 1972-1974: U.S. Geological Survey Circular, v. 177, 13 p.

Biddle, K.T., 1991, The Los Angeles basin: An overview, *in* Biddle, K.T., ed., Active Margin Basins, American Association of Petroleum Geologists Memoir 52, p. 5-24.

Blake, G.H., 1991, Review of the Neogene Biostratigraphy of the Los Angeles basin and implications for basin evolution: in Biddle, K.T., ed., Active Margin Basin, American Association of Petroleum Geologists Memoir 52, p. 135-184.

Boles, J.R., Miller, G. F., and Wright, T.D., 2010, Modern oil generation and pyrolysis at >800^{0}C from spontaneous combustion in a landslide of Miocene shale, California *in* Proceedings, Geological Society of America National Meeting, Denver, Colorado.

Brabb, E, E., and Parker, J, M., 2003, Location and age of foraminifer samples collected by Chevron petroleum geologists in California: U.S. Geological Survey Open File Report 03-167, version 2.0.: http://pubs.usgs.gov/of/2003/of03-167/ [Accessed, November 2016]

California Department of Conservation, Division of Oil, Gas, and Geothermal Resources: California Oil and Gas Fields, 1992, Volume 2, Southern, Central Coastal, and Offshore California Oil and Gas Fields, 645 p.

Cardozo, N., and Allmendinger, R. W., 2013, Spherical projections with OSX Stereonet: Computers & Geosciences, v. 51, p. 193 - 205, doi: 10.1016/j.cageo.2012.07.021

Conrad, C.L., 1983, Lithostratigraphy of the Monterey Formation of the Palos Verdes peninsula, Los Angeles County, California [Masters Thesis]: Los Angeles, California State University, 96 p.

Compton, J.S. and Siever, R. (1984). Magnesium mass balance calculations for the Monterey Formation, Santa Maria basin, California (abstract), *in* Garrison, Robert E., Miriam Kastner, and Donald H. Zenger, eds. Dolomites of the Monterey Formation and Other Organic-rich Units: April 18-21, 1984. Vol. 41. Society of Economic paleontologists, 1984.

Conrad, C.L., and Ehlig, P.L., 1987, The Monterey Formation of the Palos Verdes peninsula, California: An example of Sedimentation in a Tectonically Active Basin within the California Continental Borderland, *in* Larue, D.K., and Steel, R.J., eds., Cenozoic marine sedimentation, Pacific Margin: SEPM Pacific Section Special Publication, v. 28, p. 103-116.

Chang, A.S., and Grimm, K.A., 1999, Speckled beds: Distinctive gravity-flow deposits in finely laminated diatomaceous sediments, Miocene Monterey Formation, California: Journal of Sedimentary Research, v. 69, p. 122–134.

Chang, A.S., Grimm, K, A., and White, L, D., 1998, Diatomaceous Sediments from the Miocene Monterey Formation, California: A Lamina-Scale Investigation of Biological, Ecological, and Sedimentary Processes: PALAIOS, v. 13, p. 439-455.

Dibblee, T.W, Jr., and Ehrenspeck, H.E., 1993, Geologic Map of the Point Dume Quadrangle, Los Angeles and Ventura Counties, California: Dibblee Geological Foundation Map No. DF-48, scale 124,0000, colored.

Dolan, J. F., K. Sieh, and T. K. Rockwell (2000). Late Quaternary activity and seismic potential of the Santa Monica fault system, Los Angeles, California, Geol. Soc. Am. Bull, v. 112, p. 1559–1581

Ellis, D, V., 1987, Well Logging for Earth Scientists: Elsevier Science Publishing Co., Inc. New York, p. 1-685.

Föllmi, K.B., 1996, The Phosphorus cycle, Phosphogenesis and Marine Phosphate-Rich Deposits: Earth Science Reviews, volume. 40, issue 1-2, p. 55-124.

Garrison, E. G, 1992. Recent Archaeogeophysical Studies of the Paleoshorelines of the Gulf of Mexico, *in* Johnson, L.L., and Stright, M., eds., Paleoshorelines and Prehistory: An Investigation of Method: Boca Raton, CRC Press. p. 103-116.

Garrison, R.E., Hopple, B.W. and Grimm, K, A., 1994, Field Guide to the Monterey Formation between Santa Barbara and Gaviota, California; Pacific Section AAPG, Vol. GB72, p. 67–84.

Garrison, R.E., and Kastner, M., 1990, Phosphatic sediments and rocks recovered from the Peru margin during ODP Leg 112, *in* Suess, E., von Huene, R., et al., Proceedings Ocean Drilling Program Scientific Result, Volume 112: College Station, Texas, Ocean Drilling Program, p. 111–134, doi: 10 .2973 /odp .proc .sr .112 .145 .1990

Hoots, H.W., 1930, Geology of the eastern part of the Santa Monica Mountains, Los Angeles County, California: United States Geological Society Professional Paper 165-C, p. 134-183.

Ingle, J. C., Jr., 1981, Origin of Neogene diatomites around the north Pacific Rim, in Garrison, R. E., and Douglas, R. G., eds., The Monterey Formation and related siliceous rocks of California: Los Angeles, Pacific Section, Society of Economic Paleontologists and Mineralogists, p. 159–179.

Isaacs, C. M., 1981, "Lithostratigraphy of the Monterey formation, Goleta to Point Conception, Santa Barbara Coast, California. In: Guide to the Monterey Formation in the California coastal area, Ventura to San Luis Obispo, C.M. Isaacs (Ed.). Los Angeles, vol. 52, p. 9-23. Pacific Section American Association Petroleum Geologists.

Isaacs, C. M., 1983, "Compositional variation and sequence in the Miocene Monterey Formation, Santa Barbara coastal area, California. In: Fine-Grained Sediments: Deep Water Processes and Environments". D.K. Larue and R.J. Steel, eds. Los Angeles p. 117-132. Pacific Section American Association Petroleum Geologists.

Isaacs, C.M., and Petersen, N.F., 1987, Petroleum in the Miocene Monterey Formation, California, *in* Hein, J.R., ed., Siliceous Sedimentary Rock-hosted Ores and Petroleum: Evolution of ore fields: New York, Van Nostrand Reinhold, p. 83-116.

Kamerling, M.J., and Luyendyk, B.P., 1979, Tectonic rotations of the Santa Monica Mountains region, western Transverse Ranges, California, suggested by paleomagnetic vectors: Geological Society of America Bulletin, v. 90, p. 331 – 337.

Lanners, K. B., 2013, "Chemostratigraphy of Hemipelagic Facies of the Monterey Formation and Equivalent Sedimentary Rocks, Los Angeles Basin, California" thesis] California [Masters Thesis]: Los Angeles, California State University, 96 p.

Malmborg, W.T., West, W.B., Brabb, E.E., and Parker, J.M., 2008, Digital coordinates and age of more than 13,000 foraminifers samples collected by Chevron petroleum geologists in California: U.S. Geological Survey Open File Report, 2008-1187, 3 p., 2 database files: http://pubs.usgs.gov/of/2008/1187/[Accessed November, 2016].

Mariner, R.H., Minor, S.A., King, A.P., Boles, J.R., Kellogg, K.S., Evans, W.C., Landis, G.A., Hunt, A.G., and Till, C.B., 2008, A landslide in Tertiary marine shale with superheated fumaroles, Coast Ranges: California, Geology, v. 36, p. 959-962.

McCulloh, T.H., and Beyer, L. A., 2003, Mid-Tertiary Isopach and Lithofacies Maps for the Los Angeles Region, California: Templates for Palinspatic Reconstruction 10 17.4 Ma, U.S. Geological Survey Professional Paper 1960, p. 1-32.

Meister, P.; Bernasconi, S. M.; Vasconcelos, C.; McKenzie, J. A., 2008, Sea level changes control diagenetic dolomite formation in hemipelagic sediments of the Peru Margin. Marine Geology 252, 2008, p. 166-173.

Nicholson, C., Sorlien, C.C., Atwater, T., Crowell, J.C., and Luyendyk, B.P., 1994, Microplate capture, rotation of the western Transverse Ranges, and initiation of the San Andreas transform as a low angle fault system: Geology, v. 22, p. 491-495.

Pisciotto, K.A., and Garrison, R.E., 1981, Lithofacies and depositional environments of the Monterey Formation, California: in Garrison, R.E., and Douglas, R.G., eds., The Monterey Formation and related siliceous rocks of California, Society for Sedimentary Geology, p. 97-122.

Redin. T., 1991, Oil and Gas Production from Submarine Fans of the Los Angeles Basin, in Biddle, K.T., ed., Active Margin Basins: American Association of Petroleum Geologists, p. 35-134Rumelhart, P.E., and Ingersoll, R.V., 1997, Provenance of the upper Miocene Modelo Formation and subsidence analysis of the Los Angeles basin, southern California: Implications for paleotectonic and paleotectonic and paleogeographic reconstructions: Geological Society America Bulletin, Vol. 109, p. 885-899.

Schlumberger, 2009, Log Interpretation Charts: Schlumberger, 225 Schlumberger Drive, Sugar Land, Texas 77478, www.slb.com, p., 194.

Schwalbach, J., Gordon, A., and O'Brien, C. 2007. Reservoir Characterization of Monterey Formation Siliceous Shales: Tools and Applications. AAPG Bulletin: 119–146.

Stanley, R.G., Wilson, D.S., and McCrory, P.A., 2000, Locations and ages of middle Tertiary volcanic centers in coastal California: U.S. Geological Survey Open-File Report 00-154, 27 p.

Stuart, C.J. 1976. Source terrane of the San Onofre Breccia-Preliminary notes, in Howell, D.G., ed., Aspects of the Geological History of the California Borderland: Pacific Section, American Association of Petroleum Geologists, Miscellaneous Publication 24, p. 309-325.

Sullwold, H.H., Jr., 1960, Tarzana Fan, deep submarine fan of late Miocene age, Los Angeles County, California: American Association of Petroleum Geologists Bulletin, v. 44, p. 433-457.

Vedder, J.G., and D. G. Howell, 1976, Review of the distribution and tectonic implications of Miocene debris from the Catalina Schist, California continental borderland and adjacent coastal areas, in D.G. Howell, ed., Aspects of the geologic history of the California continental borderland: Pacific Section, AAPG Miscellaneous Publication 24, p. 326-340.

Woodring, W. P., Bramlette, M.N., and Kew, W.S.W., 1946, Geology and paleontology of Palos Verdes Hills California: U.S. Geological Survey Professional Paper 207, p. 145.

Wright, T.L., 1991, Structural geology and tectonic evolution of the Los Angeles Basin, California, in Biddle, K.T., ed., Active Margin Basins: American Association of Petroleum Geologists, p. 35-134.

Yerkes, R.F. and Campbell, R.H., 1979, Stratigraphic Nomenclature of the Central Santa Monica Mountains, Los Angeles County, California, U.S. Geol. Soc. Contributions to Stratigraphy, Bull. 1457-E, p. E25 – 29.

Yerkes, R.F. and Campbell, R.H., 1980, Geologic Map of East-Central Santa Monica Mountains, Los Angeles County, California. U.S. Geol. Soc. Miscellaneous Investigation Series: Map 1-1146.

Yerkes, R.F., McCulloh, T.H., Schoellhamer, J.E., and Vedder, J.G., 1965, Geology of the Los Angeles Basin California: An Introduction: Geological Survey Professional Paper 420-A